ΠΑΝΕΠΙΣΤΗΜΙΟ ΠΕΙΡΑΙΩΣ

ΣΧΟΛΗ ΝΑΥΤΙΛΙΑΣ ΚΑΙ ΒΙΟΜΗΧΑΝΙΑΣ

ΤΜΗΜΑ ΒΙΟΜΗΧΑΝΙΚΗΣ ΔΙΟΙΚΗΣΗΣ & ΤΕΧΝΟΛΟΓΙΑΣ

Διδακτορική Διατριβή

Σχεδίαση Βιοαισθητήρων με Τεχνοοικονομικά Κριτήρια για την Εφαρμογή τους στον Περιβαλλοντικό Έλεγχο Υδάτινων Οικοσυστημάτων

Γεωργόπουλος Ν. Κωνσταντίνος

Επιβλέπουσα
Αναπληρώτρια Καθηγήτρια
Σιοντόρου Χριστίνα

Πειραιάς, 2021

UNIVERSITY OF PIRAEUS

SCHOOL OF MARITIME AND INDUSTRIAL STUDIES

DEPARTMENT OF INDUSTRIAL MANAGEMENT AND TECHNOLOGY

PhD Thesis

Techno-Economic Design Requirements for Integrating Biosensors

in Environmental Monitoring of Aquatic Ecosystems

Georgopoulos N. Konstantinos

Supervisor
Associate Professor
Siontorou Christina

Piraeus, 2021

Advisory committee

Siontorou Christina	Associate Professor, Supervisor Department of Industrial Management and Technology, School of Maritime and Industrial Studies University of Piraeus
Sidiras Dimitrios	Professor, Department of Industrial Management and Technology, School of Maritime and Industrial Studies University of Piraeus
Karalekas Dimitrios	Professor, Department of Industrial Management and Technology, School of Maritime and Industrial Studies University of Piraeus

Συμβουλευτική επιτροπή

Σιοντόρου Χριστίνα	Αναπληρώτρια Καθηγήτρια, Επιβλέπουσα Τμήμα Βιομηχανικής Διοίκησης και Τεχνολογίας, Σχολή Ναυτιλίας και Βιομηχανίας Πανεπιστήμιο Πειραιά
Σιδηράς Δημήτριος	Καθηγητής, Τμήμα Βιομηχανικής Διοίκησης και Τεχνολογίας, Σχολή Ναυτιλίας και Βιομηχανίας Πανεπιστήμιο Πειραιά
Καραλέκας Δημήτριος	Καθηγητής, Τμήμα Βιομηχανικής Διοίκησης και Τεχνολογίας, Σχολή Ναυτιλίας και Βιομηχανίας Πανεπιστήμιο Πειραιά

Dissertation committee

Siontorou Christina	Associate Professor, Supervisor Department of Industrial Management and Technology, School of Maritime and Industrial Studies University of Piraeus
Sidiras Dimitrios	Professor, Department of Industrial Management and Technology, School of Maritime and Industrial Studies University of Piraeus
Karalekas Dimitrios	Professor, Department of Industrial Management and Technology, School of Maritime and Industrial Studies University of Piraeus
Sakellariadou Fani	Professor, Department of Maritime Studies, School of Maritime and Industrial Studies University of Piraeus
Georgakellos Dimitrios	Professor, Department of Business Administration, School of Economics, Business and International Studies University of Piraeus
Topakas Evangelos	Associate Professor, Department of Synthesis and Development of Industrial Processes, School of Chemical Engineering National and Technical University of Athens
Bakeas Evangelos	Associate Professor, Department of Chemistry, School of Science National and Kapodistrian University of Athens

Εξεταστική Επιτροπή

Σιοντόρου Χριστίνα	Αναπληρώτρια Καθηγήτρια, Επιβλέπουσα Τμήμα Βιομηχανικής Διοίκησης και Τεχνολογίας, Σχολή Ναυτιλίας και Βιομηχανίας Πανεπιστήμιο Πειραιά
Σιδηράς Δημήτριος	Καθηγητής, Τμήμα Βιομηχανικής Διοίκησης και Τεχνολογίας, Σχολή Ναυτιλίας και Βιομηχανίας Πανεπιστήμιο Πειραιά
Καραλέκας Δημήτριος	Καθηγητής, Τμήμα Βιομηχανικής Διοίκησης και Τεχνολογίας, Σχολή Ναυτιλίας και Βιομηχανίας Πανεπιστήμιο Πειραιά
Σακελλαριάδου Φανή	Καθηγήτρια, Τμήμα Ναυτιλιακών Σπουδών, Σχολή Ναυτιλίας και Βιομηχανίας Πανεπιστήμιο Πειραιά
Γεωργακέλλος Δημήτριος	Καθηγητής, Τμήμα Οργάνωσης και Διοίκησης Επιχειρήσεων, Σχολή Οικονομικών, Επιχειρηματικότητας και Διεθνών Σπουδών Πανεπιστήμιο Πειραιά
Τόπακας Ευάγγελος	Αναπληρωτής Καθηγητής, Τομέας Σύνθεσης και Ανάπτυξης Βιομηχανικών Διαδικασιών, Σχολή Χημικών Μηχανικών Εθνικό Μετσόβιο Πολυτεχνείο
Μπακέας Ευάγγελος	Αναπληρωτής Καθηγητής, Τμήμα Χημείας, Σχολή Φυσικών Επιστημών Εθνικό και Καποδιστριακό Πανεπιστήμιο Αθηνών

"To fulfil the dreams of your youth is the best that can happen because nothing creates more self-esteem and confidence than achieving one's own goal."

To all those who supported me,

and gave me the strength

to conclude this thesis

Contents

Table of Tables

Table of Figures

Acknowledgements

By completing this research, I strongly feel the need to thank certain people for their valuable contribution and support. I would like to express my gratitude to the supervisor, Assoc. Prof. C. Siontorou, for her guidance and patience, as well as for her insightful suggestions and advice. I owe a deep debt of gratitude to Prof. D. Sidiras for his support. I also thank the staff and PhD students of the Laboratory of Simulation of Industrial Processes for their collaboration all these years. Finally, I thank my wife and my son for their patience, understanding, and support.

The development of the bench-scale metal-supported self-assembled lipid membranes and the related experimental work has been performed in the Laboratory of Simulation of Industrial Processes. The experimental work on the potentiometric nanosensor has been performed in the Laboratory of Environmental Chemistry of the Department of Chemistry at the National and Kapodistrian University of Athens (under the supervision of Prof. Dimitrios Nikolelis. I would like to thank him and his staff for their help in both, the expertise and the availability of materials and equipment.

Publications

The work described herein has been published in the following scientific journals:

1. Siontorou CG, **Georgopoulos KN**, Nalantzi M-M, Designing biosensor networks for environmental risk assessment of aquatic systems. *Critical Reviews in Environmental Science and Technology* 2017;47:40-63 (IF: 8.302/ Q1)
2. Siontorou CG, **Georgopoulos KN**, Nikoleli G-P, Nikolelis DP, Karapetis SK, Bratakou S, Protein-based graphene biosensors: optimizing artificial chemoreception in bilayer lipid membranes. *Membranes (Basel)* 2016;6:43 (IF: 3.094/ Q2)
3. Siontorou CG, **Georgopoulos KN**, A biosensor platform for soil management: the case of nitrites. *Journal of Cleaner Production* 2016;111:133-142 (IF: 7.246/ Q1)

An overview of the work, has been included in the following book chapter:

1. Siontorou CG, Psychoyios VN, Nikoleli G-P, Nikolelis DP, Karapetis S, Bratakou S, **Georgopoulos KN**. Rapid detection of pathogens and toxins, in Food Process Engineering and Quality Assurance (eds Mohan CO, Carvajal-Millan E, Ravishankar CN, Haghi AK) Apple Academic Press, 2018: 9781315232966.

Part of the work has been also published in the following journals (selection from Conference Proceedings)

1. **KN Georgopoulos**, CG Siontorou, A planar bilayer lipid membrane biosensor based on enzymes in the service of environmental monitoring, published in Water Pollution XIII. Vol 209, 2016, WIT PRESS.
2. Siontorou CG, **Georgopoulos KN**, Stimuli-Responsive Platforms for Integrated Multifunctional Intelligent Systems, published in *Chemical Engineering Transactions* Vol. 39, 2014, 811-816, ELSEVIER.

Part of the work has been also presented in the following Conferences (acceptance after review)

1. Siontorou CG, **Georgopoulos KN**, Tyrosinase Biosensor for Phenol Monitoring in Water, *Proceedings of the International Conference on Chemical, Agricultural and Biological Sciences (CABS)*, 2015.
2. **KN Georgopoulos**, C. G. Siontorou, Enzyme biosensors - Co-immobilization of enzymes for the construction of multi enzymatic biosensor, *Proceedings of the International Conference on Science, Ecology, and Technology (ICONSETE*), 2015.

Summary

The aim of this work was to design and develop biosensors for monitoring aquatic ecosystems with built-in environmental specifications based on techno-economic criteria. The objectives of the work included (i) the design and development of a methodological framework for modelling aquatic ecosystems, with a view to identifying both, critical quality parameters (target analytes) that should be monitored and environmental constraints that should be considered when designing the biosensors, (ii) the design, development, validation and evaluation (by means of computational and physical simulation) of target- and environment- specific field biosensors, and (iii) the study of the technological frame, including the cost and the marketability aspects for these devices.

Modelling of aquatic systems utilised an ontological platform in order to identify critical interactions within the ecosystem at different scales. Biosensors have been developed on a lipid membrane platform coupled to an electrochemical transducer for detecting peroxide, phenols, and nitrates in water and sediment samples (from the zone and/or the benthos). The development of such systems on the basis of their intended use and their evaluation under real environmental conditions and samples has not been reported before in literature. The replacement of the lipid platform with polymerized membranes and the conversion of the transducer to zink oxide nanowalls or graphene nanosheet electrodes yielded nanosensors with improved analytical characteristics, as indicated with a cholesterol-cholesterol oxidase system.

The up-to-date technological frame of biosensors is also discussed on the basis of technology adsorption and process capability, including the identification of critical barriers to industrial production and competitiveness.

Περίληψη

Σκοπός της διατριβής ήταν ο σχεδιασμός και η ανάπτυξη βιοαισθητήρων βάσει περιβαλλοντικών προδιαγραφών και τεχνο-οικονομικών κριτηρίων για την παρακολούθηση της ποιότητας υδάτινων οικοσυστημάτων. Οι στόχοι της διατριβής περιλάμβαναν (i) το σχεδιασμό και την ανάπτυξη ενός μεθοδολογικού πλαισίου για τη διαμόρφωση υποδειγμάτων των υδάτινων οικοσυστημάτων, κατάλληλων για τον προσδιορισμό των κρίσιμων παραμέτρων ποιότητας (προσδιοριστέοι παράγοντες) που πρέπει να παρακολουθούνται καθώς και των περιορισμών που πρέπει να λαμβάνονται υπόψη κατά το σχεδιασμό των βιοαισθητήρων λόγω της λειτουργίας τους στο περιβαλλοντικό πεδίο, (ii) το σχεδιασμό, την ανάπτυξη, τη διερεύνηση της αξιοπιστίας και την αξιολόγηση (μέσω υπολογιστικής και φυσικής προσομοίωσης) βιοαισθητήρων πεδίου εξειδικευμένων για το περιβάλλον λειτουργίας και τις παραμέτρους παρακολούθησης και (iii) τη μελέτη της εμπορευσιμότητας των βιοαισθητήρων που αναπτύχθηκαν με βάση το υπάρχον τεχνολογικό πλαίσιο, τις ευκαιρίες εφαρμογής, της ικανότητας υιοθέτησης νέας τεχνολογίας και των προβλημάτων στη βιομηχανική παραγωγή.

Η μοντελοποίηση των υδάτινων συστημάτων βασίσθηκε σε μια οντολογική πλατφόρμα προκειμένου να καθίσταται δυνατός ο εντοπισμός των κρίσιμων αλληλεπιδράσεων εντός του οικοσυστήματος σε διαφορετικές κλίμακες. Οι βιοαισθητήρες αναπτύχθηκαν σε μια πλατφόρμα λιπιδικών μεμβρανών που συνδέεται με έναν ηλεκτροχημικό μεταλλάκτη για τον προσδιορισμό υπεροξειδίου, φαινολών και νιτρικών σε δείγματα νερού και ιζημάτων (από την παράκτια ζώνη ή/και τον βυθό). Η ανάπτυξη τέτοιων συστημάτων βάσει της προβλεπόμενης χρήσης τους και η αξιολόγησή τους υπό πραγματικές περιβαλλοντικές συνθήκες και με πραγματικά δείγματα δεν έχει αναφερθεί προηγουμένως στη βιβλιογραφία. Η αντικατάσταση της λιπιδικής πλατφόρμας με πολυμερισμένες μεμβράνες και η μετατροπή του μεταλλάκτη σε ηλεκτρόδια νανοδομών οξειδίου του ψευδαργύρου ή γραφενίου οδήγησαν σε νανοαισθητήρες με βελτιωμένα αναλυτικά χαρακτηριστικά, όπως διαπιστώθηκε στο σύστημα χοληστερόλης - οξειδάσης της χοληστερόλης.

Το σύγχρονο τεχνολογικό πλαίσιο των βιοαισθητήρων διερευνήθηκε, επίσης, με βάση την ικανότητα υιοθέτησης της τεχνολογίας, συμπεριλαμβανομένου του εντοπισμού κρίσιμων εμποδίων στη βιομηχανική παραγωγή και την ανταγωνιστικότητα.

1. Thesis overview

Pollution of aquatic systems (marine, lake or river) adversely affects public health and the quality of ecosystems. Sources of pollution are numerous and pervasive, including municipal and industrial waste, agricultural runoff, accidental spills or systematic discharges (Bashir *et al.*, 2020). The categories of pollutants include microbiological agents (e.g., bacterial toxins), endocrine disruptors (e.g., dioxins, perchlorates, polychlorinated biphenyls), heavy metals (e.g., Cr, Pd, Hg), acute poisoning chemicals (e.g., arsenic and cyanides), eutrophication agents (fertilizers) and agrochemicals (pesticides, insecticides).

Effective site treatment and remediation presupposes the timely and reliable detection of any stressor or pollutant that, through a cascade of interactions, degrades the quality of the site (Siontorou and Batzias, 2014a). Such an approach critically depends upon an ecological-relevant and cost-effective metrological scheme to support decision making and policy development (Burger, 2008). Engineering, however, reliable environmental gauzes is not an easy task. Any ecosystem can be described as a complex and multifaceted ecological network, composed of a multitude of sub-systems of varying nature (biological, geochemical, hydrological, ecological, physical, etc.) and scale (micro-, meso- and macro-) (Siontorou *et al.*, 2017). The function of the ecosystem relies on the interaction between its sub-systems and its tolerance to stress; thereby, monitoring of quality parameters goes beyond the mapping of a handful of chemicals and abiotic parameters (e.g., temperature, pH), that may or may not represent the critical and representative degradation profile.

Developing devices for environmental applications necessitates the inclusion of environmental constraints and criteria at the design phase, in order to ensure that the resultant device is techno-economically suitable for the intended task (Siontorou *et al.*, 2017). Environmental parameters and quality indicators (target analytes) can be derived from ecosystem modelling capable to map system's complexity in a comprehensive way.

Biosensor platforms provide the versatility required for integrating environmental, metrological and operational parameters at the design phase (Siontorou and Batzias, 2014b). Biosensors utilise a biochemical system (enzyme, antibody, receptor, DNA,

etc.) to interact, specifically and sensitively, with a target analyte so as to produce an event that is translated into an electric signal by a physicochemical transducer (Thévenot *et al.*, 1999). In effect, any target analyte can be coupled to a biochemical system of adequate affinity and combined with a suitable (as per the biochemical system, the intended use or the metrological specifications) transducer. Electrochemical systems are commonly used owing to their simplicity, miniaturization potential and low cost. Biosensor systems based on lipid membranes have been proven more suitable to handle environmental samples and detect reliably low or ultra-low concentration levels (Saem *et al*., 2020).

The aim of this work was to design and develop biosensors for monitoring aquatic ecosystems with built-in environmental specifications based on techno-economic criteria. The objectives of the work included (i) the design and development of a methodological framework for modelling aquatic ecosystems, with a view to identifying both, critical quality parameters (target analytes) that should be monitored and environmental constraints that should be considered when designing the biosensors, (ii) the design, development, validation and evaluation (by means of computational and physical simulation) of target- and environment-specific field biosensors, and (iii) the study of the technological frame, including the cost and the marketability aspects for these devices.

The thesis is structured as follows: Chapter 2 presents the methodological framework for modelling aquatic ecosystems, Chapter 3 deals with the design criteria of the biosensor platform, Chapter 4 states the materials and describes the methods used for the construction of biosensors, Chapter 5 discusses the validation and implementation of the devices developed, Chapter 6 investigates the technological frame, highlighting cost and marketability issues, and Chapter 7 presents the conclusions of this work and also some suggestions for future research.

2. Aquatic ecosystems - Monitoring needs and modelling aspects

2.1. Introduction

The modelling of aquatic systems is nowadays commonly linked to environmental management and policymaking. A metrological system is also indispensable, but critically relies on modelling to identify the monitoring parameters that represent the quality of the entire ecosystem.

As an established practice, modelling takes the form of a set of semi-empirical equations that are based on the perception of the modeler for the ecosystem (Sillero, 2011). The main scope of ecosystem modelling is to describe the status of the system in such a way that any changes can be predicted at a given degree of reliability. Generally, reliable spatiotemporal predictions are feasible with a multi-parameter and complex model that can describe the multifaceted ecological network with its many sub-systems of a varying nature (biological, geochemical, hydrological, ecological, physical, etc.) and their interactions (Knoke and Seifert, 2008). Any given ecosystem reaches a thermodynamically steady state through a multitude of interactions between different scales: molecular processes, under certain biotic and abiotic conditions, trigger changes in other systems of the same scale that are gradually progressed towards higher scales that affect lower scales, and so forth (Arhonditsis and Brett, 2004). Notwithstanding, the majority of the models suggested in the literature are only limited either to one scientific domain (e.g., ecology or hydrology) (Sillero, 2011) or to one scale, usually the scale that it is easier to provide measurements for (Knoke and Seifert, 2008). These models have been used successfully to describe part of the ecosystem but have proven unsuitable for the entire system (Bennett *et al.*, 2013). The Sidi Kerair port and Sidi Kerair coastal resort (Frihi, 2001) in Egypt, is a pertinent example. It was noticed that the long-term erosion of coastal areas due to tidal activity affected negatively the flora of the region and resulted in great economic impacts. According to a mechanistic model of the area, the construction of retaining walls behind a breakwater construction would protect the coast. Unfortunately, these constructions aggravated the existing problem because they kept the waters stagnant, leading to the spread of the algae that restricted further the growth of local flora, almost to extinction. Moving to a

hydrogeochemical model, the problem of solid residue deposition has been solved by the development of lagoons that substituted previous constructions. Another example comes from the attempts to save the North Sea herring in the 1980s. Based on a trophic transfer model, the area was overseeding with herring but populations kept declining (Cushing, 1983). Upon mapping the hydrogeochemical patterns, unfavorable to herring environmental conditions have been highlighted leading to suitable interventions.

In developing an optimal model, it is necessary to define the scales to be included and their interconnection in order to identify (Siontorou, 2014): (i) the critical procedures of the same type and scale that link abiotic to biotic parameters, (ii) critical procedures of the same scale but of different types that extent the link between abiotic and biotic parameters, and (iii) critical procedures of different types on different scales that express or drive the link between abiotic and biotic parameters.

Small scales may be modeled through site hydrology, provided that detailed information on small-scale topography is available (Hesse *et al.*, 2008). Larger areas may rely on geomorphology, provided that small-scale data is reliable and representative enough to calibrate large models (Liu *et al.*, 2008). Ecology may be proven more relevant and reliable, provided that information from hydrological and geomorphological studies are available (Knoke and Seifert, 2008). Data or models from other sources may be also needed, e.g., meteorology or microbiology, thus making the field multidisciplinary (Naveh *et al.*, 2007). Consequently, pollution responses are necessarily treated though semi-qualitative and semi-empirical terms, increasing uncertainty manifold in decision making (Liu, 2008).

Multiple scales and parameters can be efficiently handled through ontological platforms (Siontorou *et al.*, 2017). Ontology may incorporate all scientific areas and the interactions of many sub-systems in a way suitable to enhance the reliability of the spatiotemporal predictions needed for decision making. The methodological framework and its implementations are presented hereinafter.

2.2. Methodology

The presented methodology aimed at mapping all the physicochemical and biochemical processes of an aquatic ecosystem with a view to identifying the path(s) of a pollutant entering the system (Siontorou *et al.*, 2017). Modeling followed a four-phase iterative process.

Phase 1: Description of the System

Water quality, other quality issues and site exploitation plans have been considered in this phase in order to accurately reflect the critical ecological strains. The prospects, plans, and views of all stakeholders should be taken into early consideration so that any model developed bears the suitable perception as a built-in parameter. Trade-offs between economic exploitation and environmental protection, commonly observed in aquatic ecosystems, may highlight the need to monitor otherwise rendered as non-priority parameters or the need to set up a denser monitoring network.

Phase 2: Functional Analysis

At this phase, the goal was to prioritize the functions of the system. The system was decomposed into autonomous subsystems using hydrogeochemical and environmental criteria, dependent upon the nature of the problems to be solved and/or the prevailing conditions. The ecosystem was considered as an input-output system of energy and mass. Thus, each ecosystem has three main parts: the input energy-mass, the system itself that transforms the input energy-mass, and the output energy-mass (Fig. 1).

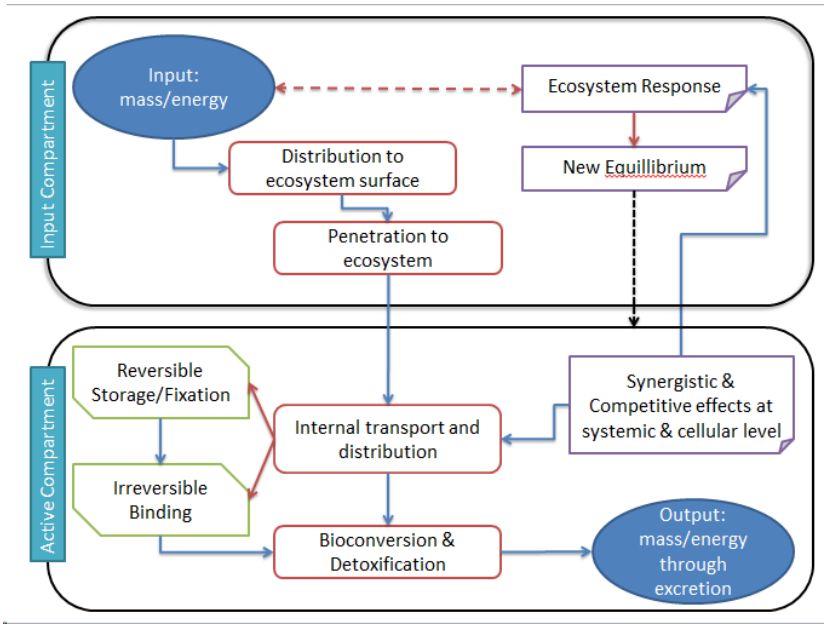

Figure 1. Simplified compartment model of an ecosystem and the interactions within and between the compartments.

Under normal working conditions, the energy and mass inflow and outflow are carefully and steadily balanced; when inflow changes significantly, the ecosystem itself changes and outflow fluctuations are observed. When budgets are fixed, there is usually

only one critical variable that dominates the other variables. The monitoring of this variable provides useful information for the entire system; for example, the pH values are indicative of the microbiological production that build the trophic chain.

Following a compartment model, the input compartment is responsible for the distribution of inflow to the surface of the ecosystem, and once it penetrates the system it can be stored/accumulated or subjected to bioconversion and eventually exit the system (Fig. 1). The input compartment host macro-scale relations, whereas the systemic and cellular effects take place in the active compartment and propagate towards higher scales.

Phase 3: Systemic Analysis

At this phase, the functional model turned into an ontological matrix of elements. The ontological platform has been developed according to the procedure described in Siontorou *et al.* (2012). Briefly, the ecosystem has been decomposed into subsystems based on the critical interactions and the flow of information (i.e., the compartments and sub-compartment shown in Fig. 1). Each sub-system has been analyzed into its constituent elements and processes (taxonomy, *is-a* relations), whereas the interactions between the subsystems (at any scale) provided the partonomic relations (*part-of* relations) and the information network within and between the subsystems (Fig. 2).

Each subsystem was described by nodes, each node referring to a basic parameter. The links between the nodes represented the parameter interactions. The ontology was structured around each subsystem of interest (e.g., the most influencing or the most sensitives), with upstream and downstream extensions, according to the procedure proposed by Kotis *et al.* (2006). The resultant network contained strong links (i.e., links with high in and out degrees), that describe the constraints of each subsystem, and weak links (i.e., links with low in and out degrees), that were eliminated. Further, the nodes that host the stronger links represent the critical parameters that should be monitored.

Phase 4: Physical Analysis

The analysis was completed by defining the interfaces and flows between the subsystems. This phase produced superstructures, the synergy of which yielded the entire system. The superstructures have been used to re-evaluate phases 2 and 3.

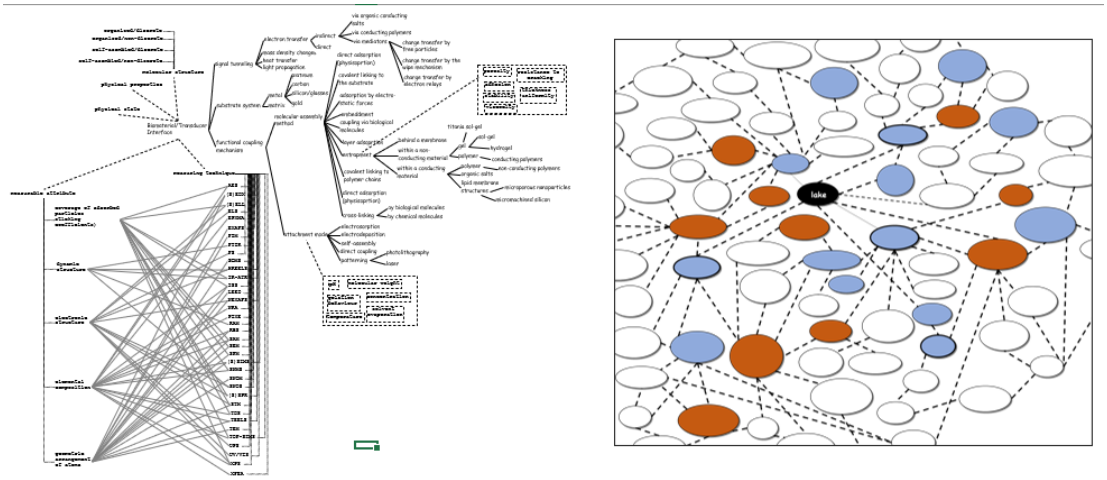

Figure 2. Excerpt from a lake (as a general concept) ontology. (left) Taxonomy of the active compartment. (right) ontology overview illustrating the partonomy relations of the same scale (blue) and of different scales (red) and of different processes (white). The size of the nodes represents the size of the respective taxonomy.

2.3. Model validation

2.3.1 Coastal ecosystem stress assessment

The coastal area of Palaia Fokea and Legrena in the Saronic Gulf has been chosen for model validation, based on the criteria of (a) stakeholder plans for exploitation and (b) contamination input. The area is touristically developed and hosts a number of settlements and aquaculture farms, whereas the bay receives the polluted waters from the Piraeus port and the Athens riviera (Fig. 3). Generally, Saronic Gulf is a marine region with extensive contamination (Zacharias *et al.*, 2005); urban wastewater from all the surrounding areas reached the Gulf without treatment for many years, whereas sea currents support a very slow cleansing process.

Phase 1 has been limited to coast profiling. The implementation area has coarse mixed sedimentary beaches with sand, grains, and pebbles. Exposure to the wave is uniform, and the characteristics of the sediments along the beach are relatively homogeneous. Both offshore and coastal sediment transfers cause changes in shoreline, with the latter acting much longer, creating coastal variability, especially during spring and summer. The coastal area has been shown to accumulate chlorinated organic pesticides and nitrogen fertilizers (Galanopoulou *et al.*, 2005), possibly from the sewage effluent received in the past and the nearby agricultural activities. The site geology and the rainwater streams support natural anti-stress processes, maintaining the quality of

seawater at a higher level than expected. Since the establishment of the settlements, water quality has degraded with an increase in coliforms, signs of nitrogen eutrophication and the appearance of resistant to heavy metals bacteria.

Figure 3. The area of Palaia Fokea and Legrena is rapidly growing with several settlements and a mixed pollution profile.

Many natural processes take place in the bay, involving waves, streams, effluents, sewage, sediments, etc., that regulate critical system parameters and confer a seasonal coastline profile. Further, local climate and geomorphology affect these natural processes in various ways. The occurring changes disturb the local biochemistry that controls the population of many sea or seashore species (Evangeliou *et al.*, 2011).

The functional model (Phase 2) that was created is presented in Fig.4, involving usual inflow (top) and stress inflow (bottom). Systemic analysis (Phase 3) showed that the critical parameters include nutrient loading, sediment resuscitation, short wave radiation, light dimming, water temperature balance and salinity conditions. Node minimization revealed nitrogen as most critical, since it appears to be the main nutrient that controls the site phytoplankton biomass, which fosters coliforms and other bacteria; nitrogen monitoring will make it possible to clarify the state of the ecosystem under study. The physical model (Phase 4) is shown in Fig. 5 (top).

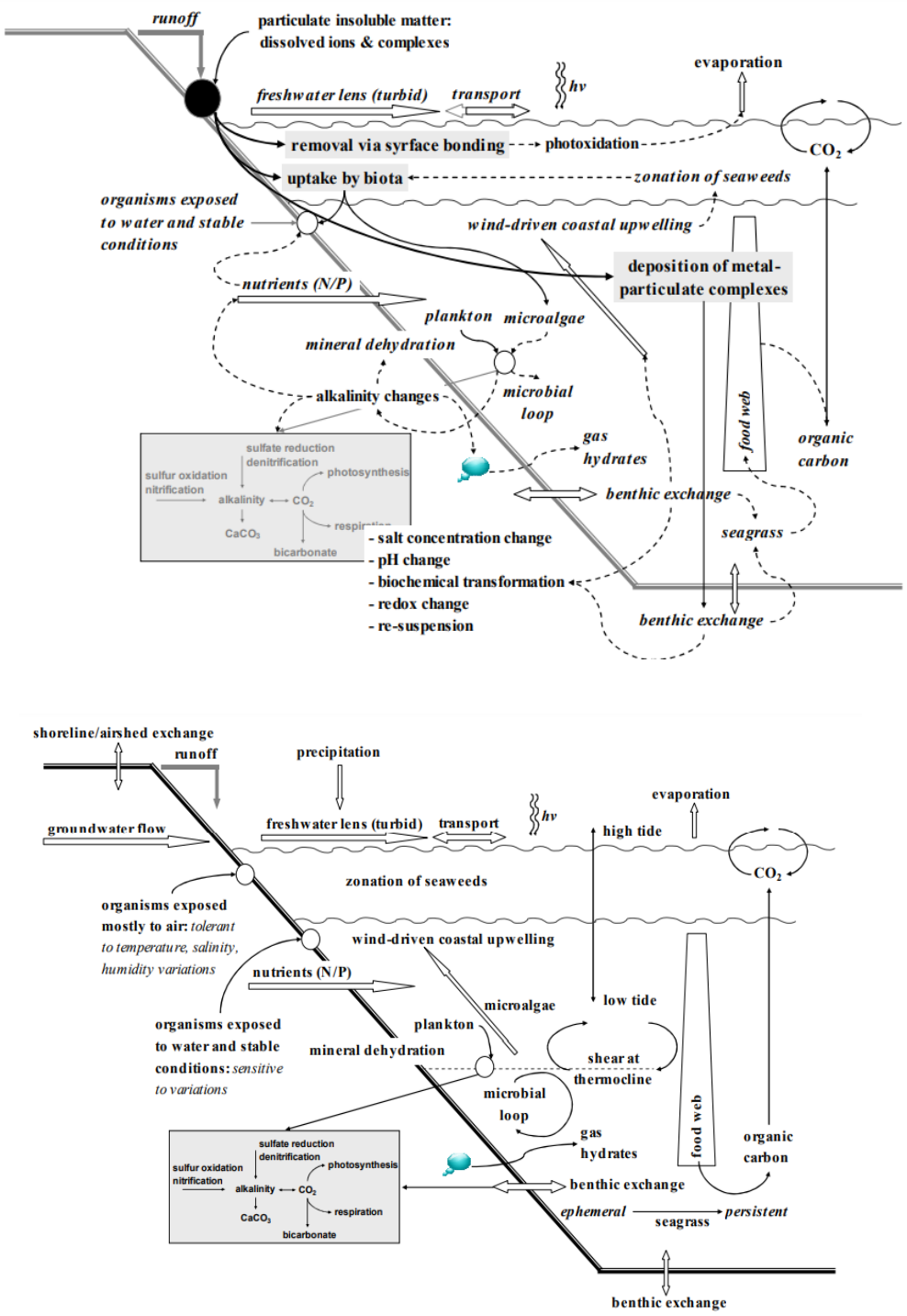

Figure 4. The functional model produced for the shoreline of the study area. (top) Overview of the ecosystem under usual inflow: benthic exchange produce ascends by the wind-driven coastal upwelling and through the food web. (bottom) Example of system shifting due to stress: the inflow of insoluble compounds has short-term effects at the meso-scale that propagate to the micro-scale, and medium-term effects on the macro-scale. The inflow is initially trapped in the turbid zone and partly removed by adsorption, photodegradation and evaporation. Vertical diffusion facilitates its uptake by biota below the low tide zone (plankton, algae, microbes), changing alkalinity that shifts ionization equilibria to modify energy production (box in grey), mineral dehydration, nutrient availability and gas hydrate

supply. Benthic exchange and re-suspension affect ephemeral and persistent sea grass species that transfer the impact to the upper levels of the food web. Coastal upwelling transfer the impact to the surface to affect seaweeds that trigger the cycle again. Primary mechanisms are shown with lines in bold, initial effects are indicated by straight lines, whereas dotted lines indicate the propagation of the adverse effects to other elements or scales.

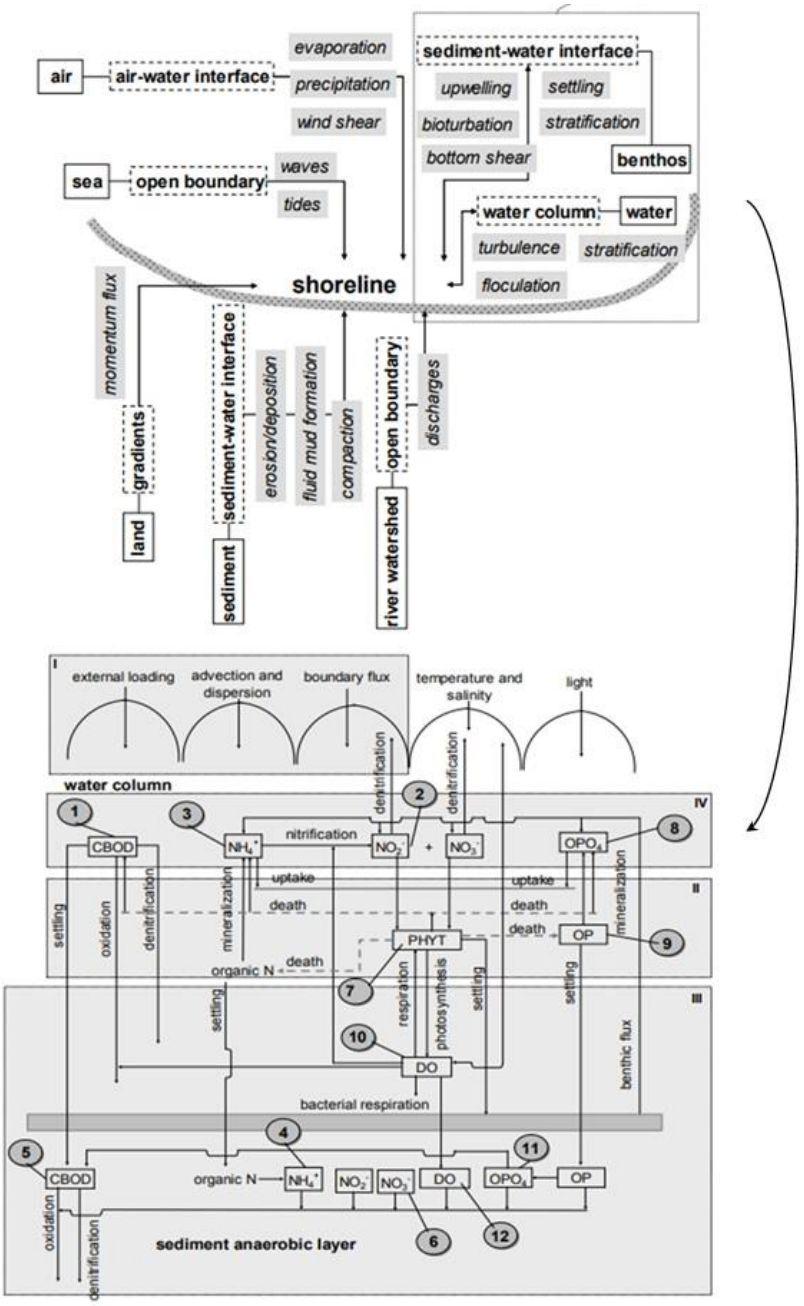

Figure 5. (top) Part of the physical model designed for the study area. (bottom) The ontological output for the benthos and water column systems that, actually, form a superstructure with nitrogen as input-output. Boxed items are the nodes with stronger links (i.e., higher in and out grades): DO (dissolved oxygen). PHYT (phytoplankton as carbon). CBOD (demand for biochemical oxygen in coal). NH_4^+ (ammonium nitrogen). NO_3^- / NO_2^- (nitrate and nitrite nitrogen). OPO_4 (ortho-phosphorus or inorganic

phosphorus). OP (organic phosphorus). Numbers inditate the nodes that represent the critical parameters to be monitored. Reprinted from Siontorou et al., Crit. Rev. Environ. Sci. Technol., 2017, under Thesis/Dissertation Reuse Request to Taylor & Francis.

Part of the ontological matrix produced in Phase 3 is shown in Fig. 5 (bottom). Using nitrogen as input, it describes the basic transformation process that includes photosynthesis, respiration, nitrification, uptake, benthic flux, denitrification, sediment suspension, and external loads, emphasizing on the water column and the anaerobic sediment layer.

In conclusion, the model developed for the Palaia Fokea and Legrena bay indicated that the critical stressors for site quality are: (a) nitrogen loading due to agricultural runoffs and fish farm effluents, and (b) sedimentary iron inputs, due to car disposal at sea. Both stressors affect seagrass populations that impact bacterial growth. These results agree with some recent studies for the quality of the area (Marbà *et al*., 2008, Papageorgiou *et al*., 2010).

2.3.2 Oil weathering at sea

Following the oil spill from the tanker Agia Zoni in the Saronic Gulf in September 2017, the model produced for the Palaia Fokea and Legrena shoreline has been re-visited in order to model the most likely degradation processes of oil constituents in the area.

Oil weathering is a multi-scale, complex process that involves physical, chemical and microbial processes occurring in parallel and/or sequentially, depending on abiotic parameters and local conditions (Balogun, 2021). Besides chemical activity, modelling has to consider the dominant physical processes and the biodegradation potential of the area. Fig. 6 presents part of the Phase 3 output, putting emphasis on the *in situ* degradation of polycyclic aromatic hydrocarbons (PAHs) contained in the oil slick. The ontological platform, provided the relevant partonomic relations to describe several processes co-occurring within a micro- or macro-region of the oil slick: inputs, fates, and effects.

PAHs may be formed as the oxidation product of C-20 to C-40 oil constituents, Oxidation of petroleum constituents, necessitating the estimation of kinetic parameters for both directions. The ontological platform used two levels of knowledge (upper and

lower) that communicate through the middle level hosting the most probable to occur chemical processes at the sea surface.

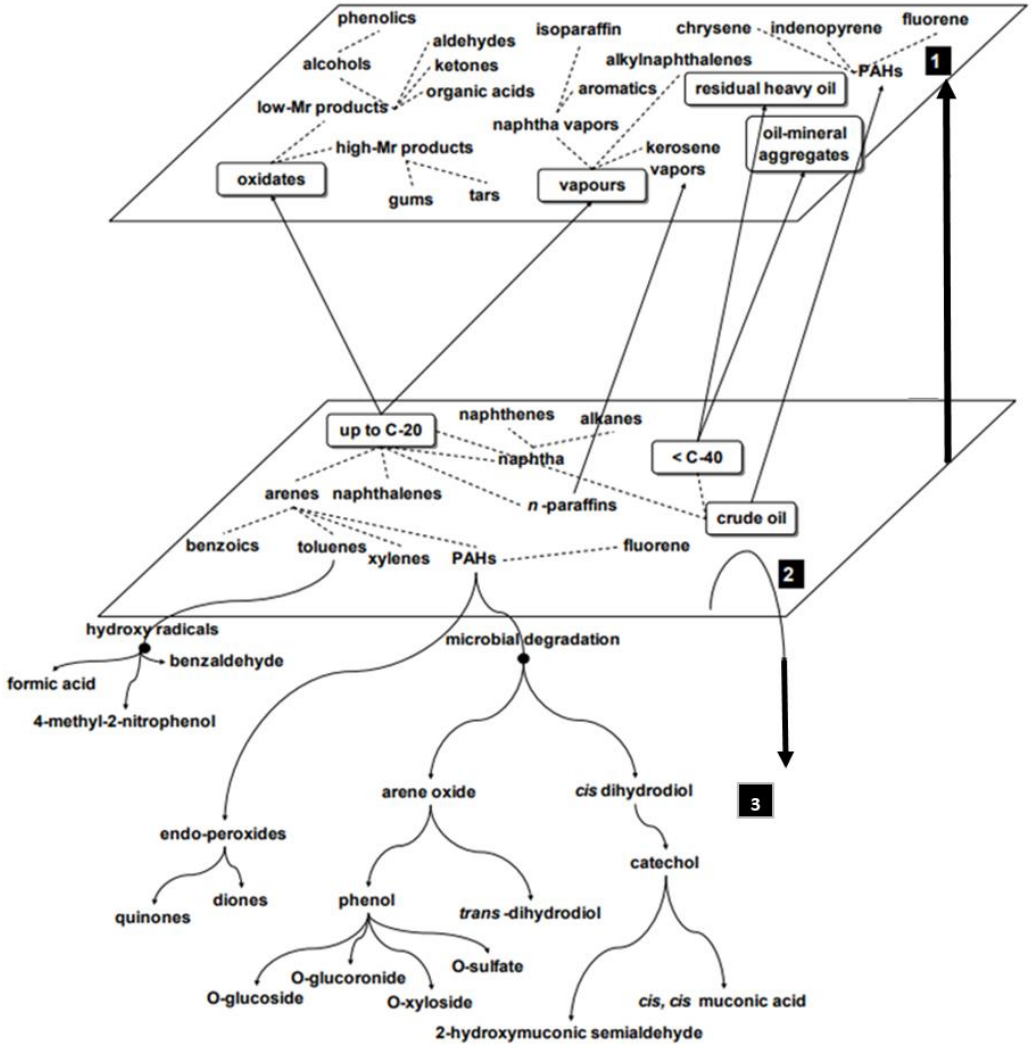

Figure 6. Schematic representation of the oil weathering ontology. Strait lines represent taxonomic (is-a) relations, whereas dotted lines indicate partonomic (part-of) relations. Level 1 includes chemical processes that are likely to occur due to the prevailing physical processes, level 2 shows the initial processes that occur at sea surface, and level 3 include biodegradation and photodegradation processes.

The interplay between physical, chemical, and biological processes lead to multi-scale weathering and transport model; when chemical processes dominate, weathering and diffusion is fast. These results agree with recent monitoring studies at the area that have detected, low levels of naphthalenes after the 8th day following the accident, possibly indicating that the primary mechanism was evaporation, trace nitrophenols at the 30th day after the accident, indicating some degree of photooxidation and increasing levels of biodegraded PAHs after the 85th day following the accident (Parinos *et al.*, 2019).

2.3.3 Lake sediment formation

The various implications of Phase I have been tested using a case of environmental quality parameters dependent upon the economic exploitation of ecosystem resources. For example, when a lake forms sediment under various physical or chemical processes, environmental and economic impacts may occur. Sapropel, for example, a salt derived from plant residues that accumulate in lake sediment, has a high value for agriculture and industry (Benkovitz *et al.*, 2020). The accumulation of sapropel at the bottom of the lake yields adverse effect long-term, reducing the capacity of the lake and its irrigation uses. The removal of sediment from the lake bed and its financial exploitation implies a net benefit. However, the extraction of sapropel from the lake sediment is currently a high-cost process with low efficiency. This scenario has been considered as a techno-economic trade-off at Phase I implementation.

If the total benefit is defined as B, then the maximum value of the periodic R_{opt} removal can be calculated by maximizing B: R_{opt} (R) = B_1(R) + B_2(R) where B_1 is the economic benefit and B_2 is the environmental benefit from sediment removal, due to sapropel marketing and lake preservation, respectively. The benefit B_1 is an increasing function of R and as operating costs are rising while capital costs decrease over time, the rate of increase of this function decreases. The benefit B_2 is a decreasing function of R and as the sediment is decreasing lake quality decreases, as well, the rate of decrease of this function increases over time. R_{opt} can be calculated as the abscissa of the B_{max} = (B_1 + B_2) max when MB_1 = MB_2, where MB_1=dB_1/dR and MB_2=$|dB_2/dR|$ are the marginal values of B_1 and B_2, respectively (Fig.7).

Any increase in the economic benefit, i.e., due to the improvement of the sediment processing methods, will shift B_1 upwards to B_1', leading to R_{opt} shifting to R_{opt} ', i.e., the same profits can be obtained at lower sediment removal.

The final result is dependent on several other variables and parameters that quantify the behavior of the whole system, such as the catchment area, the river entering the lake, the water coming out of the lake, water from other sources, irrigation water demand, sources of pollution or environmental policy-making through taxes and subsidies. Notwithstanding, the exploitation plans for aquatic ecosystems directly affect the critical quality parameters.

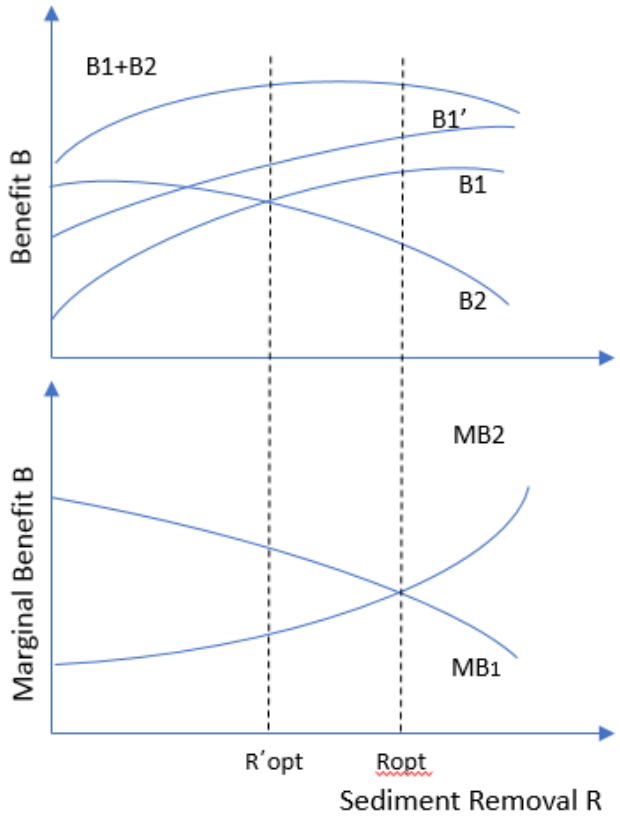

Figure 7. The dependence of sediment removal, R, on the economic benefit, B_1 and the environmental benefit, B_2. R_{opt} represents the optimal degree of removal. When the partial benefits shift, R_{opt} shifts, as well; for example, when the economic benefit increases R_{opt} shifts to lower values.

Recent data suggest that sapropel is of low significance of lake salinity, affecting brine concentrations with an extremely low rate; if removed, the impact of the geochemical processes triggered on the lake ecosystem might follow at higher rates (Simon *et al.*, 2017).

2.4. Concluding Remarks

The methodology developed for the modelling of aquatic ecosystems has been proven suitable for identifying critical quality parameters and constraints so as to support the design of metrological networks. In many cases, quality monitoring and assessment necessitate environment-specific measuring devices. In some cases, site-specific monitoring devices might be called for, especially when the critical parameters involve pollution degradation products or trace concentrations. The development of reliable environment- and site-specific biosensor devices is discussed in the following chapters.

3. Design criteria of the biosensor platform

3.1 Biosensors

3.1.1 The concept

Chemical sensing aims at extracting information relating to the chemical composition of any given sample, preferably continuously and rapidly (Luka *et al*., 2015). Sensors have two main parts: (i) a chemically sensitive layer, responsible for chemical detection, and (ii) the signal transducer that converts the chemical output into an electric signal. The amount and reliability of chemical information obtained depend on the analytical characteristics of the sensor. When the chemical sensitive layer is replaced with a biochemical one (Fig. 8), the device is called biosensor (Thévenot, 1999). The combination of biological systems with physicochemical transducers enables biosensors to convey natural analytics on a well-established technological platform.

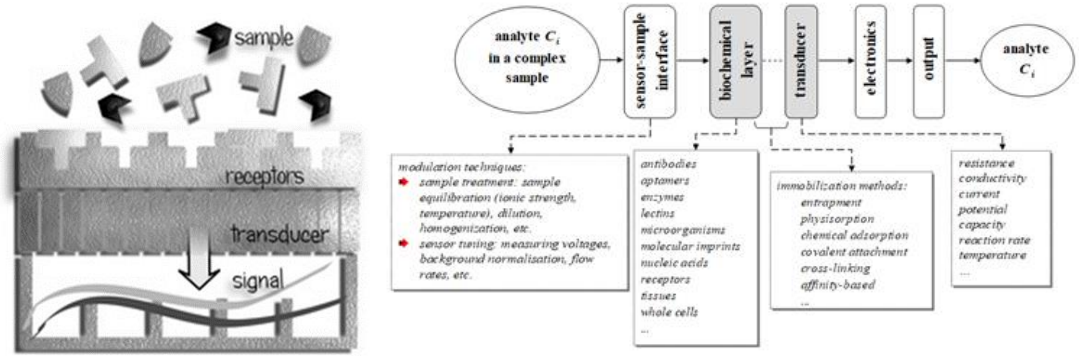

Figure 8. Schematic representation of a biosensor. (left) There are several substances in the sample but only one, the analyte, that can interact with the receptors. The bio-reaction is readily picked up by the transducer that generates a signal related to the concentration of the analyte in the sample. (right) Overview of the biosensor architecture, and commonly used materials, techniques and methods for device construction. Reprinted from Siontorou et al., Crit. Rev. Environ. Sci. Technol., 2017, under Thesis/Dissertation Reuse Request to Taylor & Francis.

The field of biosensors has progressed rapidly over the last decades. The market success of the glucose biosensor in the 1960s[1] created new scientific and commercial frontiers which are still expanding today. The latest research is focused towards (Zhai and Cheng, 2019):

[1] The first biosensor was demonstrated in 1962 to measure blood glucose using the Clark's electrode. In 1975, the YSI analyzer was launched, paving the way for the glucose meter.

- optimization of the biosensors stability: standardization of the integration of the biochemical system, development of nanosystems, sensor packaging and microfluidics
- design of market-ready systems: development of biosensors intended for niche applications where a competitive advantage exists, cost analysis of the construction process, scale-up of construction, quality control protocol development, integration of online system diagnostics.
- adsorption of technological progress: exploitation of quantum dots, use of nanotools and nanomaterials in existing biosensor platforms, 3D printing construction.
- expansion of potential applicability: development of drug delivery vehicles, pharmaceutical control assays, electrophysiology models, artificial sensory organs, energy harvesting, personalised health monitoring systems, clinical diagnostic imaging, etc.

The mechanism of sensing is similar to natural chemoreception (Siontorou *et al*., 2017): a biological system, e.g., enzyme, antibody, DNA, receptor, or cell, selectively interacts with the chemical moiety to be detected, which serves as substrate, antigen, adduct, ligand or metabolic substance, respectively, to produce a biochemical signal, i.e., a reaction product or changes induced by the reaction. The transducer translates this biochemical information into a signal that provides information about the chemical moiety to be detected.

The biorecognition system (bioelement) is immobilized on, i.e., is in close contact with, the transducer and the biological reaction takes place at the sensor's interface with the sample (Fig. 8). The most commonly used biorecognition processes are bio-catalysis (enzyme formats) and bio-affinity (immunological formats). Detection can be direct, i.e., the transducer monitors the reaction that the analyte participates in, or indirect, i.e., the analyte reaction triggers a cascade of reactions that produce the measurand moiety. Indirect detection is used for signal amplification purposes in order to lower detection limits or for improving selectivity and sensitivity (Siontorou and Batzias, 2014a). While the use of natural bioelements remains within the research focus, many biomimicking or bioinspired materials have been proposed, such as molecularly imprinted polymers, aptamers, biohybrids and stimuli-responsive polymers (Clegg *et al.*, 2019) with a view to impart more target-specific properties or improve device ruggedness.

Enzyme systems offer adequate selectivity, fast kinetics and rapid assays to handle single analytes in various samples, while receptors can be used for multiple analytes or toxic compounds (Siontorou *et al.*, 2017). Immunochemical systems are generally slower and cumbersome but mostly preferred in clinical applications (Bhalla *et al.*, 2016). DNA biosensors are more expensive but yield better interrogation platforms (Kavita, 2017). Biomimicking materials tend to be more target-specific but the full range of nature's capability has not been demonstrated yet (Clegg *et al.*, 2019).

Effective conversion of the biological recognition event into an analytical signal is essential for sensing. Common transducers are piezoelectric, thermal, magnetic, electrochemical, or optical, although hybrid systems may be used to optimize signals by combining phenomena (Bhalla *et al.*, 2016); fluorescence, for example, can be handled by electrochemical and optical transducers. Electrochemical systems are mostly preferred due to their simplicity, low cost, miniaturability and well-established protocols (Grieshaber *et al.*, 2008). Moreover, since natural chemoreception involves some kind of electron exchange, electrochemistry is the most relevant and direct means for structuring biomimicking platforms.

Biochemical reactions typically generate a measurable current (amperometric biosensors), potential or charge accumulation (potentiometric biosensors), or alteration of medium conductance (conductometric biosensors) (Grieshaber *et al*., 2008). The close proximity of the bioelement to the transducer surface renders electrodes, as per materials, dimensions, surface modulation, and geometry, critical to detection. Electrochemical sensing utilizes two-electrode systems, i.e., a reference electrode and a working electrode, or an auxiliary electrode may be added for three-electrode systems (Fig. 9). Electrodes are made of conductive and chemically stable materials, such as silver wires with a silver chloride coating (Ag/AgCl), carbon-based or zink-based nanomaterials, composites, polymers, etc. Compared to metals, composites, and polymers, nanomaterials are more susceptible to external stimuli owing to their higher surface-to-volume ratio and they generally yield devices with extremely low detection limits (Barry and O' Riordan, 2015).

At a variety of combinations between biomaterials and transducers, commercial biosensor systems (Fig. 10) are used for clinical, food and environmental analysis, as well as for biothreat assessment (Bahadir and Sezgintürk, 2015).

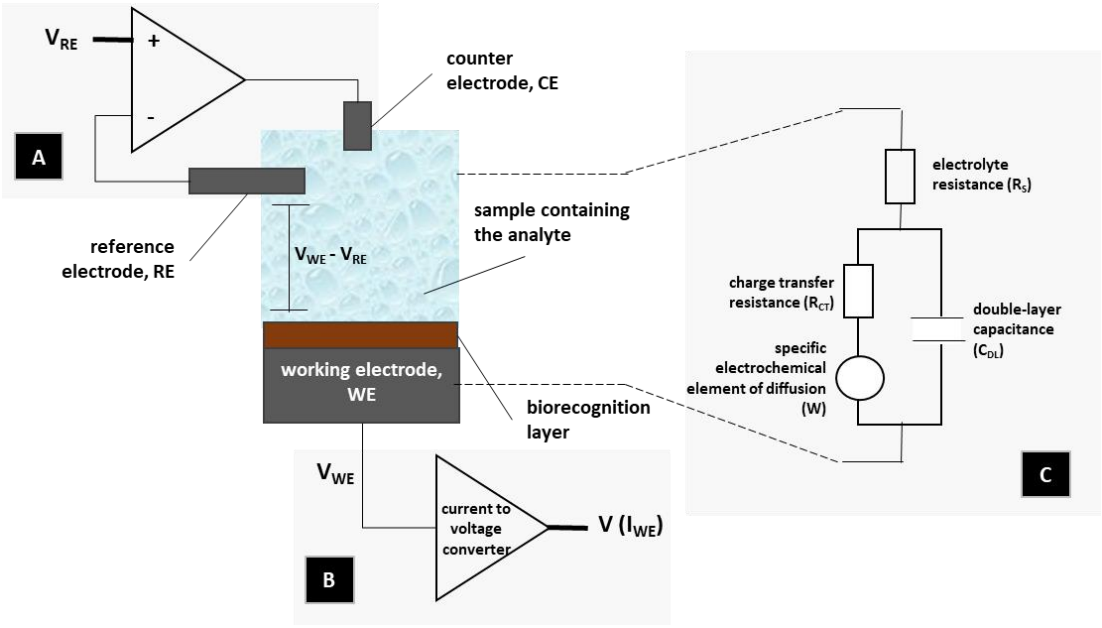

Figure 9. Overview of an electrochemical three-electrode biosensor. The biorecognition events occur at the surface of the working electrode. Panel A shows the control circuitry and panel B the measurement circuitry. The biochemical reaction leads to charge displacement, accumulation or transport that alter the potential between the reference and the working electrode, which is converted to an electric signal. The electrochemical cell can be modelled with the Randles equivalent circuit (panel C), where the biorecognition layer plays the role of a capacitor and its interface with the transducer depends on charge transfer and diffusion. In effect, the bioelement-transducer interface is a voltage-responsive surface. Not drawn in scale.

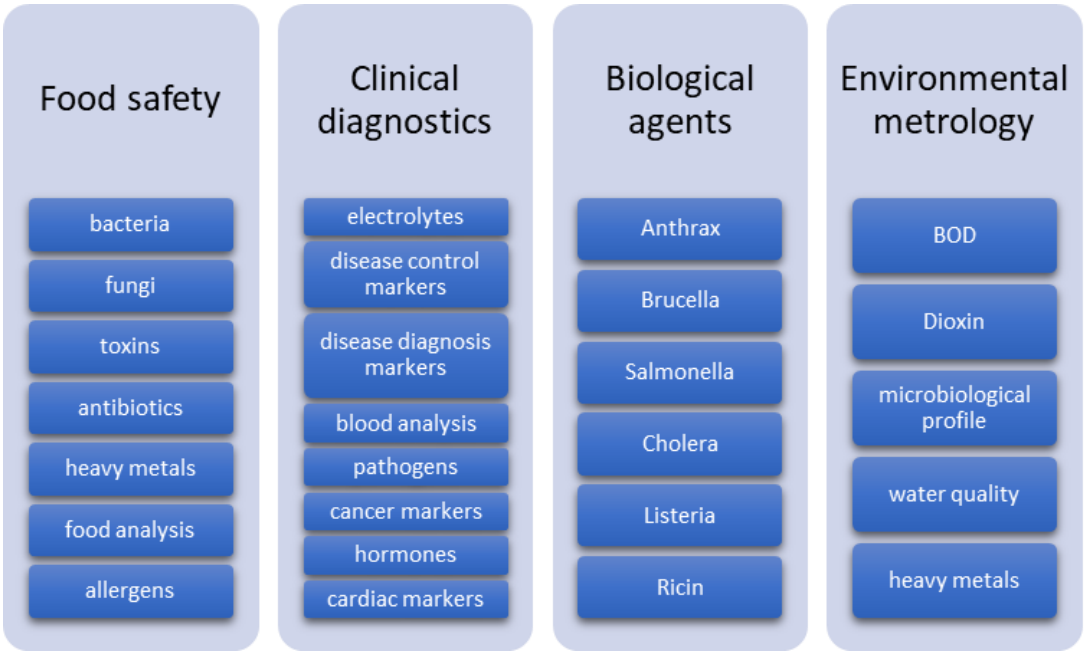

Figure 10. Commercial biosensor systems and their applications.

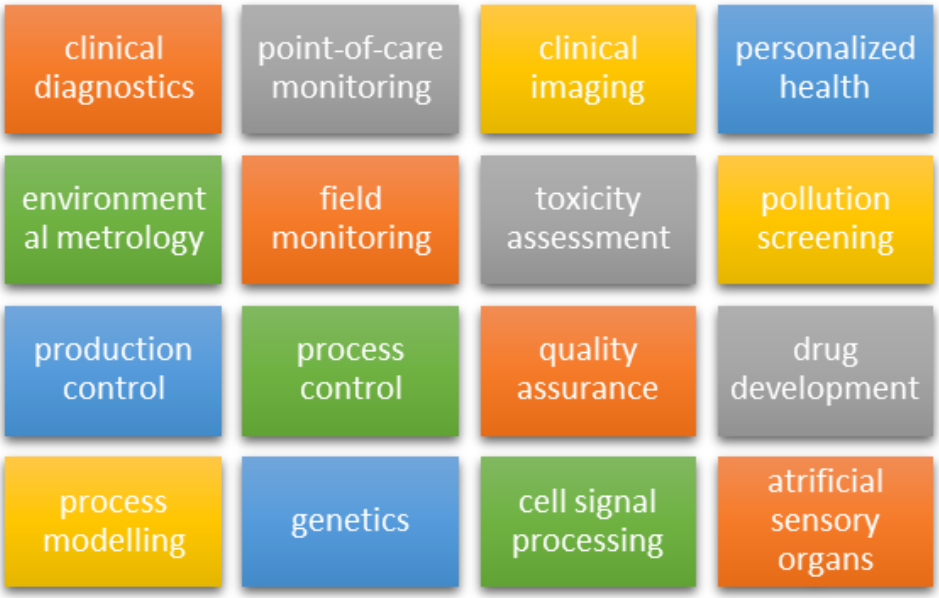

Figure 11. Research trends in biosensing.

Biosensor research (Fig. 11) expands the applicability potential by rapidly adopting the emerging technology to address the ever-increasing number of analytes and samples, the ever-decreasing detection limits required, the interest in telemetry and the need for size reduction (Olson and Bae, 2019).

3.1.2 The features

In each measuring system, criteria need to be established for describing the operation of the system, for evaluating the performance of the system and for comparing this performance to other measuring systems. A biosensor measuring system can be described by its analytical parameters: (a) the calibration curve, yielding a workable relation between the response of the system and the concentration of the analyte (Stoytcheva *et al*., 2009), (b) the linear range, defined as the analyte concentration range where the change in the response of the system is directly proportional to the change in analyte concentration (Mohanty and Kougianos, 2006); for reliable and accurate measurements, a broad linear range (greater than two orders of magnitude) is required, otherwise, signal processing techniques should be used (Justino *et al.*, 2017), (c) the sensitivity, calculated from the slope of the calibration curve in the linear range and defined as the proportion of change in the response of the system when the concentration of the analyte increases by a unit degree; sensitivity is largely dependent upon transduction, the analyte diffusion towards the bioelement and the affinity of the

bioelement for the analyte (Grieshaber *et al.*, 2008), (d) the detection limit, characterized as the lowest analyte concentration that can be reliably determined, calculated as the analyte concentration that triggers a signal with a magnitude three times that of noise (i.e., the response of the system in the absence of the analyte); detection limit requirements depend on the intended use of the sensor and becomes critical when detecting extremely low analyte concentrations and/or at small sample volumes (Stoytcheva *et al*., 2009), and (e) selectivity, defined as the capability to reliably detect the analyte in complex matrices; it is usually stated as the maximum permissible concentration of potential inhibitors that cause a measurement error greater than 5% (10% in environmental samples) (Zhu *et al*., 2015).

Operational parameters characterize the function of the biosensor as a device and include stability, reproducibility, shelf lifetime and operational lifetime. Stability is linked to the ability of the device to retain its analytical and structural characteristics intact during the course of an assay (Stoytcheva *et al.*, 2009). It critically depends on the integration of the bioelement with the transducer and the mode of sensor operation; for example, flow-through systems tend to slowly detach the bioelement from the surface of the transducer, expressed as an electrode drift (Siontorou *et al.*, 2010). Biosensing entails a compromise between firm bioelement attachment, that adds to sensor stability, and unrestricted bioelement interaction with its environment and the analyte, that triggers and maximizes biorecognition events. The efficiency of natural chemoreception is based on fluid, loosely attached systems with the necessary degrees of freedom to sustain thermodynamic equilibria; the expression of this efficiency on a device has not been demonstrated yet on any biosensor system (Morales and Halpern, 2018). Cell biosensors are more promising, provided that culture control is adequate and a very sophisticated signal processing technique is used to discriminate cellular signaling (Siontorou and Batzias, 2014a). Sensor instability may be also caused by the inactivation (degradation or structural deformation) of the bioelement or by sensor fouling (Siontorou *et al*., 2010).

The term '*reproducibility'* is used to quantify both, the repeatability of measurements and the repeatability of the sensor construction process. A coefficient of variation (CV) less than 10% is considered acceptable for repeatability and accuracy of measurements (Chen *et al.*, 2020). The reproducibility of construction is evaluated by the analytical characteristics of a number of devices assembled within a given testing period in order

to ensure that the device behaves systematically within day timescale and between days and analysts. It should be emphasized that most publications deal with construction reproducibility on the basis of laboratory assembly protocols (Siontorou and Batzias, 2014b).

Shelf-lifetime refers to the period that the sensor retains its analytical characteristics at storage; bioelement stability is the limiting factor (Panjan *et al.*, 2017). Operational stability (otherwise called ruggedness) refers to the ability of the device to operate under working conditions and is defined by a fit-for-purpose design and validation, device assembly and packaging (Bahadir *et al.*, 2015). The stability under storage and the stability under operation are both critical characteristics of a biosensor, if commercialization is sought for.

3.2 Stimuli-responsive platforms

3.2.1 Bioinspired smart surfaces

Multifunctional intelligent surfaces are versatile and self-adjustable micro- and nanostructures (natural, semi-synthetic, or synthetic) that can detect and respond to changes in their surrounding environment (Motornov *et al*., 2010). The mechanism to generate a response mimics natural chemoreception: external stimuli induce changes that alter the physicochemical state of the surface to a degree adequate for recording this change. It should be noted that natural processes have been evolved through millennia to optimize the synergy between ordered architectures through genetic control and gene expression that yielded a signal transduction and amplification mechanism at such sophistication that it is too difficult to interpret even today. Each cellular recognition event relies on a surface that is altered by charge changes, phase transitions, ion flux, or potential gradients. Although the event *per se* can be easily simulated on an artificial surface, the underlying entropy cannot (Siontorou and Georgopoulos, 2014). In any natural system, ion transport is controlled by diffusion, molecular mobility has to overcome viscosity and the surface moves towards the sample. In any artificial system, ion transport is controlled by bulk flow, molecular mobility has to overcome inertia and the sample is pushed towards the surface.

Pre-assembly engineering (Ponzoni *et al.*, 2012) or post-assembly modulations (Mendes, 2008) are commonly used in order to construct an intelligent surface with an

adequate degree of functionality. The former involves a fit-for-purpose and customized design while the latter produces a generic platform that can be modified as the need arises. Notwithstanding, efficiency depends on the construction of carefully aligned responsive molecular blocks within a hierarchical architecture that ensures the propagation of the response to the macro-level. Control over processes at the molecular level is not easy, thus moieties that can self-assemble into ordered structures are a highly preferred class of materials (Weiss, 2008). Lipids can self-organize into thermodynamically stable ordered forms (micelles, liposomes, membranes) retaining enough fluidity to accommodate changes without critical perturbation of their structure. Their use in biosensor construction dates back to early 1970s and they have been extensively studied as lipid membrane biosensor platforms, although latest applications include drug delivery and regenerative medicine (Siontorou and Georgopoulos, 2014).

3.2.2 Lipid membrane platforms

A lipid membrane is fluid 2D nanoconstruct formed by at least two lipid sheets linked through non-covalent hydrophobic interactions (Gould, 2018). In two-layer formats (bilayer lipid membrane, BLM), the polar heads of the lipids are oriented towards the hydrophilic phase, whereas the non-polar tails face inwards to form a hydrophobic zone, through a thermodynamically driven interplay between van der Waals attraction and steric repulsive force (Siontorou, 2015). BLMs in suspension between two aqueous compartments have been demonstrated at a thickness of 2-5 nm to exhibit a 100 MΩ cm^2 resistance, 0. 5-0.8 μF/cm^2 capacitance and a few picoamperes (pA) transmembrane ion current[2] (Nikoleli *et al.*, 2019). Protein molecules can be physisorbed on the membrane surface retaining favorable 3D conformational rotation. The reaction between the protein on the membrane and an analyte on the membrane-electrolyte interface results in a change that is unavoidably transferred on the membrane surface, impacting the surface charge density, the dipolar potential, the molecular packing or the membrane fluidity (Siontorou, 2015); such an impact results in a transient or permanent perturbation of the lipid continuity that modifies the transmembrane ion flux, manifested as an ion current signal (Fig. 12).

[2] The first reconstituted bilayer has been described by Mueller, P; Rudin, D O; Tien, H I; Wescott, W C (1962). "Reconstitution of cell membrane structure in vitro and its transformation into an excitable system". Nature. 194 (4832): 979–980.

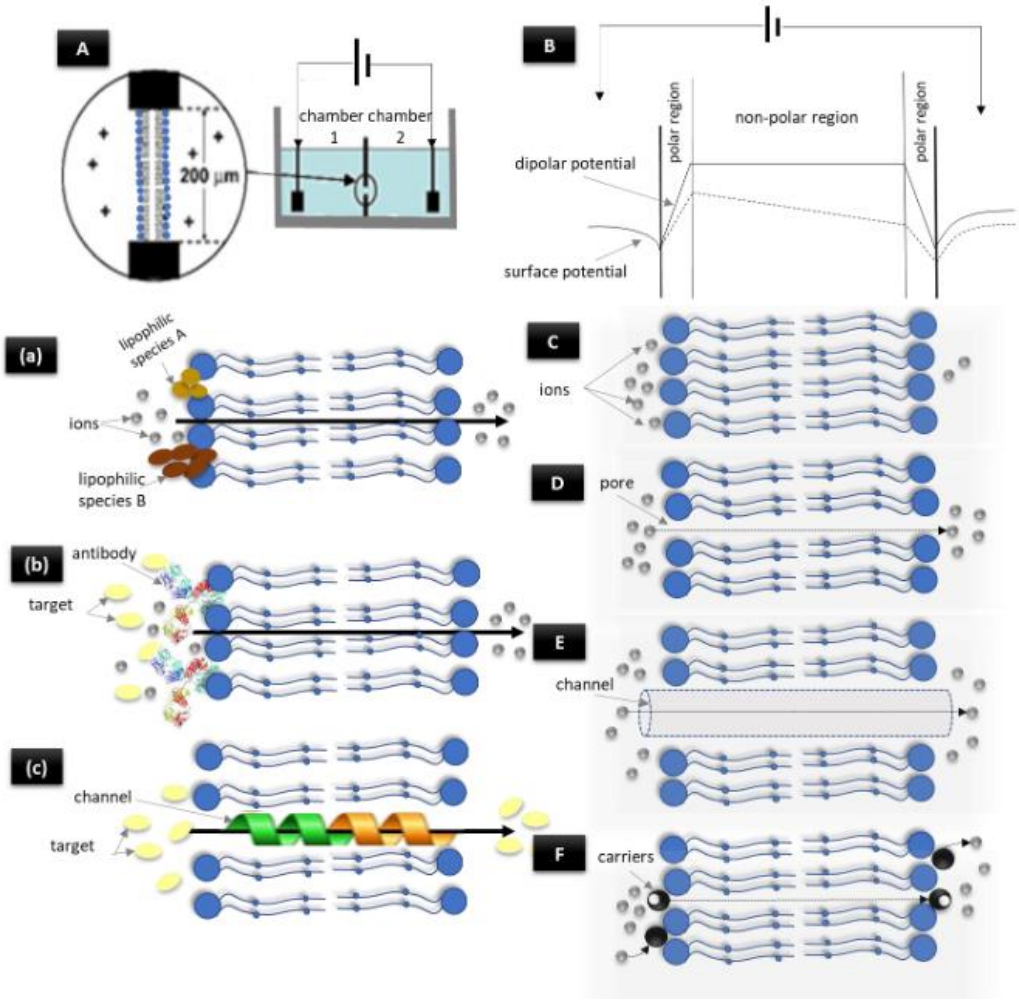

Figure 12. Protein-analyte and protein-lipid interactions of bilayer lipid membranes in suspension. (A) Experimental set-up. (B) Transmembrane potential profile. The lipid-based transduction and amplification may be due to ion flux through the membrane as the result of chemical gradient (C), pores induced by external voltage, charge density fluctuations or molecular perturbation(D), protein channels (E), or ion carriers (F). Lipid-protein interactions include alterations due to molecular aggregation and local perturbation (a), molecular packing and fluidity alterations due to immunocomplexation (b), or protein absorption in the hydrophobic zone. Not drawn in scale. Reprinted from Nikoleli et al., Appl. Sci., 2019, published from MDPI under an open access Creative Common CC BY license.

In effect, the lipid bilayer serves both, as an immobilization matrix for the bioelement and as a signal transduction and amplification system. Although remarkably responsive, the reconstituted membranes are extremely fragile and are currently used for electrophysiology modelling (Zakharian, 2013). To enhance stability, a variety of construction methods has been proposed, mostly involving the support of the bilayer on a surface (Fig. 13). Generally, self-assembly and metal supports produce rugged systems but the discriminatory capabilities are compromised (Siontorou, 2015).

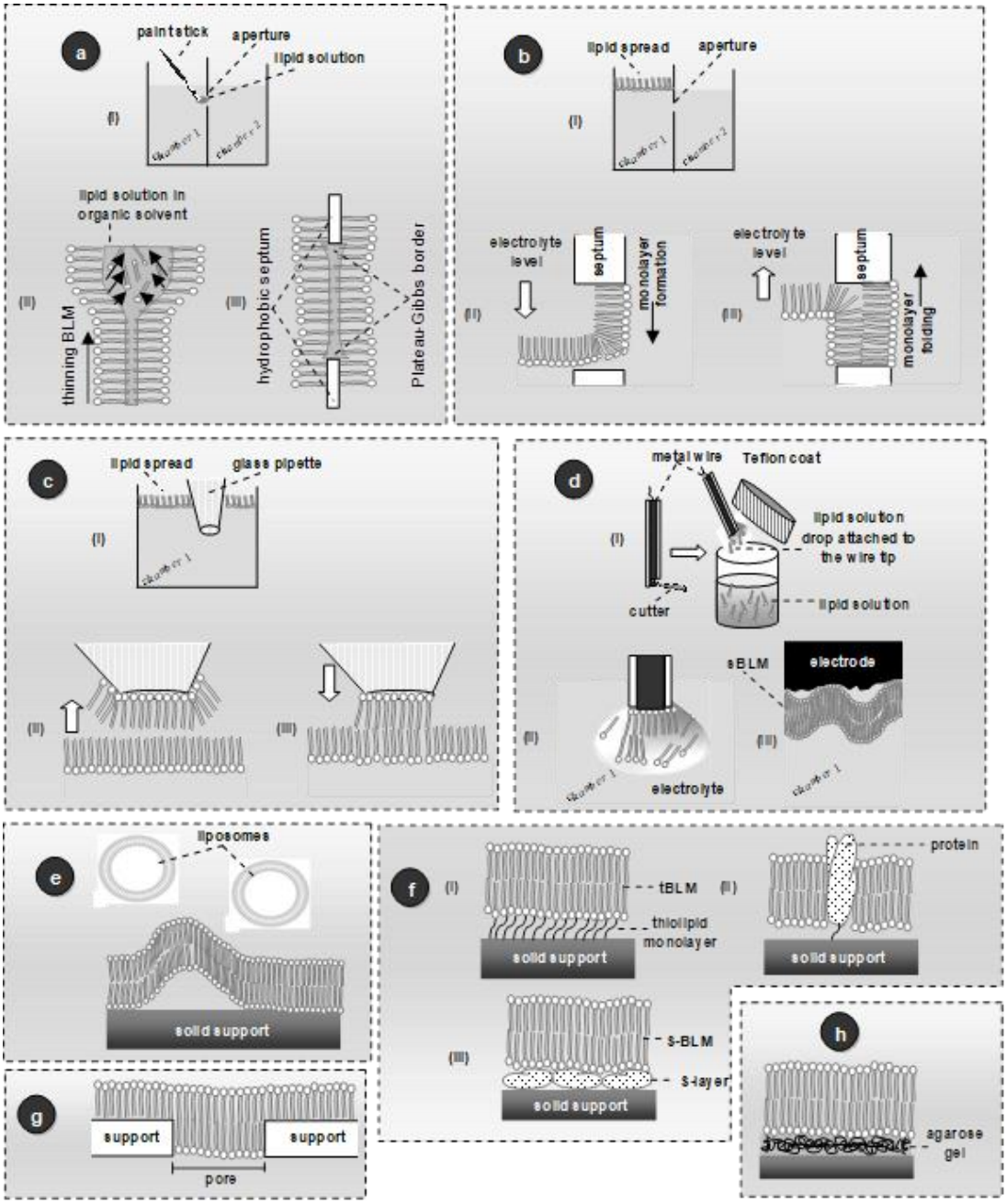

Figure 13. Bilayer lipid membrane construction methods: (a) Lipid painting: (i) lipids in organic solvent are painted on a mm-diameter aperture on a hydrophobic septum that separates two electrolyte chambers; (ii) as the solvent is pushed towards the rim of the aperture, lipids form two opposing layers that form the bilayer; (iii) the solvent forms a Plateau-Gibbs border that sustains the bilayer, (b) Monolayer folding: (i) when lipids are spread on electrolyte surface they spontaneously form a monolayer and the solvent evaporates; (ii) lowering the electrolyte below the aperture, the monolayer covers the aperture (iii) re-filling the chamber, forces the monolayer to fold into a bilayer, (c) Tip-dip: (i) lipids are spread on the surface of electrolyte to form a monolayer; (ii) the removal of the glass pipette forces the monolayer to attach on the tip; (iii) re-immersing the pipette, forces a second monolayer to attach on the first, (d) self-assembly on metal support: (i) the tip of wire is immersed in lipid solution; (ii) when transferred into electrolyte, a monolayer anchors onto the tip; (iii) gradually, a second monolayer is starting to form and the structures is reducing to a bilayer, (e) Vesicle fusion: when lipid vesicles are placed on a solid support, they rupture and spontaneously form a bilayer, (f) Tethering: (i) through thiolipids; (ii) through proteins;. (iii) through a proteinaceous surface (S-) layer lattice, (g) Supporting on micro-porous materials: bilayer membranes form on the spaces between the supports, (h) Gel-cushioning: gels support and hydrate the membrane. Not drawn in scale. Reprinted from Siontorou, Advanced Bioelectronic Materials, 2015, with permission from John Wiley and Sons.

Vesicle-induced bilayer formation is not easy to control but it allows for a large variety of bioelement integration methods and fine-tuning in responsivity (Oshima and Sumitomo, 2017). Tethering is more susceptible to customizations but as transmembrane ion flux is prohibited, only surface interrogation techniques may be used for signal transduction (Rebaud *et al.*, 2014).

The equivalent circuitry of these bilayer formats is shown in Fig. 14. Modelling is complicated in supported membranes or membrane arrays (Siontorou, 2015). Many techniques, such as Langmuir-Blodgett, screen printing, droplet interface, nanopatterning, or polymerization, have been proposed to guide the bilayer process or to produce multi-layer and diversified architectures. As control over process and ruggedness increases, the bioelement-lipid and lipid-lipid interactions are sub-optimized (Barry and O' Riordan, 2015). A very carefully managed trade-off exists between sensor development and sensor efficiency.

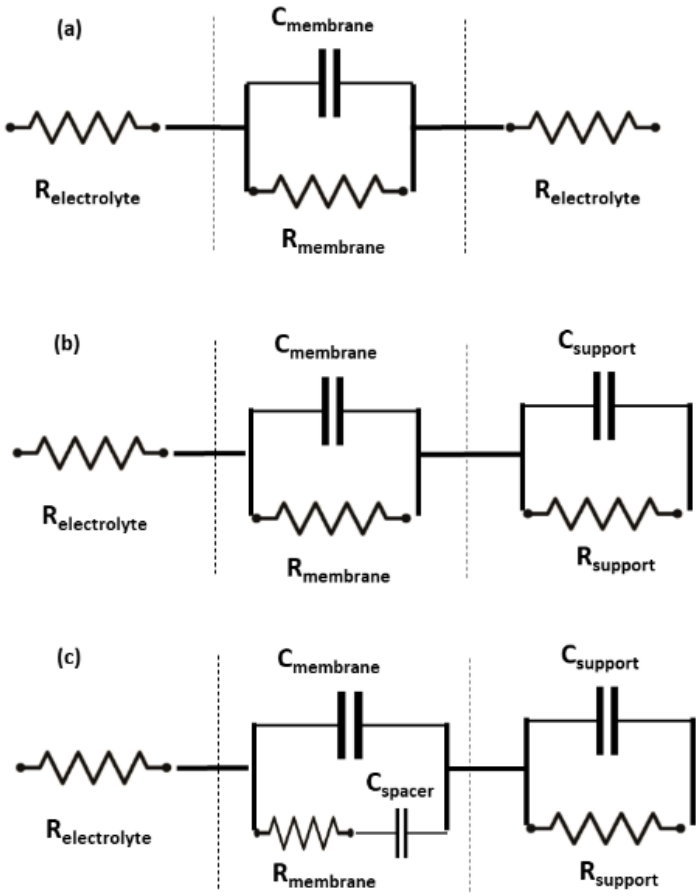

Figure 14. Equivalent circuitry for (a) a bilayer in suspension; (b) a bilayer floating on the electrode surface; (c) a bilayer anchored on the electrode surface through a spacer. In the latter case, spacer interferes with the membrane system. Reprinted from Nikoleli et al., Appl. Sci., 2019, published from MDPI under an open access Creative Common CC BY license.

A lipid layered construct spontaneously guides the orientation and thermodynamic stability of bioelements, prevents loss of biological function and integrity, and favors biomolecular interactions (Siontorou and Georgopoulos, 2014). Avoiding the cumbersome and multi-step schemes to involve crosslinkers and stabilizers, physisorption is an easy, one-step and straightforward means for constructing a biorecognition surface. The process is highly effective and reproducible but marginally controllable and nonamenable to precision engineering (Siontorou, 2015).

In platforms that use supported but suspended membranes, the bioelement may be simply added in the bulk electrolyte; high-magnitude transient signals appear, indicative of the adsorption of the bioelement on the membrane; these signals gradually decrease in magnitude and frequency to reach a stable background current within 10-20 min of bioelement addition (Nikolelis and Siontorou, 1995). The biorecognition complex retains its stability and functionality for flow rates up to 20 ml/min (Nikolelis and Siontorou, 1995), membrane phase shifting (Nikolelis and Siontorou, 1996) and temperatures up to 40 ^{o}C (Siontorou *et al*., 1998). The interaction between the bioelement and the analyte is recorded as picoampere (pA) transient (of ms duration) ion current changes, indicative of transmembrane ion flux alterations; i.e., at increasing ion current, pore formation allows more ions to cross the membrane, while in decreasing currents, the lipid molecules compress to hinder ion movement (Siontorou, 2015). Detection range is largely dependent upon bioelement loading: the more bioelements attach on the membrane surface the more analyte molecules can be detected; but there is a limit to the number of bioelements that a single membrane can host without collapsing.

A similar approach can be followed in metal-supported platforms, as well, but the background noise is higher, at the nanoampere (nA) range, and the behavior of the lipid-bioelement complex towards a biorecognition event differs (Siontorou *et al*., 1997). Although the self-assembly process traps an ultra-small quantity of electrolyte between the metal surface and the lipid monolayer, the bilayer faces uneven stresses between its two interfaces (the metal and the bulk electrolyte). Thus, any change in the membrane structure is rapidly expressed as changes in the elasticity modulus (Hianik, 2011). Further, as the electrolyte reservoir on one side of the membrane is not adequate to drive ion exchange, the analyte-bioelement interaction is manifested as permanent ion current increases. Detection range is largely dependent upon the biorecognition events:

the more analyses performed on the same sensor, the more the current is rising; practically, detection ends when the microampere (μA) level is reached.

3.2.3 Pre-assembly engineering and post-assembly modification

The properties of any membrane can be tuned, to a certain degree, by lipid composition, membrane microenvironment, biorecognition system and membrane support materials and geometry. The selection of lipids is critical to built-in membrane functionality and possibly signal amplification processes. The lipid-lipid interactions guide the molecular packing and fluidity of the membrane, as well as its electrochemical profile, mostly surface charge density and dipolar potential. Phosphatidyl choline (PC) yields fluid membranes with no discernable charge identity that work well with most surface proteins and most sample matrices (Siontorou, 2015). In complex biosensor formats, multilayered membranes or synthetic biorecognition arrays, electrostatic interactions between the membrane layers or the membrane and the bioelement can be achieved with the use of charged lipids (e.g., phosphatidyl serine, phosphatidyl inositol, phosphatidic acid, etc.). The ionic strength of the reconstitution electrolyte provides the necessary ions to support a transmembrane potential within a pH range, while membrane defects can regulate membrane surface electrochemistry (Hianik, 2011).

Preferably, the structural or electrochemical changes induced by the biolement-analyte interaction should be adequate to generate a measuring response. If not, considering that the device response (i.e., the signal) depends, more or less, upon pore formation, the membrane can be engineered to contain defect sites that would maximize poration. Voltage-induced poration has been utilized in the monitoring of gating phenomena (Rems *et al.*, 2020), and grafting-driven poration have been proposed for clinical application (Duan *et al.*, 2017). The formation of asymmetric membranes (Shukla *et al.*, 2019) or mixed lipid membranes (Sabirovas et al., 2020) can provide some degree of poration and has been proposed for signal amplification and decrease of detection levels. More mechanismic strategies include the guiding of some kind of charge accumulation at domains on the membrane surface and the use of lipid mixtures that can accommodate these accumulations as pores. For example, the incorporation of small amounts of the negatively charged dipalmitoyl phosphatidic acid (DPPA) in phosphatidyl choline membranes seeds nanodomains with negative charges that can attract positive ions from the bulk electrolyte to form aggregates on the surface of these

nanodomains (Nikoleli *et al*., 2019); the ion-lipid electrostatic interactions interrupt lipid-lipid interactions structuring pores that enhance transmembrane ion flux.

The selection of a suitable biorecognition system depends upon a plethora of criteria and conditions, involving the target analyte, the transduction system, the measurement requirements (i.e., detection limit, detection range, time of response, assay duration, working environment), and the sample matrix (Siontorou, 2015). In the case of discrimination between structurally similar compounds, sensor specifity can be mostly designed on antibody-antigen interactions (Kiani and Rahimpour, 2020), whereas receptors may require some prost-assembly manipulation to enhance resolution (Lang *et al.*, 2021). Enzyme substrates are used for robust environmental sensors (Nikoleli *et al*., 2019) and DNA strands may be more suitable for genetic targets (Aziz *et al*., 2021). The lipid membrane *per se* can be used for the detection of lipophilic compounds providing that partition coefficients are adequate to support detection in complex samples (Siontorou, 2015).

Electrode material and geometry also plays a role, especially in metal-supported platforms. In general, the thinner and smoother the metal surface the lower the detection limit but the higher the noise level (Saem *et al.*, 2020). A necessary compromise should be made between detectability and measurement reliability. The conducting properties of the support are also important for signal amplification, although only nanomaterials can yield a high response at low background noise (Siontorou *et al.*, 2016).

Post-assembly modifications are normally part of device optimization and usually follow a variety of approaches ranging from sophisticated analyte conjugation to simple manipulations of the membrane microenvironment. For example, gramicidin channels are routinely used to verify the bilayer membrane thickness but can serve as a bioelement as well for detecting the range of ions that can transport (ammonium, potassium, sodium, calcium and lithium, in ion selectivity order). Ammonium can be detected at a lithium-based electrolyte, whereas potassium monitoring requires the complexation of the other alkali metals in the sample (Nishio et al., 2020). Adjusting pH or temperature may also enhance the sensor's response, especially when chemical structures are pH- or temperature-susceptible (Matthews *et al*., 2021). These settings can be, also, used for counteracting matrix effects in complex samples (Siontorou et al., 1997). Sample flow rate can be also adjusted to minimize non-specific reactivity, provided that the flow rate values is adequate to support target-bioelement interaction

kinetics, high enough to prohibit non-specific interactions and low enough to retain the bioelement on the membrane surface (Nikolelis and Sontorou, 1996).

3.3 Environmental design

Designing for the environment poses a variety of challenges that should be carefully considered. Environmental samples are inherently extremely complex because the measurand concentration is largely unknown and hard to predict, especially when it accumulates, degrades or enters the ecosystem through numerous sources (Chen *et al.*, 2010). Further, sample matrix may contain a variety of non-target substances at a variety of concentrations that could alter assay results leading to over- or under-estimations of the analyte in the sample, or even to sensor fouling, especially when the matrix involves proteins (Martins *et al.*, 2011).

Typically, matrix effects are considered during device validation and not during device design, leading to the development of outstanding laboratory set-ups that failed to work with real environmental samples (Siontorou *et al.*, 2010). Evidently, detection in complex matrices renders sensor selectivity extremely important for counteracting sample effects (Siontorou *et al.*, 2017); biorecognition systems with extremely high specificity should be selected in order to decrease cross reactivity. Further, to successfully tackle non-specific interactions, very rugged sensing platforms should be developed. Post-validation with the standard analytical technique of evaluating recovery rates at spiked samples (laboratory prepared simulated matrices) may not be adequate to assess the suitability of the sensor for environmental applications; validation with spiked real environmental samples becomes indispensable.

The concentration range of the analyte in the ecosystem to be monitored may vary from trace to large levels (Siontorou *et al.*, 2017). No reliable biosensor can be designed for more than ten orders of magnitude, meaning that low concentrations and high concentrations should be detected with different devices and possibly different strategies. Alternatively, a low-to-medium concentration range sensor can be developed but, at higher analyte levels, the sample should be diluted before the assay (Siontorou and Georgopoulos, 2016). Further, non-aqueous samples, e.g., soil, cannot be assayed *as is* but require some kind of pre-treatment to produce aqueous extracts; that involves multiple dilutions that lower the analyte concentration in the assay sample. Taken sample dilution under consideration, the detection limit of the sensor becomes critical.

Commonly, environmental biosensors report low detectability during device development, but when applied to real environmental samples, detectability rises at least 10 times (Siontorou and Georgopoulos, 2016).

It has long been accepted that site-specific monitoring rises the need for developing customized sensors (Hanrahan *et al.*, 2004). Designing a flexible platform that can be quickly converted to a variety of different sensors by simply assembling different biorecognition systems on the platform and tuning accordingly the bioelement-platform interface is feasible using lipid membrane technology (Siontorou, 2015). Notwithstanding, designing for the environment presupposes a basis for engineering towards either the design of one system capable of a very large number of assays and a long operational lifetime or the design of a system capable of a limited number of assays (even single-shot device), easily replicated for multiple sensor parallel construction (horizontal scale-up), each with a long storage lifetime. The biology of the device may perplex decisions, since biorecognition systems, unless synthetic, exhibit an operational lifetime shorter than that of the sensor components, thus preventing the design of a multiple-assay system. Switching to limited-shot devices, the storage conditions that biology requires may not be compatible with the optimal conditions for the sensor components. A feasible alternative may be the design of a quick and simple device assembly prior to operation.

In situ monitoring presents an additional set of requirements, related to the autonomy of field devices, e.g., power supply, auto-calibration, online fault diagnostics, etc. (Budi *et al.*, 2018), issues concerning data collection and processing, e.g., signal transmission, wireless networking, etc. (Martins *et al*., 2011), the ability of devices to operate without supervision in an ever-changing environment, e.g., temperature changes between day and night, wind disturbances, precipitation levels, flora development, nuisance from small animals, etc. (Hesse *et al*., 2008), as well as, small sample volumes and high sample throughput capabilities (Siontorou *et al*., 2017). Further, network design should take into consideration the reliability of the measurements, which inevitably draws for redundancy; especially in monitoring remote and inaccessible areas, false positive signals may pose a more serious problem than false negative ones. In effect, reliability and sensitivity should be re-defined in *in situ* monitoring (Batzias *et al*., 2011). In analytical terms, reliability is the measure of the ability of a detection system to produce accurate decisions about the possible existence of an alarming state. In operability

terms, reliability is measured by the probability of detecting an alarming state, given that such a state does not exist; a system is reliable if that probability is low, i.e., if the measuring system consistently detects actual alarming states without generating incorrect signals. Likewise, sensitivity is re-defined as the extent of the alarming state that a system is capable of detecting and the time required for the system to issue a corresponding signal.

Considering the cost of the device, some issues may be raised regarding materials, construction and assembly processes, device performance and competitiveness over alternative instrumentation (Siontorou and Batzias, 2014b). Thus, designing for the environment, possibly with a view to marketing, necessitates techno-economic evaluations and trade-offs based on niche applicability, either on analyte targeting or on analytical performance, in order to gain a competitive advantage.

3.4 Concluding remarks

In view of the above, the critical points to consider when designing for site-specific applicability (Fig. 15), certainly go beyond the typical analytical development and validation protocols. Evidently, biosensor development should adapt to engineering processes for producing science-driven, technology-based and market-in-view devices.

Figure 15. Design criteria for environmental-relevant and site-specific biosensors for monitoring aquatic ecosystems.

4. Materials and methods

4.1 Materials and reagents

Lipid membranes have been formed using egg phosphatidyl choline (egg PC Type XVI-E) and dipalmitoyl phosphatidyl choline (C16:0) (DPPC), both purchased from Sigma-Aldrich and stored at -20 ^{o}C. Lipid solutions could be kept refrigerated (0-4 ^{o}C) for up to 2 months. The lipid mix solution for the preparation of polymerized membranes contained also methacrylic acid (Aldrich-Chemie), ethylene glycol dimethacrylate (Aldrich-Chemie), and 2,20-azobis-(2-methylpropionitrile) (AIBN) (Merck), used without further purification.

Teflon coated silver wires (diameters of 0.1, 0.25, 0.5 and 1.0 mm from Sigma) and glass microfiber filters (with nominal pore sizes 0.7 and 1.0 mm from Whatmam Scientific Ltd) were used as lipid membrane supports. ZnO nanowall and graphene electrodes have been synthesized and assembled *ad hoc*.

The biorecognition systems used herein included peroxidase (type XII from horseradish, 1.7 mg solid, Sigma-Aldrich), tyrosinase from mushroom (polyphenol oxidase, E.C.1.14.18.1, 5370 U/mg, Sigma), bovine methemoglobin (Sigma-Aldrich) and cholesterol oxidase (EC 1.1.3.6, 28 U/mg, Sigma-Aldrich). All bioelements have been diluted/reconstituted in buffer to obtain stock solutions, except from cholesterol oxidase that was diluted with 10 mM of tris-HCl buffer solution. When not in use, stock solutions were kept refrigerated (4–8 ^{o}C).

The chemicals used were of analytical-reagent grade apart from peroxide solution 3% m/m (commercial grade) and high purity phenol (Fluka >99.5%). Catechol has been obtained from Sigma. Nitrite standard solutions were prepared from the dilution of 0.015 g of $NaNO_2$, dried for 4 h at 105 ^{o}C. The cholesterol stock solution was prepared in water (50 mL) containing 2% (v/v) 2-propanol and 2% (v/v) Triton X-100 in a bath at 60 ^{o}C to avoid precipitation.

Electrolyte solutions were prepared from KCl and HEPES (N-2-hydroxyethyl-piperazine-N´-2-ethanosulfonic acid); equimolar concentrations (0.05 M) of KH_2PO_4 and Na_2HPO_4, in NaCl (0.9% m/v) electrolyte, were mixed together to prepare phosphate-buffered solutions (PBS).

Water used was either distilled through a filtering system or purified by passage through a Milli-Q cartridge filtering system (Milli-Q, Millipore, El Paso, TX, USA).

4.2 Apparatus

The electrochemical set-up used for the metal-supported biosensors described herein is presented in Fig. 16. A two-electrode configuration system was assembled, i.e., a sensing wire hosting the lipid membrane/bioelement complex on its tip immersed in electrolyte and a reference Ag/AgCl electrode. A power source (SourceMeter® KEITHLEY 2400) supplied a 25 mV DC potential and the current between the sensing and the reference electrodes was measured with an electrometer (System Electrometer KEITHLEY 6514) that also served as a current-to-voltage converter. For potentiometric systems, the reference electrode was connected to a potentiometric transducer and detection was based on the redox potential caused by oxygen/hydrogen peroxide ratio shifts. LabVIEW (National Instruments Co., Austin, TX, USA) properly customized for small currents was used to store and process signal data. All experiments were performed at 25 ± 1 ºC.

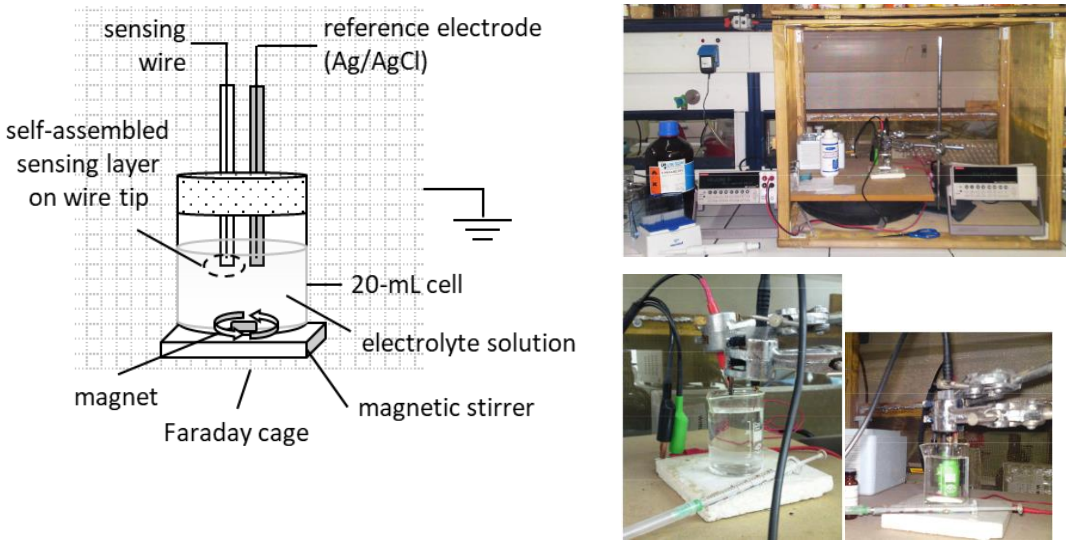

Figure 16. (left) Overview of the electrochemical set-up for metal-supported biosensors. The sensing wire is connected to the power supply source and the reference electrode to the electrometer; the applied potential at the sensing electrode is positive relative to ground. The electrochemical cell and electronic equipment are placed in a grounded Faraday cage. Not drawn in scale. (right) The bench-scale system in the Laboratory of Simulation of Industrial Processes.

4.3 Lipid membrane construction and bioelement attachment

Metal-supported lipid membranes were constructed from a stock lipid solution of 2.5 mg/mL (in 80% v/v n-hexane and 20% v/v absolute ethanol), as previously described (Siontorou *et al*., 1997; 1998): the sensing wire was tipped just before its immersion in the lipid solution (Fig. 17a); upon removal, a small drop of lipids remained attached on the tip (Fig. 17b); the wire was subsequently immersed in the electrolyte solution (Fig. 17c) and a 25 mV voltage was applied between the electrodes.

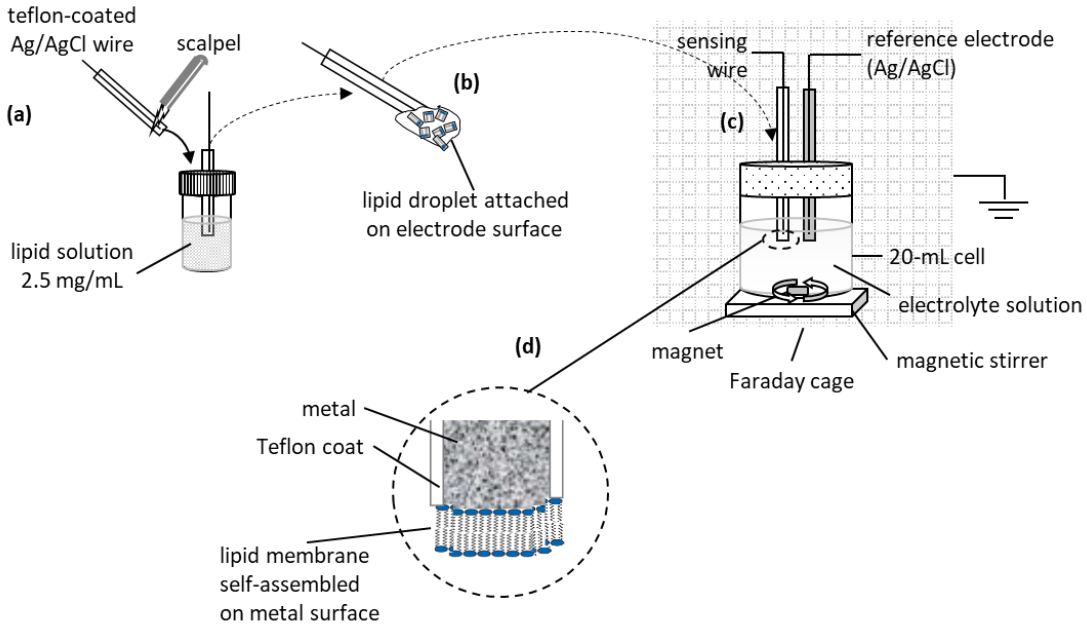

Figure 17. Simplified diagram of the construction of metal-supported lipid membrane biosensors. The sensing wire is tipped and immediately dipped in the lipid solution (a). When transferred into the electrolyte solution (b), the self-assembly process is initiated at the metal-electrolyte interface. The lipids spontaneously organize into a micellar formation, orienting their polar heads tangent to the metal surface in order to securely place their hydrophobic tails inwards. The micellar formation thins due to electrostatic interactions to multi-layer formats, that finally degrade into a lipid bilayer (d). Not drawn in scale. Adapted from Fig. 1 in Siontorou and Georgopoulos, J. Clean. Prod., 2016.

The lipid self-assembly process could be monitoring through current stabilization (Fig. 18); a steady background current of ca. 1 nA could be reached within ca. 10-15 min for a simple PC membrane on a 0.5 mm silver wire; slightly longer stabilization times (ca. 20 min) have been observed with thinner wires or mixed-lipid membranes.

The immobilization of the bioelement on the lipid membrane surface could be performed by adding the bioelement in the electrolyte solution after membrane formation under mild stirring. Physisorption being a slow process, a stable background current could be reached within 10-20 min, depending on the bioelement (Fig. 19);

usually, as the size and polarity increase, the required stabilization time for the conjugate increases. Owing to the steric hindrance displaying on the lipid-electrolyte interface by the voluminous protein moiety, the immobilization of the biolement raised background currents ten-fold. Alternatively, the bioelement could be added in the lipid mixture prior to membrane formation, so that immobilization could occur during the self-assembly process. As observed, current stabilization required > 45 min, the background current was much higher (20-25 nA) and sensor reproducibility (as indicated by the sensor's response towards a given analyte concentration) decreased by 42%.

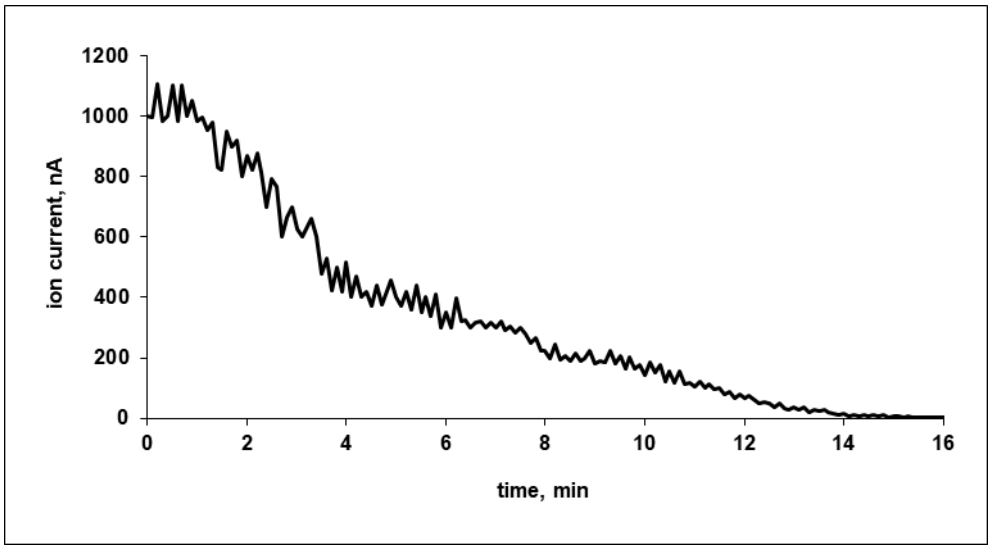

Figure 18. Recording showing the stabilization of the lipid membrane (from phosphatidyl choline) on 0.5 mm Teflon coated silver wire (0.1 M KCl with HEPES, pH 6.5) at 25 ºC under stirring.

The polymerized membranes have been prepared according to established techniques (Nikolelis *et al.*, 2006;2008). UV irradiation or thermal polymerization could be used. Briefly, dipalmitoyl phosphatidyl choline (5 mg) was mixed with methylacrylic acid (0.070 ml), ethylene glycol dimethacrylate (0.8 ml), 2,2-azobis-2-methylpropionitrile (8 mg) and acetonitrile (1.0 ml). Following nitrogen spurging for 1 hour and 30 min sonication, the lipid membrane forming mixture could be kept refrigerated (0-4 ºC) for up to 6 months. An aliquot of this mixture (0.15 ml) was spread on the glass fiber microfilter and irradiated using the UV deuterium lamp for 4 h. Alternatively, thermal polymerization was performed at 80 °C for 16 h.

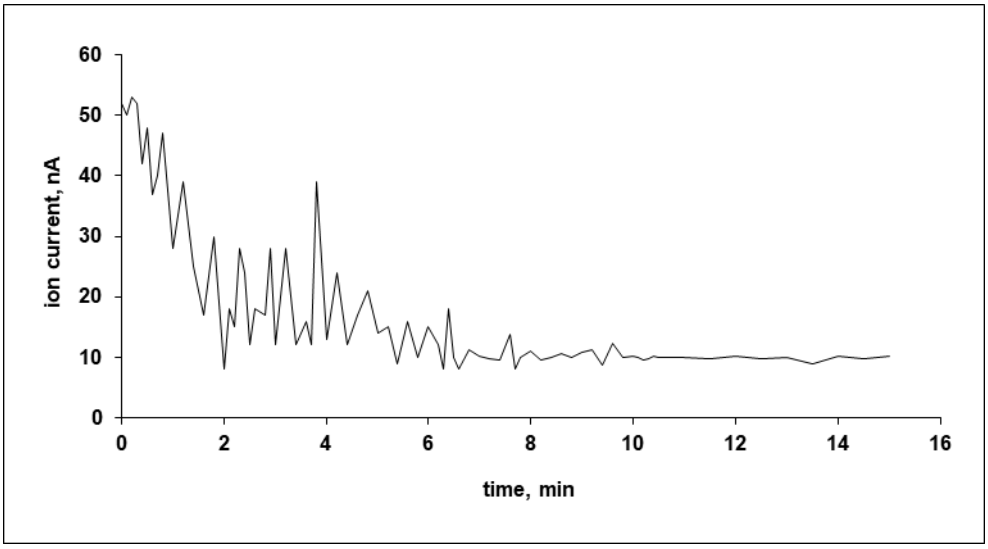

Figure 19. Recording showing the stabilization of the lipid membrane (from phosphatidyl choline) on 0.5 mm Teflon coated silver wire (0.1 M KCl with HEPES, pH 6.5, 25 ^{o}C) after the addition of methemoglobin (20 μL of a 10 mg/mL stock solution) in the bulk electrolyte under stirring.

The bioelement was spread on the microfilter immediately after the addition of lipid membrane forming mixture so that polymerization and immobilization occur at one step. If the bioelement was not temperature sensitive, thermal polymerization could be also used, yielding comparable results.

Following the sonochemical method (Nayak *et al*. 2012), zinc nitrate hexahydrate ($Zn(NO_3)_26H_2O$) and hexamethylenamine ($C_6H_{12}N_4$), at equimolar concentrations (50mM), were dropped on 1cm^2 aluminium foil. The nanowalls could be collected using the scotch tape method. Graphene nanoelectrodes were prepared using a graphene dispersion of 0.4 mg/ml in N-methyl-pyrrolidone, homogenized by mild sonication for 180 h and centrifuged at 700 rpm for 2 h (Nikoleli *et al*., 2012). The nanostructures were transferred on a 0.25 mm copper wire and the solvent was allowed to evaporate. The filter-membrane-bioelement was placed on the nanoelectrode to conclude sensor construction.

All metal-supported biosensors described herein have been constructed and validated in the Laboratory of Simulation of Industrial Processes of the Department of Industrial Management and Technology at the University of Piraeus. Nanosensors have been constructed and validated in the Laboratory of Environmental Chemistry of the Department of Chemistry at the National and Kapodistrian University of Athens.

4.4 Treatment of environmental samples

Lake samples have been collected from Koumoundourou Lake (Attiki, Greece) and used without further treatment. Soil and sediment samples have been simulated using AgroMAT Ag-2 standard (sandy soil) containing 15-22 ppm phosphorus, 79-88 ppm potassium, 2.5-3.2 % m/m organic matter, 5 ppm nitrates, <400 ppm divalent cations and a pH value of 5.7 (SCP Science, QC, CA). Real soil samples were collected from a field in a small mountainous settlement of Northern Greece (Ioannina Prefecture: 3941'29.040"N; 212'17.880"E; 750 m altitude; 982 mm mean annual precipitation). Soil samples (simulated and real) were treated according to the following: after left overnight at room temperature, the samples were dried at 105 ^{o}C for 4 h; dried soil was mixed with 2 M KCl (10 ml for every mg of sample), gently shaken, and filtered through pre-washed filters (Whatman filter paper No. 42, Whatman, UK). Soil extracts were immediately analyzed.

Matrix effects for aqueous environmental samples have been simulated using solutions of varying compositions between anions (carbonates, nitrates, chloride, sulfates, sulfides, cyanides, and phosphates), cations (calcium, magnesium and ammonium ions), glucose, uric acid, amino acids (alanine, aspartic acid, glutamine, glycine, phenylalanine, tryptophan, and tyrosine).

5. Development of custom-tailored environmental biosensors

5.1 Peroxide biosensor – Proof-of principle for PAHs biosensing

The modelling of oil weathering at sea, presented in Chapter 2, revealed the critical contribution of petrogenic polycyclic aromatic hydrocarbons (PAHs) in the acute open sea pollution. Under certain conditions (wind, temperature, sea currents, microbial ecology), the degradation pathways described in Fig. 6 fail to manage more 10-15% of PAHs input, especially in phytoplankton rich areas (Duran and Cravo-Laureau, 2016); in cases as such, PAHs accumulate in sediments is eminent (via vertical sinking), posing a threatening condition for open sea and coastal ecosystems; the impact is expected to be critical for the estuarine zone that may also receive PAHs from land sources. Extending the ontological network to include the fate of sediment PAHs under the conditions prevailing in Saronic Gulf shoreline (as stated in Parinos *et al.*, 2019), microbial aerobic degradation has been highlighted as a critical process (Fig. 20). Biodegradation is mostly carried out by four consortia, in which proteobacteria, e.g., *Pseudomonas spp..*, dominate (Thomas *et al*., 2020).

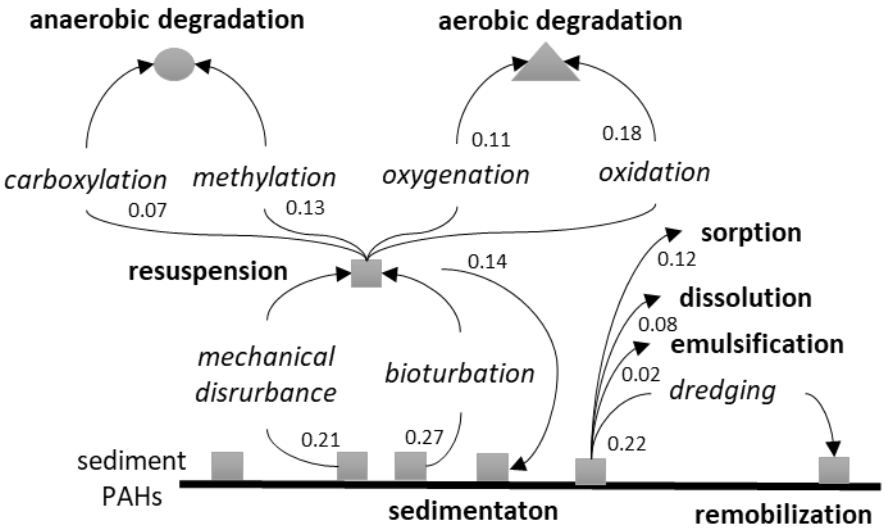

Figure 20. Schematic representation of sediment PAHs fate ontology under Saronic Gulf conditions (systemic analysis). Processes are indicated in bold, drivers to processes (partonomy) are indicated in italics. Numbers indicate in-out degrees, i.e., the link likelihoods between the nodes.

This species has been suggested for the development of bioluminescent biosensors (Paton *et al.*, 2009), using naphthalene as a PAH model. Cellular response against PAHs

commonly involves oxygenation that breaks down the aromatic ring, readily monitored through cell respiration (Werlen *et al*., 2004); since all reactions involve electron transfer, amperometric enzyme biosensors could be also utilized for direct (Liu *et al.*, 2007) or indirect (Liu *et al.*, 2009) PAHs detection.

Heme-containing redox bacterial enzymes, such as horseradish peroxidase (HRP), are known to oxidize organic electron donor substances, such as PAHs, yielding high-oxidation-state intermediates in the presence of hydrogen peroxide or oxygen (La Rota Hernandez *et al*., 2008). A generic and simplified hydrogen peroxide mediated model is shown below:

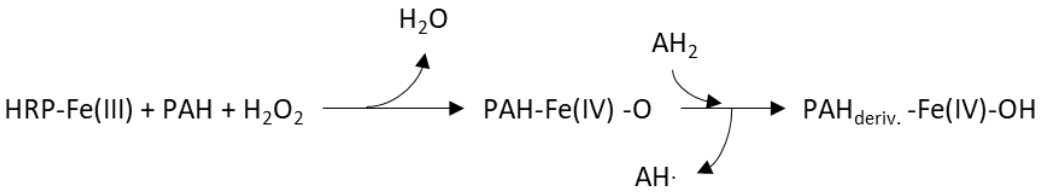

The monitoring of the redox reaction is prone to interference by other electroactive compounds, commonly anticipated in a water sample. Sensor development is feasible using complicated and possibly multilayered interference suppression schemes. The monitoring of peroxide consumption is less prone to interference and has been investigated herein for the development of a metal-supported lipid-membrane biosensor with incorporated HRP for the indirect detection of PAHs (Georgopoulos and Siontorou, 2016). To our knowledge, such an approach has not been proposed to literature so far.

5.1.1 Construction of the HRP metal-supported lipid membrane sensor

A sensing wire of 0.1 mm diameter was used to support lipid membranes from phosphatidyl choline (PC) in 0.1M KCl electrolyte solution (pH 6.5±0.1). The mean stabilization time for the self-assembly of the lipid membranes was 22±3 min (n=15), whereas the background current was 120±10 pA (n=15) and the noise level (random spikes) was 33±5 pA (n=15). The minimum applied voltage to bring about a non-linear relation between ion current and voltage (breakdown voltage) was 105 mV. Values between 100 and 500 mV have been reported in literature for such systems (Hianik, 2011); lipid membranes in suspension exhibit higher tolerances (ca. 350 mV) (Nikoleli *et al.*, 2019). Following membrane collapse, *in situ* regeneration, i.e., re-formation of the membrane from the lipids in dispersion, presented a high failure rate (>60%) and

low reproducibility, necessitating the construction of a new platform. These results render the ruggedness of the sensing system quite adequate for bench-scale development, but marginally suitable for the engineering of environmental devices.

Once formed and stabilized, the sensing wire-lipid membrane conjugate remained functional (i.e., electrode drift <5%) within the electrolyte solution for 30 h, even at moderately high ambient temperatures; however, at temperatures higher than 30 ^{o}C, the noise level increased by 20%. Outside the electrolyte solution, i.e., in air, stability has been demonstrated for ca. 10 min.

For enzyme immobilization, 5μl of the stock HRP solution (giving a final bulk concentration of 1.17μg/ml) were injected in the bulk electrolyte under mild stirring. The sensing wire-lipid membrane-HRP assembly stabilized within 20±5 min (n=10) to a background current of 122±11.5 pA (n=10), comparable to that obtained with the lipid platform without the enzyme. The latter indicates that the enzyme does not induce membrane poration; thus, enzyme-membrane interactions are not predominantly electrostatic. The noise levels recorded were 26±6 pA, slightly lower than those recorded for the lipid membrane without the enzyme, possibly indicating a reduction in membrane fluidity. The results may demonstrate aggregation phenomena on the membrane-electrolyte interface. This is further supported by the results obtained at lower enzyme levels, which gave similar stabilization times and background currents, but increased noise to levels unsuitable for sensing; the use of 0.17 μg/ml HRP bulk concentration yielded a background current of 123±8.5 pA (n=3) within 18±3.4 min (n=3) at 85±16 pA (n=3) noise levels.

The sensing wire-lipid membrane-HRP assembly was stable (<5% drift) for 9 hours of continuous operation. Stability in the air has been demonstrated for ca. 10 min.

5.1.2 Peroxide detection

The lipid membrane without the enzyme produced a small response towards peroxide, possibly due to slight increases in the surface charge density of the lipid bilayer induced by the accumulation of the charged molecules on the membrane-electrolyte interface. At the presence of peroxide in the bulk electrolyte, a permanent ion current increase was recorded, the magnitude of which could be linearly related to the concentration of peroxide in the bulk; the time required for signal generation, i.e., to establish 99% of steady-state current, was on the order of a few seconds, supporting the view of rapid

alterations at the surface of the membrane. This response probably demonstrated initial enzyme-analyte interactions but the response time was too short to accommodate any downstream interactions; at any case, the sensor was not built to monitor reduction currents and, further, after the appearance of the ion current increase corresponding to the addition of the analyte, no signal was recorded for 15 mins.

Peroxide was added at stepwise injections of 20 μl of the analyte solution and its cumulative concentration in the bulk was calculated after each injection. The results are shown in Table 1 and the calibration graph in Fig. 21; the individual addition of standard analyte concentrations gave similar signals, within the error of measurement. The lipid membrane exhibited a linear response towards peroxide within a concentration range of 0.05-1.58 mg/ml, although the reliability of the response towards low analyte concentrations (as judged by the standard deviation of the mean current values obtained) is marginally acceptable. The detection limit was 109 μg/ml; non-membrane HRP sensors have reported peroxide detectability at 1.92 ng/ml (Liu *et al.*, 2009) or 0.72 ng/ml (Liu et al., 2007).

Table 1. Analytical characteristics and performance of the peroxide sensor at different enzyme loadings.

Concentration of peroxide in the bulk (mg/ml)	Sensor response (ΔI, nA) without the enzyme (±SD, *n*)	Sensor response (ΔI, nA) with 0.34 μg/ml HRP (±SD, *n*)	Sensor response (ΔI, nA) with 1.17 μg/ml HRP (±SD, *n*)
0.05	0.102 (±0.4369, 5)	0.983 (±0.2362, 9)	0.840 (±0.222, 20)
0.11	0.182 (±0.4510,5)	2.050 (±0.3334, 10)	4.316 (±0.3112, 20)
0.16	0.390 (±1.3822,5)	2.854 (±0.3736, 14)	6.155 (±0.3990, 20)
0.21	0.442 (±2.2561, 5)	4.013 (±1.1957, 14)	9.852 (±1.050, 20)
0.26	1.155 (±3.477, 5)	5.021 (±2.246, 10)	11.06 (±2.665, 20)
0.53	2.766 (±1.402, 5)	13.79 (±3.6721, 10)	24.22 (±3.899, 20)
0.79	4.930 (±2.258, 5)	20.87 (±3.5346, 5)	34.05 (±4.422, 20)
1.05	7.672 (±2.054, 5)	28.11 (±5.1757, 5)	47.67 (±6.588, 20)
1.32	9.118 (±3.104, 5)	36.57 (±5.4163, 5)	58.201 (±6.999, 20)
1.58	10.44 (±1.578, 5)	43.44 (±2.454, 5)	69.45 (±6.777, 20)
Noise level (nA)	0.033 (±0.005, 15)	0.182 (±0.023, 5)	0.122 (±0.0115, 10)
Linear range (mg/ml)*	0.05-1.58	0.05-1.58	0.05-1.58
Detection limit$ (μg/ml)	109	70.8	18.9
Sensitivity#	7.2823	28.44	44.65

**from the calibration curve; $at S/N = 3; # as nA per unit analyte concentration*

The monitoring of the HRP-peroxide interaction occurring in the bulk, i.e., with the enzyme unbound, gave no discernible membrane response. Small transient ion currents,

possibly due to small-scale electrostatic changes at the surface of the membrane, have been recorded without a clear relation to analyte concentration.

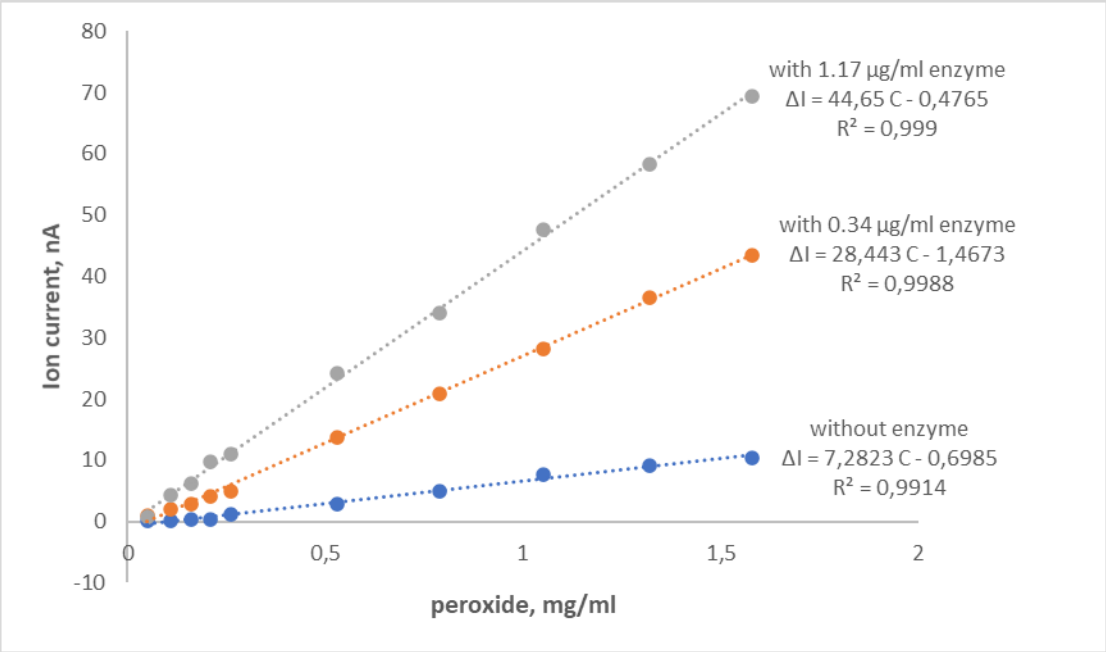

Figure 21. Calibration graphs for the peroxide sensor incorporating 0.34 µg/ml and 1.17 µg/ml HRP (as concentration in bulk). The lipid membrane exhibits also some selectivity towards peroxide, at levels much lower than those of the HRP systems (PC lipid membranes, 0.1M KCl electrolyte, pH 6.5±0.1, 25°C).

The response of the sensor incorporating 0.34 µg/ml HRP (as concentration in bulk) towards peroxide gave similar permanent increases of the ion current (Fig. 22), but at a four times higher sensitivity that decreased the detection limit to 70.8 µg/ml. When the HRP concentration increased to 1.17 µg/ml, sensitivity increased further by two-fold and the detection limit achieved was 18.9 µg/ml. Given the selectivity of the lipid membrane to peroxide, non-specific interactions could be ruled out, without, however, affecting the linearity of the response. Some drift of the ion current was noticed, especially at high peroxide levels and long use; however, the maximum value observed was 1 nA/min, increasing significantly after 9 hours of sensor use.

The effect of pH on the response of the sensor has been investigated in the range 6-8 (Fig. 23). HRP systems, in general, exhibit an optimum response at pH 7 when the redox reaction is monitored. In the present study, the optimum pH for peroxide consumption is 6.5.

No interference has been reported from glucose, uric acid and amino acid mixtures, i.e., compounds that are known to interact HRP, at varying concentrations up to 0.1M.

Similar results have been also reported by other HRP sensors working at a pH value of 6.5 (Liu *et al*., 2008; 2009).

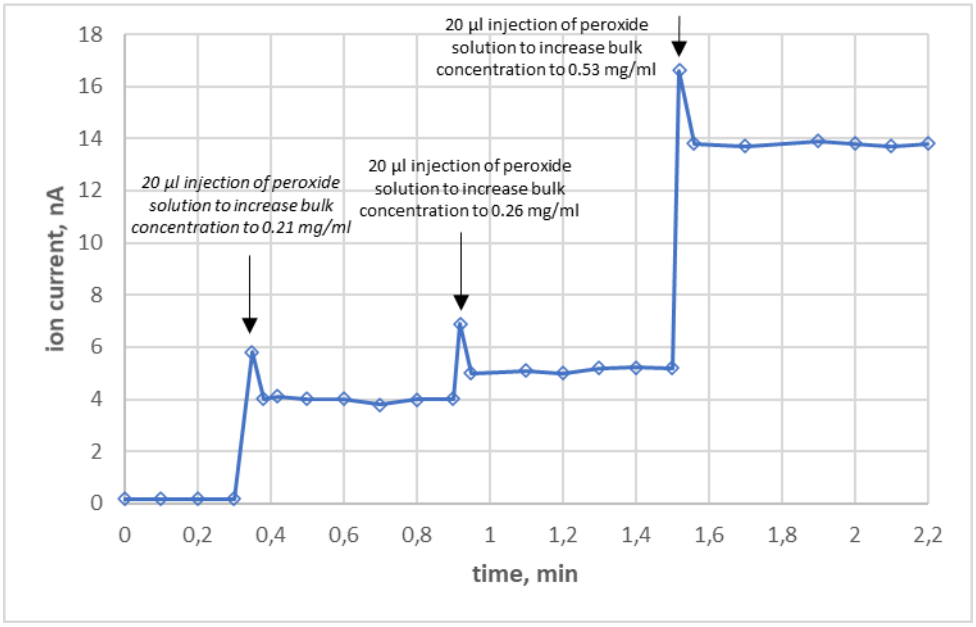

Figure 22. Recording obtained from the response of the sensor incorporating 0.34 µg/ml HRP (as concentration in bulk) to stepwise additions of peroxide under stirring (PC lipid membranes, 0.1M KCl electrolyte, pH 6.5±0.1, 25 ºC).

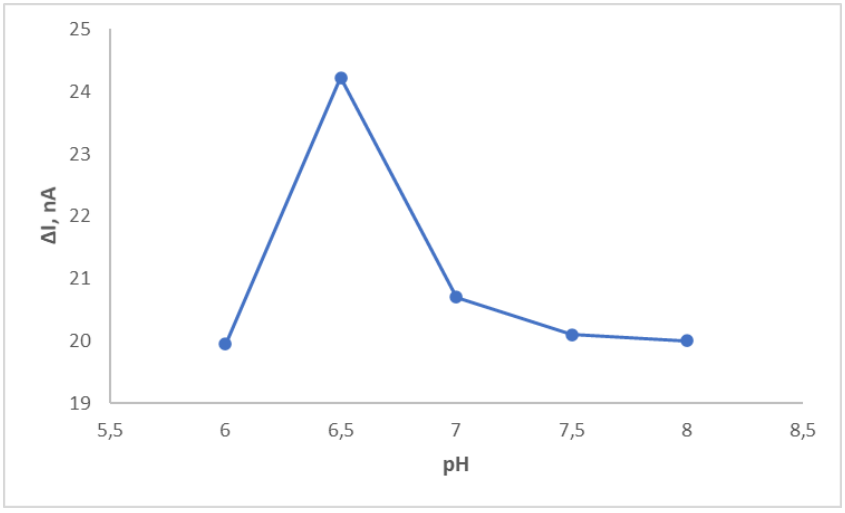

Figure 23. Effect of pH on the response of the lipid membrane sensor incorporating 1.17 µg/ml HRP towards 0.53 mg/ml peroxide. (PC membranes, 0.1M KCl electrolyte buffered with HEPES, 25 ºC).

5.1.3 Evaluation of the results

The construction of site-specific models of aquatic ecosystems for guiding biosensor development has been proven suitable to deliver critical environmental parameters and customized detectors. In effect, the local anti-stress response mechanisms can be used

as molecular tools for developing tailored to the environment measuring systems; utilizing multiple layers of knowledge, abiotic parameters can be effectively linked to biotic ones. Thereby, the biosensors developed are capable to assess the impact of pollution than the pollution itself, providing valuable information for environmental management schemes.

The results presented herein for the metal-supported enzyme biosensor built on horseradish peroxidase to quantitate peroxide and can be regarded as proof-of-principle for the detection of PAHs (Georgopoulos and Siontorou, 2016). Although the electrochemical study alone is not adequate to draw comprehensive conclusions, necessitating an in-depth investigation of the enzyme-lipid interactions and the mechanism of signal generation, quantitative detection has been demonstrated. Such detection strategy has not been reported in the literature, while it is more straightforward and easier to apply than the more complex redox formats. Undoubtedly, the HRP-PAHs-peroxide system should be further examined, starting from studies using naphthalenes and gradually including anthracenes and higher PAHs; the discriminatory capability of the sensor towards different PAHs is yet unknown, but even a cumulative response might be adequate for environmental screening. Moreover, more elaborate optimization and interference studies are required along with extended validation with real samples.

The selectivity of the lipid membrane *as is* to peroxide did not affect the reliability of the measurements in the system presented. The enzyme sensor responds to the increase of the analyte concentration in the sample, although similar signals are obtained by discrete additions, proving the reproducibility of the response. Also, detection is not prone to interference from compounds that are known to interact with HRP. The operational stability (i.e., 9 hours of continuous operation without affected reliability) is quite satisfactory for applicability. The use of 1.14 μg/ml of the enzyme presented the best results but the detection limit achieved is higher than that of other HRP systems. The electrochemical behavior of the system, especially the breakdown voltage and the noise levels, render the ruggedness of the sensor marginally suitable for environmental applications. The use of sensing wires with larger diameters may yield a more rugged device but detectability is not expected to reach the nano-range. The adaptation, however, of the biochemical system to a nanoplatform might provide more fit-for-purpose results.

5.2 Phenols biosensor

Phenolic and polyphenolic compounds are widely distributed in the environment from municipal waste, industrial effluents, agricultural runoffs and natural processes. High toxicity has been demonstrated for more than 165 phenolics (WHO, 2018); chlorophenols produced during the chlorination of water have an established mutagenic potential. Life threatening (acute or chronic) toxicity levels for humans and aquatic life are in the range of 9-25 mg/l, whereas the water purity standard is set within 1-10 ng/ml, depending on the drinking water source (WHO, 2018). Thus, the rapid and reliable detection of low phenolics concentrations in water is vital to environmental management.

Implementing the modelling methodology described in Chapter 2 (Fig.24), site-specifity as per the dominancy of degradation pathways for phenolics in water could not be established. Phenol compounds may undergo biodegradation or photooxidation, without excluding interactions with inorganic moieties followed by physical processing (Anku *et al.*, 2017); environmental conditions do not play a critical role in the prevalence of any pathway. Further, degradation results in the complete mineralization of phenolics, thus degradation products cannot be used as indices of a particular process. In view of the above, phenols stand as the critical to ecosystem target analyte.

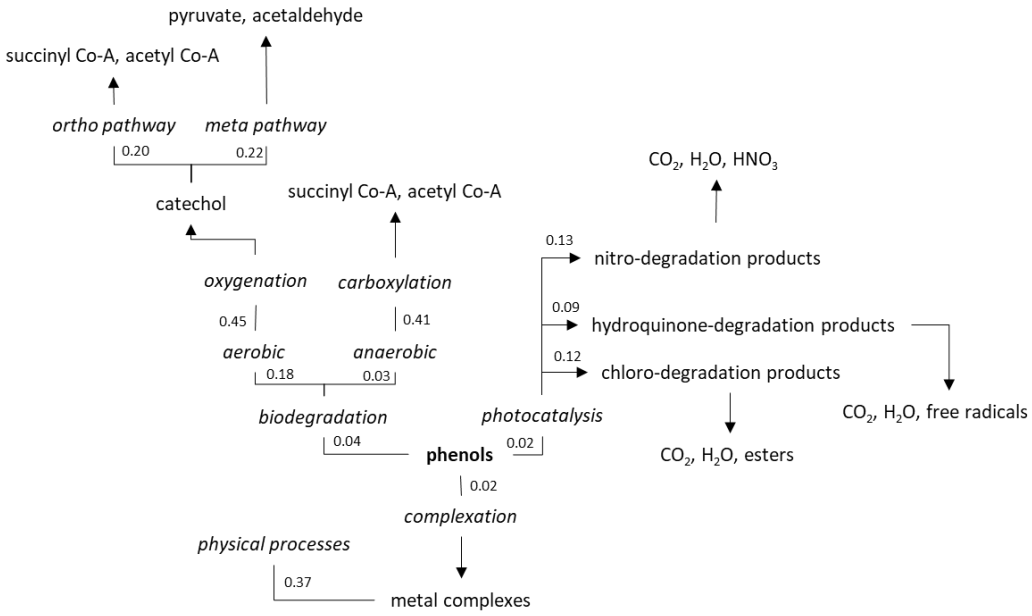

Figure 24. Schematic representation of the general ontological model for the fate of phenolics in water (systemic analysis). Processes (partonomy) are indicated in italics. Numbers indicate in-out degrees, i.e., the link likelihoods between the nodes.

Phenol detection has been proposed with liquid chromatography, combined with UV (Yang *et al.*, 2006) or electrochemistry (Vanbeneden *et al.*, 2006), or gas chromatography combined with mass spectrometry (Peng *et al.*, 2006) or flame ionization (Fiamegos *et al.*, 2003). Field instrumentation is feasible with quantum dots-immunoassays (Zhang *et al*., 2014) or microchip capillary electrophoresis (Wu and Lin, 2006). Biosensing has been also suggested, based on the amperometric detection of tyrosinase-catalyzed oxidation of phenol (Adamski *et al*., 2010; Guan *et al.*, 2013; Yildiz *et al*., 2007); sensing is focused either on the redox reactions or the reduction of the produced quinone (Fig. 25). The reported detectability ranges between 1-10 ng/ml (Adamski et al., 2010; Yildiz et al., 2007); liposome-based sensing decreased detectability to 8.5 pg/ml (Guan *et al.*, 2013). However, enzyme kinetics remain unclear (Ramsden and Riley, 2014) hindering the effective amplification of the redox signal, while the manipulation of the enzyme on the surface of the transducer reduced sensor reproducibility (Guan *et al.*, 2013). Since the produced quinones are fouling agents (Yildiz *et al*., 2007), a narrow linear range of detection was used; problems with enzyme leaching have been also reported (Adamski et al., 2010). Optimized sensors have been developed on complex multilayer constructs of graphene-Au nanoparticle-platforms with chitosan-bound tyrosinase with a detection limit of 4.67 ng/ml (Fartas et al., 2017).

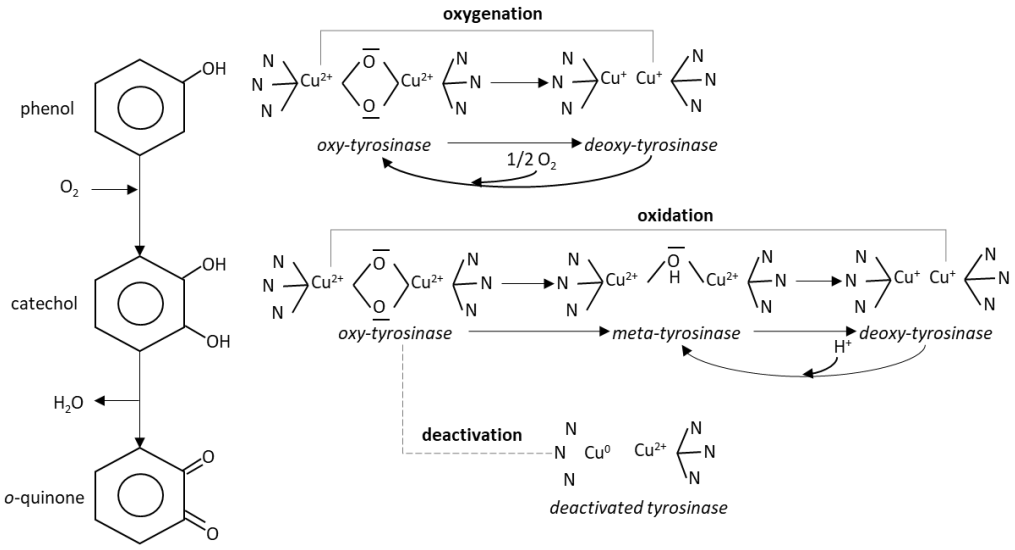

Figure 25. Tyrosinase catalyzed oxidation of phenol: the monophenol is hydroxylayted to diphenol (catechol) that is dehydrogenated to o-quinone. During the reactions the enzyme changes from oxy- to deoxy- and to meta-state. Phenol may be oxidized to o-quinone through the monooxygenase pathway, even without the formation of the intermediary catechol; the oxy- and deoxy- states are readily interchangeable. Catechol is oxidized to o-quinones through the oxidase pathway, but the deoxy- to meta-interchange may also require redox exchange with other metals. Catecholic substrates may sometimes enter the monooxygenase pathway (i.e., processed similarly to phenols) leading to copper reduction and enzyme deactivation.

To avoid fouling and electrochemical interference, the tyrosinase-phenol primary interaction (i.e., at the oxy-state) has been investigated herein for the development of a metal-supported lipid-membrane phenols biosensor (Siontorou and Georgopoulos, 2015). To our knowledge, such an approach has not been proposed to literature so far.

5.2.1 Construction of the tyrosinase metal-supported lipid membrane sensor

The metal-supported lipid membranes were constructed from phosphatidyl choline. The concentration of the lipid solution has been investigated herein in the range of 1-3 mg/ml (as concentration in bulk). The use of 2.5 mg/ml lipid solution had a 100% success rate in constructing the lipid platforms, with stabilization times achieved within 10-15 min at a 0.5 mm in diameter sensing wire; more dilute lipid solutions gave a success rate of 60%, whereas higher concentrations resulted in prolonged stabilization times.

The use of sensing wires with a diameter of 0.5 mm produced more rugged platforms (280 mV breakdown voltage) and 30% shorter membrane stabilization times than the 0.1 mm wires; the background ion current was 15.8±4.2 nA, quite higher than that observed with the 0.1 mm wires but adequate for sensing. When a 1.0 mm in diameter wire was used, the background ion current increased to 60 nA; since only currents up to 650 nA are reliable for sensing (larger currents may indicate membrane destabilization and not analytical signals), the use of 1.0 mm wires limits the analytical range.

Once formed and stabilized, the sensing wire-lipid membrane conjugate remained functional (i.e., electrode drift <5%) within the electrolyte solution for 30 h at ambient temperature. Outside the electrolyte solution, i.e., in air, stability has been demonstrated for ca. 10 min.

Enzyme integration has been investigated with lipid membranes self-assembled on a 0.5 mm sensing wire, using 0.1M KCl electrolyte solution buffered with HEPES. After the stabilization of the membrane, 10 μl of the enzyme stock solution (5 mg/ml) were injected into bulk electrolyte; the ion current stabilized within 6-8 min, giving a background current of 15±2.5 nA, (n=12), comparable to that obtained without the enzyme; thus, the enzyme-lipid interactions are not predominantly electrostatic and the immobilization of the enzyme on the membrane surface does not induce poration. The sensing wire-lipid membrane-tyrosinase assembly was stable (<5% drift) for 12 hours

stored in electrolyte at room temperature. Stability in air has been demonstrated for ca. 10 min.

5.2.2 Phenol detection

The lipid membrane exhibited no discernible selectivity towards phenol at pH 8, even at very high concentrations; no changes have been also observed in the background ion current or the noise levels. Earlier studies on the partitioning of phenol phospholipid vesicles showed that only the uncharged phenols influence the fluidity of the lipid membrane but the effect is pH-dependent. At pH 7, limited adsorption has been demonstrated but at higher pH values, phenol was insoluble in the lipid; at pH values < 5, partitioning into the hydrophobic chains was concentration-dependent (Van Dael, and Ceuterickx, 1984). Catechol, a possible intermediate in tyrosinase-phenol interaction has been found to interact weakly with the outer leaflet of a model bilayer through limited headgroup partitioning at pH 7.4 (Forsberg *et al*., 2005). No response has been recorded in the metal-supported lipid membrane sensor presented herein from the addition of catechol concentrations up to 1M at pH 8.

The monitoring of the enzyme-analyte interaction in the bulk (i.e., with unbound enzyme) produced no discernible membrane response. At pH values < 7, small transient ion currents have been recorded, possibly due to small-scale electrostatic changes at the surface of the membrane, without analytical use.

The tyrosinase membrane sensor responded to phenol additions by permanent ion current increases, the magnitude of which was linearly related to the concentration of the analyte in the bulk. The response time obtained was 10±0.75 s (n=31), suggesting rapid alterations at the surface of the membrane. This response probably demonstrated initial enzyme-analyte interactions but the response time was too short to accommodate any downstream interactions; at any case, the sensor was not built to monitor reduction currents and, further, after the appearance of the ion current increase corresponding to the addition of the analyte, no signal was recorded for 15 mins.

The signals recorded at increasing phenol concentrations had such large magnitudes that cannot be attributed simply to surface membrane alterations due to the enzyme-phenol interactions; knowing that the complexation of the enzyme with phenol changes the state of the enzyme (Ramsden and Riley, 2014), concurrent changes in the membrane packing and fluidity seem possible. Also, the response of the sensor towards

phenol was the same, regardless if the analyte was introduced by stepwise additions or as single injection. For example, when phenol bulk concentration reached 3.72 pg/ml at stepwise additions, the mean difference in ion current (ΔI) was 128.7±10.1 nA (*n*=10); single injections of 3.72 pg/ml phenol in the bulk, produced signals of 130.7±10.9 nA (*n*=10); similar results have been obtained for 13.64 mg/ml of phenol, indicating no memory effects. Thus, the sensor developed exhibits no statistically significant carryover effects and can be used for multiple analyses.

The effect of enzyme loading on signal magnitude has been studied in the range 1.25-10 μg/ml (concentration in bulk). The optimal bulk tyrosinase concentration was found to be 2.5 μg/ml; lower levels did not provide adequate sensitivity for detection (as shown by the 33% reduction in the response of the sensor to 3.72 pg/ml of phenol in the bulk), while higher levels caused membrane destabilization.

The effect of pH has been also investigated herein. Other tyrosinase biosensors have reported optimal pH values between 6 and 7 (Adamski *et al*., 2010; Guan *et al*., 2013; Yildiz *et al*., 2007); at lower values, the produced catechol may replace phenol for the enzyme binding sites leading to enzyme deactivation (Ramsden and Riley, 2014), while higher values do not favor the monooxygenase pathway (Yildiz *et al*., 2007). Using a phenol bulk concentration of 3.72 pg/ml, the highest signal, i.e., 213.8 nA, was achieved at pH 7.0 (Fig. 26); however, the destabilization of the sensor became apparent after two consecutive phenol injections, manifested as an increase of background ion current to 420 nA with multiple transient signals of high magnitude that prohibited any further use of the sensor. This effect could be possibly attributed to membrane fluidity alterations due to enzyme state shifting and/or catechol interference (provided that catechols were indeed produced *in situ*). At pH values < 7, increased noise levels were observed; at pH 5, noise levels became excessively high, with transients up to 100 nA; while phenol partitioning cannot be excluded, enzyme deactivation or desorption from the bilayer is also possible. At pH values > 8.5, the response of the sensor towards phenol dropped to 5.61% of its value at pH 7. At pH 8.0, the response of the sensor decreased by 40%, but the system remained stable and functional after ten consecutive injections, where it reached the maximum allowable current level. At this pH, no interference is expected by non-specific interactions between the analyte or the oxidation by-products.

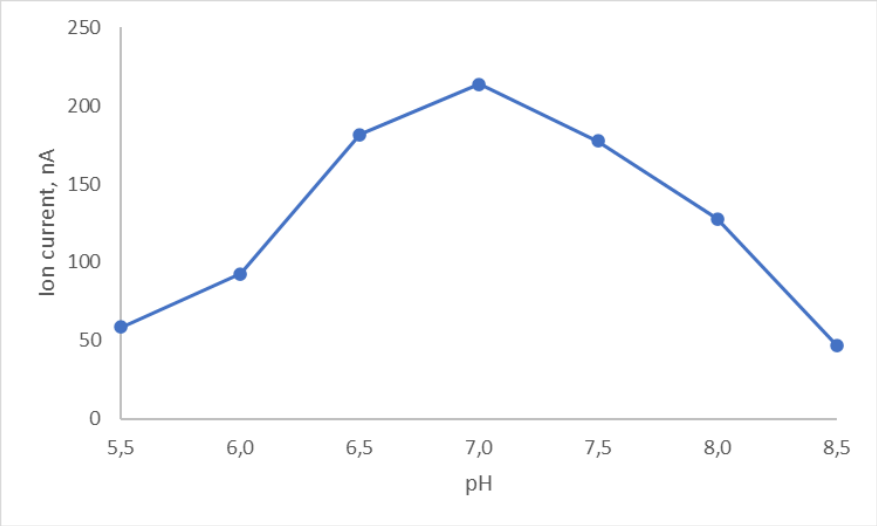

Figure 26. The effect of pH on the response of a metal-supported PC membrane incorporating 2.5 µg/ml tyrosinase (0.1M KCl buffered with HEPES, 0.5 mm diameter Teflon-coated silver wire, 25 °C) towards 3.72 pg/ml phenol (as concentration in bulk).

The calibration graph for phenol detection at the optimized conditions is shown in Fig. 27. The coefficient of determination (R^2) was 0.9997 (n=31) and the reproducibility of response was estimated to ±8-12% for within-day analyses (as relative standard error, n=31, 5.95% confidence limit) and 15.85% for between-days and analysts analyses (as relative standard error, n=24, 5.95% confidence limit).

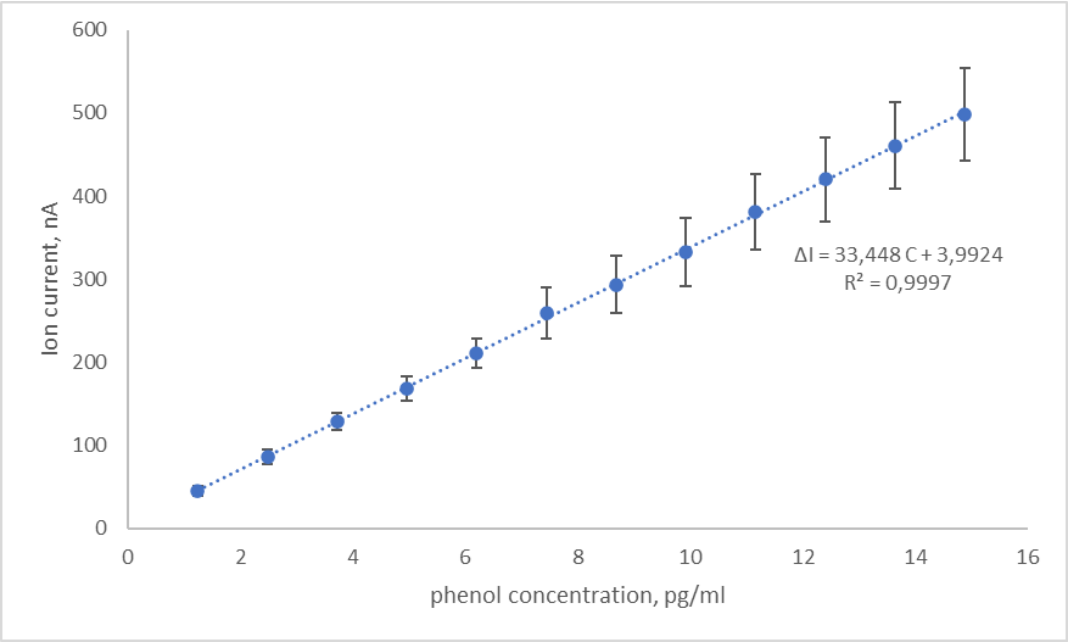

Figure 27. Calibration graph for phenol detection using metal-supported PC membranes incorporating tyrosinase (2.5 µg/ml, concentration in bulk). Experimental conditions: pH 8.0; 0.5 mm Teflon coated Ag wire; 0.1 KCl solution with HEPES, 25 °C; calibration was performed by stepwise additions of phenol standard solution under stirring. Error bars denote standard deviation (n=31).

The linear range was 1.24-15 pg/ml, with a detection limit (as S/N = 3) of 1.24 pg/ml and a sensitivity of 33.45 nA per pg/ml phenol concentration. Some drift of the ion current with time was noticed, especially at high phenol concentrations and use; however, the maximum value observed was 1 nA/min, increasing after 12 hours of storage in electrolyte at room temperature. The detection limit achieved herein is lower than that reported by other tyrosinase biosensor systems (Adamski *et al*., 2010; Guan *et al.*, 2013; Yildiz *et al*., 2007) and higher sensitivity has been demonstrated, comparable to chromatographic detection (Fiamegos *et al.*, 2003; Peng *et al*., 2006; Vanbeneden et al., 2006; Yang *et al.*, 2006), immunoassays (Zhang *et al*., 2014) or electrophoretic devices (Wu and Lin, 2006).

5.2.3 Sensor reversibility

Earlier metal-supported platforms have demonstrated the response of protein (Siontorou *et al*., 1997) and DNA (Siontorou *et al.*, 1998) lipid membrane sensors towards decreasing analyte concentrations, leading to sensor reversibility, i.e., the restoration of low ion currents that allowed the reuse of the same sensor for another experimental run. Although the reversibility mechanism has been only investigated electrochemically, decreasing the analyte concentration in the bulk yields a concentration gradient between the membrane surface and the bulk electrolyte, adequate to pull away analyte molecules from the electrolyte-membrane interface. The de-complexation of the analyte from DNA has not been proven (Siontorou *et al.*, 1998); also, limited DNA desorption was possible, as evident by the lag time required to re-establish a stable system, but the complete extraction of DNA from the membrane was not feasible without destroying the sensor.

In the sensor developed herein, the phenol-rich electrolyte was gradually removed from the electrochemical cell and replaced with phenol-free electrolyte, until the ion current dropped to acceptably low levels. Compared to calibration, the response of the sensor towards phenol was rather elevated while the sensitivity was slightly decreased, possibly indicating memory and carryover effects. Washing the sensing electrode with strongly acidic or alkaline solution has been suggested in literature (Aloraefy *et al.*, 2014); as lipids are oxidized at pH values < 4.5, only alkaline treatment has been considered herein.

Filling the electrochemical cell with 15 pg/ml phenol (the highest analyte concentration tested herein) and after receiving the corresponding signal and allowing the system to stabilize, the sensing wire was removed from the electrochemical cell and immersed in pH 8.5 buffer (0.1M KCl with HEPES) for 10 min. When the sensing wire transferred in phenol-free and enzyme-free electrolyte (pH 8.0), the ion current reduced to 28 ±1.5 nA (*n*=12), 20% higher than the background ion current within 5-6 min; the sensitivity towards phenol was not affected (within analytical error), clearly indicating insignificant or none enzyme desorption. Shorter washing times, settled ion current to higher values.

The number of repetitive assays of high phenol samples that could be achieved, including analysis, washing and re-stabilization, was 8 without observing any statistically significant reduction in signal magnitudes. The number of samples that could be assayed with the same sensor depended on phenol concentration in the sample; at 1.24 pg/ml phenol, the repetitive number of assays that could be performed increased to 15.

5.2.4 Sensor validation

Possible interference from a number of anions (carbonates, nitrates, phosphates, chloride, sulfates and sulfides) and cations (ammonium, calcium, and magnesium ions) has been studied herein with simulated water samples, at varying composition and concentration. The sensor exhibited high tolerance to interfering ions during simulation; the results showed a determinant error < 5% for bulk electrolyte concentrations up to the high mM range.

Phenol-spiked tap and lake water were used for validation studies. Spiked samples were freshly prepared from the phenol stock solution and analyzed immediately. 10-ml tap water samples were spiked with 9.4 ng/ml phenol (the upper allowable level for drinking water) and 5-ml lake water samples were spiked with 18.8 ng/ml (lower than the allowable phenol limit has been chosen in order to elucidate matrix effects). A 10-μl assay volume was used. The same sensor was used to analyze all samples with a mean analysis rate of 14 samples/h (including regeneration); the calibration graph of Fig. 27 was used for quantitation (i.e., the sensor was not re-calibrated), taken into account the dilution factors.

Tap water did not affect the sensor; lake water increased noise levels by 42.86%, necessitating the increase of the detection limit to 2.8 pg/ml. Phenol recovery in the tap water samples ranged between 93-105% (Table 2), with no positive or negative trends, indicative of standard errors. For environmental samples, the acceptable range is 80-115% (ICH, 2005). Considering sample dilutions, the lowest phenol concentration in tap water samples that could be reliably detected was 2.5 ng/ml. Table 3 presents the results from the lake water samples; a consistent positive trend was observed, possibly due to matrix effects or phenol already present in the sample. The maximum deviation was +6.6%, allowing for reliable detection of lake samples. Considering sample dilutions, the lowest phenol concentration in lake water samples that could be reliably detected was 6.1 ng/ml.

Table 2. Validation results from the recovery of phenol in tap water samples containing 9.4 ng/ml phenol.

#	Phenol detected with the sensor (ng/ml)	% Relative error
1	9.06	-3.617
2	9.36	-0.426
3	9.84	+4.681
4	9.48	+0.851
5	9.66	+2.766
6	9.18	-2.340
7	9.90	+5.319
8	9.84	+4.681
9	9.12	-2.979
10	8.76	-6.809

Table 3. Validation results from the recovery of phenol in lake water samples containing 18.8 ng/ml phenol.

#	Phenol detected with the sensor (ng/ml)	% Relative error
1	19.26	+2.447
2	18.96	+0.851
3	20.04	+6.596
4	19.56	+4.043
5	19.86	+5.638
6	19.80	+5.319

5.2.5 Evaluation of the results

The modeling methodology for determining critical environmental parameters has been proven suitable to handle multi-source pollution input and persistent pollutants with multiple degradation routes within the ecosystem.

The results presented herein for the metal-supported enzyme biosensor built on tyrosinase to quantitate phenol based on the enzyme-analyte initial interaction and not the commonly adopted monitoring of the redox cascade reactions (Siontorou and Georgopoulos, 2015); such an approach has not been proposed in literature thus far and offers many advantages for environmental monitoring. The sensitivity demonstrated was higher than that of other tyrosinase-based biosensor systems, comparable to chromatography and immunoassays, whereas the pg/ml detection limit achieved was quite lower, enabling environmental screening of phenol at concentrations within and above the environmental limits.

Operational functionality has been also demonstrated using real environmental samples; the sensor could reliably detect 2.5 ng/ml (i.e., 2.5 ppb) phenol in tap water and 6.1 ng/ml (i.e., 6.1 ppb) in lake water. Although the results from the environmental samples obtained herein should be verified further with a more extended study, proof of concept has been provided and the phenol sensor developed is readily applicable. The storage and operational stability, though, are marginally satisfactory for applicability.

Nonetheless, selectivity towards phenolics has not been studied herein. The discriminatory capability of the sensor towards different phenolics is yet unknown, but, as partition coefficients of higher phenols differ, some degree of qualitation might be possible based on aggregation kinetics on the membrane surface. For rapid environmental screening, though, cumulative responses might be adequate.

5.3 Nitrite biosensor

The need to determine nitrates (NO_3^-) and nitrites (NO_2^-) in water columns and sediments, and possibly differentiate between the two, has been already highlighted in the coastal ecosystem model discussed in Chapter 2 (Fig. 5). The nitrification-denitrification processes that take place usually involve bacteria developing in sediments (Wang *et al.*, 2016) or in the routing system of macrophytes and algae (Gao

et al., 2014); the functional analysis output of nitrogen influx is presented in Fig. 28. The entry of dissolved forms of nitrogen (ammonium, nitrite or nitrate ions) into the ecosystem is generally managed by bacteria. Ammonia is handled by the chemoautotrophs *Nitrosomonas* spp. and *Nitrobacter* spp. that convert ammonium ions to nitrites and nitrites to nitrates, respectively; bioconversion is aerobic (Wang *et al.*, 2016), although it has been also demonstrated at low oxygen levels (Gao *et al*., 2014). Denitrifying bacteria, such as *Thiobacillus denitrificans*, *Micrococcus denitrificans*, *Serratia* spp., *Pseudomonas* spp., and *Achromobacter* spp., convert nitrates to nitrogen gas under strictly anoxic conditions (Álvarez *et al*., 2013). Denitrification occurs at the accumulation sub-compartment near the water-sediment interface (Fig. 28) at rates dependent upon nitrate levels, organic carbon sources, hydroperiods, pH, temperature and the N-compounds levels of the water column (Álvarez *et al*., 2013).

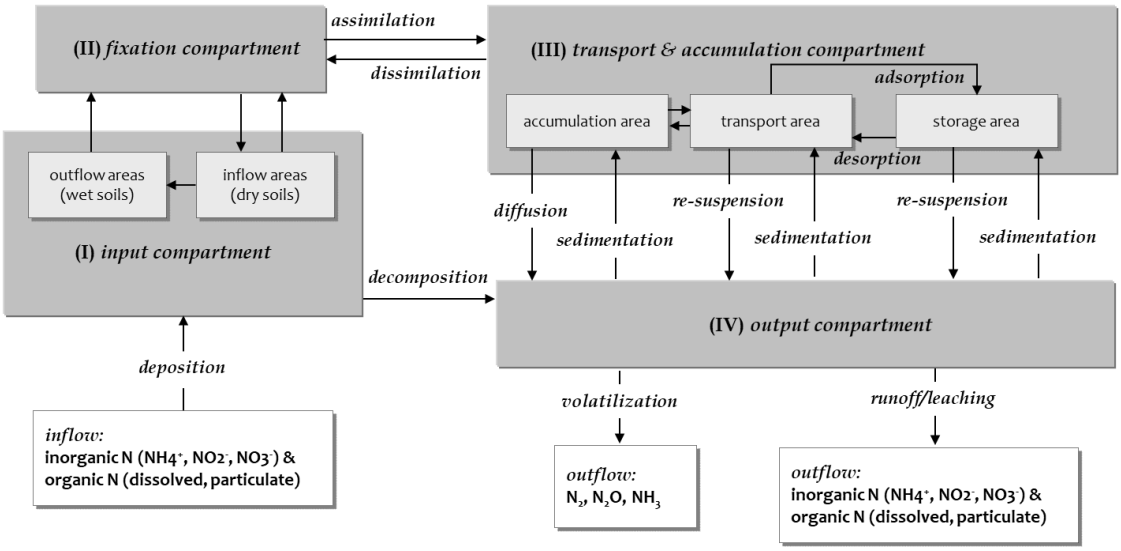

Figure 28. Modelling the nitrogen influx in aquatic ecosystem with the compartmentalization model described in Chapter 2 (the functional analysis output). Reprinted from Siontorou et al., Crit. Rev. Environ. Sci. Technol., 2017, under Thesis/Dissertation Reuse Request to Taylor & Francis).

If ammonia accumulates, herbivores, such as insects, dominate and can decimate aquatic vegetation (Ji and Brune, 2006). If nitrates accumulate, algae growth is extremely favored, eventually leading to eutrophication (Beutel *et al*., 2008). The accumulation of nitrites is indicative of anaerobic reduction of nitrates and a complete inhibition of denitrification (Gelfand and Yakir, 2008); agricultural runoff has an important role to play, emphasis given to nitrogen fertilizers and biocides.

Nitrites in irrigation are considered a major concern for agriculture (Laanbroek *et al*., 2002), readily entering the food chain (Pawełczyk, 2012). Nitrites in drinking water are

considered a serious health risk; WHO (2008) sets the upper limit to 3 μg/ml for short-term exposure and 0.2 μg/ml for long-term exposure; the EU (EC, 2007) limit is 0.5 μg/ml. The selective detection of nitrites in water, sediments and soil is indispensable, necessitating, however increased sensitivity and very low detection limits.

Nitrite detection has been proposed using chromatographic, spectroscopic and electrochemical techniques (Dutt and Davis, 2002). Spectroscopic methods have demonstrated good precision, high sample analysis rate, detection limits at 15-20 ng/ml and an extremely high cost of analysis (Ensafi *et al*., 2004; López Pasquali *et al*., 2010; Sreekumar *et al*., 2003). Chromatographic methods exhibited higher reliability of measurements with slightly higher detection limits (Michalski and Kurzyca, 2006). Field instrumentation might be feasible with chemical sensors; a detectability between 46 ng/ml (Salimi *et al*., 2008) and 92 ng/ml (Pietrzak and Meyerhoff, 2009) has been reported for a variety of environmental samples; carbon nanotube systems lowered the detection limit to 10 ng/ml (Pham *et al*., 2011).

Electrochemical or optical biosensor systems have been also developed, based on nitrite reductases or hemoproteins. Amperometric platforms on horseradish peroxidase (Liu *et al*., 2009), and nitrite reductase (Silveira *et al*., 2010; Tepper, 2010) reported detection limits of 8-10 ng/ml at simulated samples; cytochrome c (Chen *et al*., 2009) and other hemoproteins (Dai *et al*., 2008; Ding *et al*., 2010; Liu and Ju, 2003) gave similar detectability. Field validation data from a microbial biosensor for nitrates/nitrites (i.e., with no discriminatory capability) reported electrode fouling within minutes of sensor operation (Larsen *et al*., 2000). Nonetheless, detectability should be reduced manifold to compensate for the dilution of water samples and for the extraction from sediment or soil samples.

Tyrosinase-based platform development has not been considered herein, since its demonstrated selectivity towards phenol (Subchapter 5.2) would most certainly interfere with nitrite detection. The interactions between lipid membranes and hemoproteins have been previously studied on the metal-supported platforms. Carbon dioxide could be detected at 75 ng/ml on a phosphatidyl choline membrane incorporating deoxygenated hemoglobin, at anoxic conditions and pH 6; the detection limit decreased to 1.6 ng/ml when the membrane was dopped with dipalmitoyl phosphatidic acid and platelet activating factor (Siontorou *et al*., 1997). At pH 8, deoxygenated hemoglobin shifted selectivity towards cyanides (Siontorou and

Nikolelis, 1997); the detection limit achieved was 6.5 ng/ml. Methemoglobin, the oxidized form of hemoglobin, allowed detectability levels of 0.3 ng/ml. Interestingly, although no interference has been reported at pH 8 for carbon oxides, nitrates and sulfides, interference became significant at pH values < 7. A multiplex mechanism of signal generation has been demonstrated, involving mainly rapid changes of surface charge density of the lipid membrane, due to negative charge built up on the protein during complexation (Siontorou and Nikolelis, 1997), and slower changes in membrane fluidity, due to the protein shifting from the tense form to the relaxed form during complexation (Siontorou *et al*., 1997).

Methemoglobin has been investigated herein for the development of a metal-supported lipid membrane nitrite biosensor (Siontorou and Georgopoulos, 2016). To our knowledge, such an approach has not been proposed to literature so far.

5.3.1 Construction of the methemoglobin metal-supported lipid membrane sensor

The metal-supported lipid membranes were constructed from 2.5 mg/ml phosphatidyl choline solution. Membrane self-assembly was concluded within 10-15 min at a sensing wire with a diameter of 0.5 mm. Once formed and stabilized, the sensing wire-lipid membrane conjugate remained functional (i.e., electrode drift <5%) within the electrolyte solution for 30 h at ambient temperature. Outside the electrolyte solution, i.e., in air, stability has been demonstrated for ca. 10 min.

Methemoglobin was introduced in the electrochemical cell as 5-40 μl injections of a 10 mg/ml stock solution; the lipid membrane-methemoglobin conjugate stabilized within 6-8 min, regardless of protein concentration. The background ion current achieved with 10 μg/ml methemoglobin in the bulk was 10±2.5 nA, (n=52); lower levels (down to 5 μg/ml) decreased significantly sensitivity towards nitrites, while higher levels (up to 20 μg/ml) caused permanent membrane destabilization.

The background ion current recorded with a 10 μg/ml protein was comparable to that obtained without the protein; thus, the methemoglobin-lipid interactions are not predominantly electrostatic and protein immobilization on the membrane surface does not induce poration. The sensing wire-lipid membrane-methemoglobin assembly was stable (<5% drift) for 2 hours of continuous operation. Stability in air has been demonstrated for ca. 10 min.

5.3.2 Nitrite detection

The lipid membrane exhibited no discernible selectivity towards nitrite within a pH range of 6-8, even at very high concentrations; also, no changes have been observed in the background ion current or the noise levels. Previous studies have shown that nitrites accumulate inside phosphatidyl choline liposomes in concentrations well exceeding bulk concentrations without leaching (Samouilov *et al*., 2007); nitrate-induced phase shifting has been observed with charged lipid multilayer membranes, but nitrites failed to reproduce the thermodynamic effect (Vashchenko *et al*., 2017). The monitoring of the protein-analyte interaction in the bulk (i.e., with unbound methemoglobin) produced no discernible membrane response within a pH range of 6-8.

The methemoglobin membrane sensor responded to nitrite additions (as sodium nitrite) by permanent ion current increases (Fig. 29), the magnitude of which was linearly related to the concentration of the analyte in the bulk. The response time obtained was 9.85±0.67 s (n=20), suggesting rapid alterations at the surface of the membrane; as nitrite concentration increases, methemoglobin builds up negative charge that attracts cations in the membrane-electrolyte interface to increase transmembrane ion flux (Goetz *et al*., 2010; Schwab *et al*., 2009). Nonetheless, after the appearance of the ion current increase corresponding to the addition of the analyte, no signal was recorded for 15 mins.

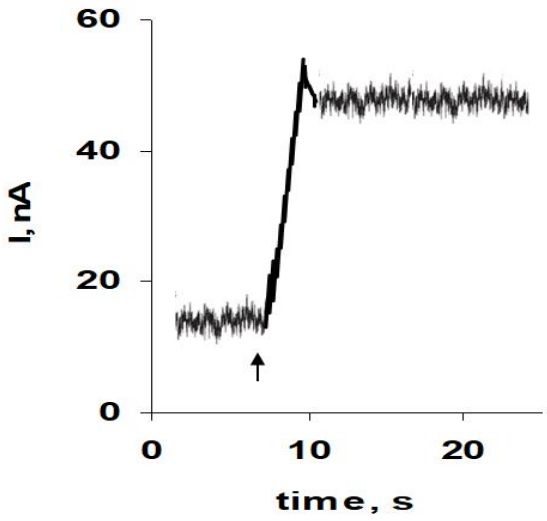

Figure 29. Recording obtained from the response of the sensor incorporating 10 μg/ml methemoglobin (as concentration in bulk) to the addition of 2.5 ng/ml nitrite (concentration in bulk) under stirring. Experimental conditions: PC lipid membrane, 0.5 mm diameter of sensing wire, 0.1M KCl electrolyte buffered with HEPES, pH 6.5±0.1, 25 ºC.

The affinity of hemoproteins to nitrites is well established, although not fully elucidated yet (Laterreur and English, 2007). At high pH values and high nitrite concentrations, low affinities have been reported (Schwab *et al.*, 2009); at low pH values and low nitrite concentrations, high affinities have been reported with oxidized hemoproteins (Goetz *et al.*, 2010). Low nitrite levels have been shown to interact with hemoglobin at concentration-dependent kinetics; high nitrite levels inhibited the interaction (Laterreur and English, 2007). Methemoglobin showed a small, but significant, affinity to 50 nM nitrite ions in cyanide-free samples at pH 8 (Siontorou and Nikolelis, 1997). Schwab *et al.*, (2009) suggested that at pH values > 7.7, nitrite forces methemoglobin to shift from the tense state to the relaxed state, leading to an increase of methemoglobin-nitrite dissociation constant; at pH 6.5, methemoglobin is at the tense state exhibiting a high affinity for nitrite and a very low dissociation constant; affinity dropped significantly when the concentration of nitrite increased to mM levels (Goetz *et al.*, 2010).

The effect of pH has been investigated herein (Fig. 30). At pH < 6.5, the noise level increased substantially, with transients up to 100 nA, possibly due to the reduction of nitrite to nitrous oxide. At pH 7.0, the response of the sensor towards nitrite decreased by 52%; response dropped by 81.2% at pH 7.5, whereas at pH 8.0, the response was reduced to noise levels. The best results have been obtained at pH 6.5; these results are in agreement with previous kinetic studies on the interaction between methemoglobin and nitrite (Goetz *et al.*, 2010; Schwab *et al.*, 2009).

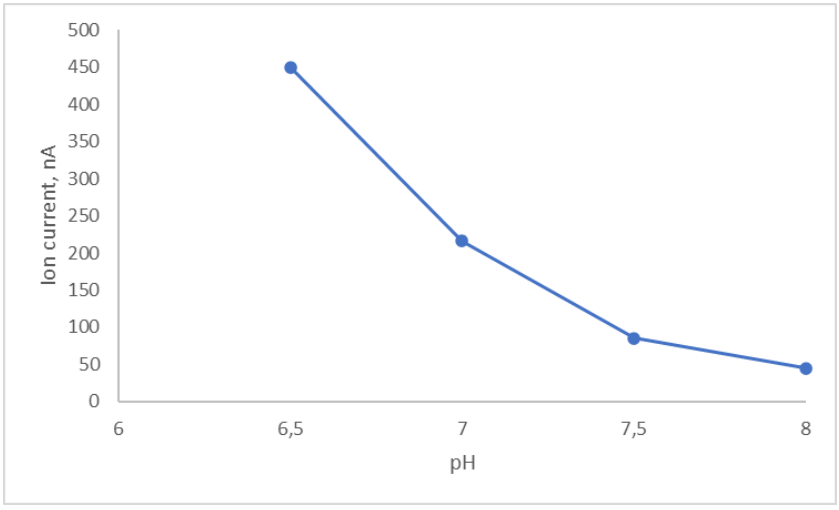

Figure 30. The effect of pH on the response of a metal-supported PC membrane incorporating 10 μg/ml methemoglobin (0.1M KCl buffered with HEPES, 0.5 mm diameter sensing wire, 25 °C) towards 62.5 ng/ml nitrite (as concentration in bulk).

The calibration graph for nitrite detection at the optimized conditions is shown in Fig. 31. Calibration was performed by stepwise additions of 0.01 g/l nitrite standard solution (as 5-10 μl injections).

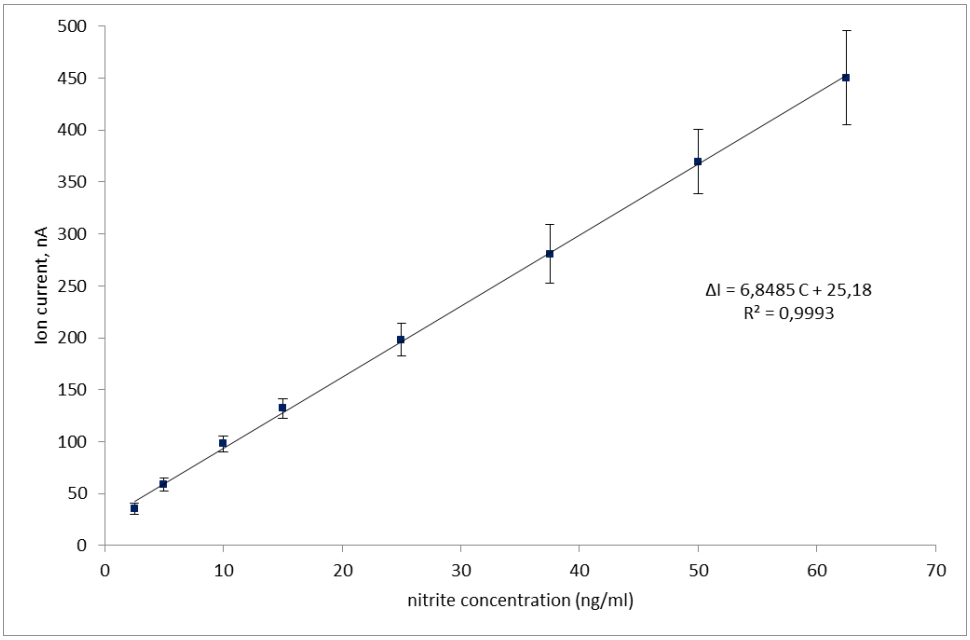

Figure 31. Calibration graph for nirite detection using metal-supported PC membranes incorporating methemoglobin (10 μg/ml, concentration in bulk). Experimental conditions: pH 6.5; 0.5 mm Teflon coated Ag wire; 0.1 KCl solution with HEPES, 25 ºC; calibration was performed by stepwise additions of nitrite standard solution under stirring. Error bars denote standard deviation (n=20).

The coefficient of determination (R^2) was 0.9993 (n=20) and the reproducibility of response was estimated to ±6-10% for within-day analyses (as relative standard error, n=20, 5.95% confidence limit). Between days and analysts precision was estimated over five days and three analysts for four nitrite concentrations (Table 4); two-way ANOVA results are also presented. A fresh sensor has been used for each analyst and day (i.e., each analyst used stepwise additions of nitrite to yield the response to the four concentrations tested), while the estimation of nitrite concentration in the bulk was based on the calibration graph of Fig. 31 (i.e., the sensor has not been re-calibrated). The results indicate the reproducibility of the response, with no positive or negative trend, indicative of standard errors and carryover effects; the error of measurement was <5% in all cases, whereas day or analyst significant effect has not been observed, as judged by the corresponding P-values.

The linear range was 2.5 – 62.5 ng/ml (as concentration in bulk), with a detection limit (as S/N = 3) of 0.9 ng/ml and a sensitivity of 6.85 nA per ng/ml nitrite concentration.

Table 4. Intermediate precision results for nitrite detection with the metal-supported lipid membrane biosensor incorporating 10 μg/ml methemoglobin (0.1M KCl buffered with HEPES, 0.5 mm diameter Teflon-coated silver wire, 25 °C)

Day	Nitrite (ng/ml)	Signal 1/ Analyst 1	Signal 2/ Analyst 2	Signal 3/ Analyst 3	Mean ± SD	Estimated nitrite concentration (ng/ml)	Error of measurement
1	2.5	45	42	39	42.0 ± 3.00	2.456	-1.76%
	10	90	98	95	94.3 ± 4.04	10.10	0.98%
	25	182	198	191	190.3 ± 8.02	24.12	-3.54%
	50	370	379	366	371.7 ± 6.66	50.59	1.19%
2	2.5	41	40	47	42.7 ± 3.79	2.553	2.13%
	10	90	88	97	91.7 ± 4.73	9.708	-2.92%
	25	192	200	198	196.7 ± 4.16	25.04	0.16%
	50	370	373	383	375.3 ± 6.81	51.13	2.26%
3	2.5	39	42	45	42.0 ± 3.00	2.456	-1.76%
	10	100	95	93	96.0 ± 3.61	10.34	3.41%
	25	188	200	195	194.3 ± 6.03	24.70	-1.20%
	50	395	365	382	380.7 ± 15.04	51.91	3.81%
4	2.5	45	41	39	41.7 ± 3.06	2.407	-3.71%
	10	103	98	100	100.3 ± 2.52	10.97	9.74%
	25	185	191	189	188.3 ± 3.06	23.82	-4.71%
	50	388	379	384	383.7 ± 4.51	52.35	4.69%
5	2.5	42	46	38	42.0 ± 4.00	2.456	-1.76%
	10	99	92	96	95.7 ± 3.51	10.29	2.92%
	25	198	190	196	194.7 ± 4.16	24.75	-1.01%
	50	345	368	356	356.3 ± 11.50	48.35	-3.29%

Two-way ANOVA results

2.5 ng/ml	Sum of squares	Degrees of freedom	Mean square	F (DFn, DFd)	P value
analyst	1.733	2	0.8667	(2,8)=0.06103	0.9412
day	1.600	4	0.4000	(4,8)=0.02817	0.9981
residual	113.6	8	14.20		

Source of variation	% of total variation	P value
analyst	1.482	0.9412
day	1.368	0.9981

10 ng/ml	Sum of squares	Degrees of freedom	Mean square	F (DFn, DFd)	P value
analyst	14.80	2	7.400	(2,8)=0.4703	0.6410
day	118.9	4	29.73	(4,8)=1.890	0.2057
residual	125.9	8	15.73		

Source of variation	% of total variation	P value
analyst	5.701	0.6410
day	45.81	0.2057

25 ng/ml	Sum of squares	Degrees of freedom	Mean square	F (DFn, DFd)	P value
analyst	122.1	2	61.07	(2,8)=2.922	0.1115
day	140.4	4	35.10	(4,8)=1.679	0.2467

residual	167.2	8	20.90		
Source of variation		% of total variation		P value	
analyst		28.42		0.1115	
day		32.67		0.2467	

50 ng/ml	Sum of squares	Degrees of freedom	Mean square	F (DFn, DFd)	P value
analyst	4.933	2	2.467	(2,8)=0.0211	0.9792
day	1368	4	342.1	(4,8)=2.929	0.0915
residual	934.4	8	116.8		
Source of variation		% of total variation		P value	
analyst		0.2138		0.9792	
day		59.30		0.0915	

Some drift of the ion current with time was noticed, especially at high nitrite concentrations and long use. The calibration of the sensor after 2 hours of continuous operation showed a 5% decrease in sensitivity; after 5 hours of continuous operation, sensitivity decreased to 45%. These results indicate that the sensor should not be used for more than 2 hours; considering the time required for sensor construction (16-23 min), the rate of analysis was estimated to 10 samples per hour for low nitrite levels and 3 samples per hour for medium-to-high nitrite levels. Since the lipid membrane platform exhibits higher stability (30h at ambient temperature), a number of lipid membrane platforms (without methemoglobin) can be simultaneously constructed and stored in order to increase daily run rates.

In order to investigate the reliability of measurement under continuous sensor operation, repeatability studies involved two sets of experiments: the first set utilized six freshly prepared sensors to assay 10 μl of nitrite standard solution; the second set utilized one sensor to assay six consecutive 10 μl injections of standard solution. Using the calibration graph of Fig. 31 (i.e., the sensor has not been re-calibrated), the coefficient of variation (as % relative standard deviation) obtained was 6.29% for the first set and 8.61% for the second set. The F-test results ($F = 1.888$, $F_{crit} = 5.05$, P-value = 0.5024) indicated no statistically significant differences between the two sets; the t-test results ($t = 0.09869$, $t_{crit} = 2.2282$) indicated that the difference of the mean values of the two sets was also not statistically significant. Thus, the sensor developed exhibits no statistically significant carryover effects and can be used for multiple analyses.

The detection limit achieved herein is 16 to 25 times lower than those reported by spectroscopic (Ensafi *et al*., 2004; López Pasquali *et al*., 2010; Sreekumar *et al*., 2003) or chromatographic methods (Michalski and Kurzyca, 2006) with comparable sensitivity. Compared to chemical microsensors (Pietrzak and Meyerhoff, 2009; Salimi

et al., 2008), the detectability of the lipid membrane sensor is 100 times lower and the sensitivity is higher by tenfold; compared to nanosensors (Pham *et al*., 2011) and biosensors (Chen *et al*., 2009; Dai *et al*., 2008; Ding *et al*., 2010; Liu and Ju, 2003; Liu *et al*., 2009; Silveira *et al*., 2010; Tepper, 2010), the detection limit of the methemoglobin sensor is 10 times lower and the sensitivity is higher by fivefold.

5.3.3 Sensor reversibility

As was stressed out during pH investigation (Fig. 30), the response of the sensor practically diminished at pH 8.0. After allowing for signal stabilization in response to 62.5 ng/ml nitrite in the bulk (the maximum nitrite concentration tested in this study), the sensing wire was removed from the electrochemical cell and immersed in pH 8.0 buffer (0.1M KCl with HEPES) for 5 min. When the sensing wire transferred in nitrite-free and methemoglobin-free electrolyte (pH 6.5), the ion current reduced to 25±2 nA, i.e., the background levels within 5-6 min (Fig. 32); the sensitivity of the sensor towards nitrites was not affected (within analytical error), clearly indicating insignificant or none protein desorption. Shorter washing times, settled ion current to higher values.

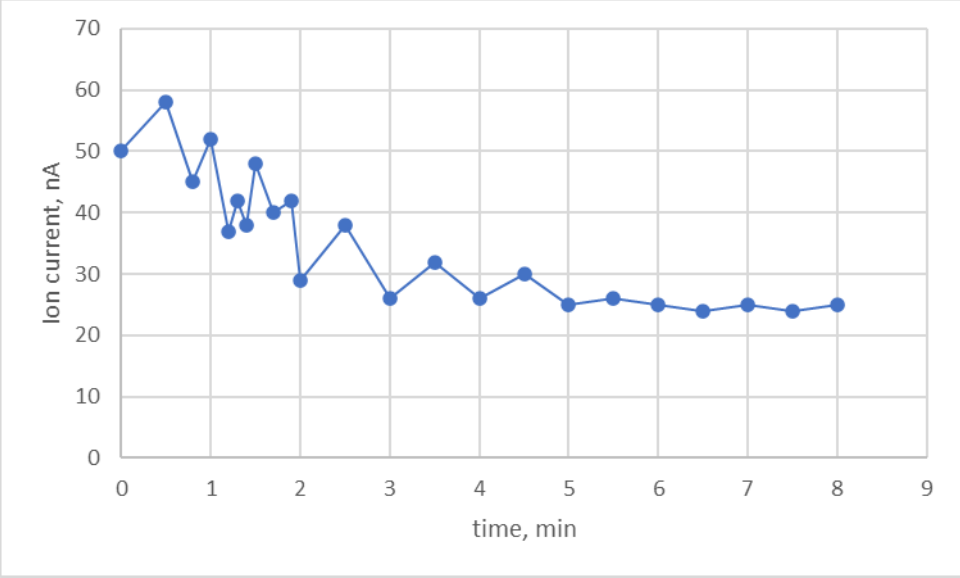

Figure 32. Recording obtained at re-immersing the sensing wire into pH 6.5 nitrite-free and protein-free electrolyte (0.1M KCl buffered with HEPES) after 5 min bathing at pH 8.0 (0.1M KCl buffered with HEPES).

The number of repetitive assays of high nitrite that could be achieved, including analysis, washing and re-stabilization, was 10 without observing any statistically significant reduction in signal magnitudes. The number of samples that could be assayed with the same sensor depended on nitrite concentration in the sample; at low

nitrite levels, the repetitive number of assays that could be performed with one sensor were 37.

5.3.4 Sensor validation

Possible interference from a number of anions (carbonates, phosphates, chloride, sulfates and sulfides) and cations (calcium, and magnesium ions) has been studied herein with simulated water samples, at varying composition and concentration. The simulation samples also contained nitrates and ammonium ions, as possibly present in an environmental sample; the mixture was supplemented by cyanides, for which methemoglobin has a known affinity (Siontorou and Nikolelis, 1997). The sensor exhibited high tolerance to interfering ions during simulation; the results showed a determinant error < 5% for bulk concentrations up to the high mM range (Table 5), either in mixtures or on their own.

Table 5.Nitrite sensor tolerance limits for interfering ions

Interferent	Max. tolerable concentration
Carbonates	87 μg/ml
Nitrates	620 ng/ml
Sulfates	96 μg/ml
Sulfides	320 ng/ml
Cyanides	260 ng/ml
Phosphates	950 ng/ml
Chloride	180 ng/ml
Calcium ions	400 ng/ml
Magnesium ions	240 ng/ml
Ammonium ions	120 ng/ml

Nitrite-spiked tap and lake water samples were used for validation studies. Spiked samples were freshly prepared from the nitrite stock solution and analyzed immediately. 10-ml tap water samples and 5-ml lake water samples were spiked with 0.5 μg/ml nitrite (the upper allowable EU level). A 0.1-ml assay volume was used. The same sensor was used to analyze all samples with a mean analysis rate of 37 samples/h (including regeneration); the calibration graph of Fig. 31 was used for quantitation (i.e., the sensor was not re-calibrated), taken into account the dilution factors.

Tap water did not affect the sensor; lake water increased noise levels by 30%, necessitating the increase of the detection limit to 2.02 ng/ml. Nitrite recovery in the tap water samples ranged between 95-102% (Table 6), with no positive or negative

trends, indicative of standard errors. For environmental samples, the acceptable range is 80-115% (ICH, 2005). Considering sample dilutions, the lowest nitrite concentration in tap water samples that could be reliably detected was 0.2 μg/ml. Recovery in lake water samples (Table 6) indicated a consistent positive trend, possibly due to matrix effects or nitrite already present in the sample. The maximum deviation was +8.6%, allowing for reliable detection of lake samples. Considering sample dilutions, the lowest nitrite concentration in lake water samples that could be reliably detected was 0.5 μg/ml.

Table 6. Validation results from the recovery of nitrite in water samples containing 0.2 μg/ml

sample	#	Nitrite detected with the sensor (μg/ml)	% Relative error
Tap water	1	0.479	-4.20%
	2	0.508	+1.60%
	3	0.485	-3.00%
	4	0.512	+2.40%
	5	0.473	-5.40%
Lake water	1	0.512	+2.40%
	2	0.536	+7.20%
	3	0.542	+8.40%
	4	0.543	+8.60%
	5	0.540	+8.00%

The performance of the sensor in soil and sediment samples has been also studied, following the extraction procedure described in Subchapter 4.4. The extract from the control (unspiked) soil sample did not produce any discernable electrode activity indicative of significant matrix effects, but increased noise level by 32%, setting the detection limit for soil extracts to 2.1 ng/ml. The soil simulated samples were spiked with 1 μg/ml nitrite ions that reached 2.5 ng/ml in the bulk, and 10 μg/ml that reached 25 ng/ml in the bulk. All samples were analyzed on the same sensor, regenerated when needed, and quantitated using the calibration graph of Fig. 31 (i.e., the sensor was not re-calibrated), taken into account the dilution factors.

The results are presented in Table 7. At low nitrite level, the mean % error was 5.48%, deviating from -7.6% to +9.0%; at high nitrite level, the mean % error was 2.61%, deviating from -3.73% to +5.03%. The reliability of measurements is very satisfactory, even at nitrite levels close to the detection limit. No positive or negative trends, indicative of standard errors, have been observed. Thus, the suitability of the sensor for

sediment and soil monitoring has been successfully demonstrated for soil levels of 2.1 μg/ml.

Table 7. Validation results from the recovery of nitrite in soil and sediment simulated samples

sample	#	nitrite detected with the sensor (μg/ml)	% Relative error
1 μg/ml	1	0.924	-7.60%
	2	0.982	-1.80%
	3	0.924	-7.60%
	4	1.041	+4.10%
	5	0.923	-7.70%
	6	1.090	+9.00%
	7	0.982	-1.80%
	8	1.042	+4.20%
10 μg/ml	1	10.09	+0.94%
	2	9.627	-3.73%
	3	10.27	+2.69%
	4	10.50	+5.03%
	5	9.802	-1.98%
	6	9.685	-3.15%
	7	9.743	-2.57%
	8	9.919	-0.81%

Nitrite accumulation has been observed in areas with increased precipitation, low temperatures that hinder biodegradation, and alkaline soil with high $N\text{-}NH_4^+$ content (Gelfand and Yakir, 2008). The site for real soil sampling (Subchapter 4.4) has been carefully selected to match these conditions: mean annual precipitation of 982 mm, temperatures < 12 ^oC for 4.5 months per year, soil pH 7.7, and over 10 years of extensive use of organic manure fertilization, assuring a high $N\text{-}NH_4^+$ content. Sampling was performed two months after the application of the fertilizer; within a half an acre area, six random samples were collected, at 30 cm below the surface, and stored in polyethylene bags. Three of these samples have been tested in a certified Laboratory, and the other three were transferred to the Laboratory of Simulation of Industrial Processes, where treated similarly to the simulated samples. The $N\text{-}NH_4^+$ content was determined by the certified Laboratory to be 10 μg/ml; this level was expected to interfere with the performance of the sensor (Table 5).

The nitrite results provided by the certified Laboratory, using the standard spectrophotometric nitrite test, were 32.1±1.15 mg/100 g soil (0.5% standard error). The nitrite results from the sensor developed herein were 33.1±1.55 mg/100 g soil (3.13% standard error); the slightly higher nitrite levels detected were possibly due to ammonium interference, but the performance of the sensor was proven reliable in analytical terms for environmental applications.

5.3.5 Evaluation of the results

The modeling methodology for determining critical environmental parameters has been proven suitable to handle complex biodegradation routes within the ecosystem.

The results presented herein for the metal-supported biosensor built on methemoglobin to quantitate nitrite indicate an improved performance over spectroscopic, chromatographic and biosensing techniques (Siontorou and Georgopoulos, 2016); such an approach has not been proposed in literature thus far and offers many advantages for environmental monitoring. Operational functionality and reliability have been also demonstrated using real environmental water and soil samples; the detection limits achieved were 0.2 μg/ml for tap water, 0.5 μg/ml for lake water and 2.1 μg/ml for soil, enabling environmental screening of nitrite at concentrations within and above the environmental limits. Although the results from the environmental samples obtained herein should be verified further with a more extended study, proof of concept has been provided and the nitrite sensor developed is readily applicable. The low operational stability (i.e., 2 hours of continuous operation without affecting reliability) can be compensated with electrode washing to reach an analysis rate of 37 samples/h.

Notwithstanding, the biosensor detection system developed herein is in fact a dual sensor, capable for the reliable detection of cyanides (at pH 8) and nitrites (at pH 6.5) at an interference-tolerant format. Such a system has not been demonstrated yet in literature, proving the high possibility of developing a flexible detector platform for ecosystem-specific and custom-tailored environmental biosensors.

5.4 Sensor miniaturization on nanotechnology-based transduction schemes

The ruggedness and stability of the metal-supported platforms developed herein are much improved as compared to the fragility of the lipid membranes in suspension (Nikoleli *et al.*, 2019) at the lowest possible performance compromise; nonetheless,

storage stability (practically 1 day in electrolyte) is not sufficient for cost-effective device development other than limited-shot probes. Further, the drivers to lipid membrane formation employed herein are not easily amenable to automation, thus sensor assembly may be considered quite trouble-some for routine analysis.

Supporting membranes on microfiltration filters yields a network of bilayers that form on the pores of the filter, without, however, improving sensor assembly and storage stability (Nikolelis and Siontorou, 1995; 1996). Methacrylate polymers provide smaller pores that guide the formation of bilayers through electrostatic forces and also maintain enough hydration to prevent membrane collapse outside the electrolyte (Nikolelis *et al.*, 2006;2008). The bioelements can be added to the lipid forming solution before polymerization. The membrane construction and bioelement integration process, described in Subchapter 4.3, is concluded within 6 hours; it has been found that polymerized bilayer-bioelement conjugates remain stable and functional after 1 month at storage. Membrane rehydration requires < 5 min and the sensor can be used for multiple assays.

These platforms are more appropriate for nanotransducer coupling (Nikolelis *et al.*, 2009). Graphene-based and zinc oxide-based nanostructures have demonstrated increased yields in terms of mechanical stability, thermal conductivity and surface-area-to-volume ratios to support rapid electron wiring (Walcarius *et al.*, 2013). Graphene nanosheets and zink oxides nanowalls have been investigated herein using the well-studied cholesterol oxidase – cholesterol interactions (Levitan *et al.*, 2010) with a view to evaluating efficacy, performance and efficiency for biosensor construction (Siontorou *et al.*, 2016). The various biosensor systems that have been proposed in literature, reported detection limits ranging between 0.77 ng/ml to 39 μg/ml (Narwal *et al.*, 2019); lipid membrane systems have reported lower detectabilities, ranging between 1.1 pg/ml to 1.35 ng/ml (Lawal *et al.*, 2018).

5.4.1 Sensor construction

An overview of the construction of the nanosensors and the biorecognition scheme employed herein are presented in Fig. 33. The cost and expertise required to fabricate both nanoelectrodes are comparable and presently quite high for bench-scale development. Graphene nanosheets were easier to handle than zinc oxide nanowalls, although the time required to prepare the graphene-based electrode was much longer.

In any case, both formats demonstrated similar standardization and scalability potential for mass production.

A successful lipid membrane platform has been demonstrated in both formats for 99% of the attempts. The reproducibility of the electrochemical response was found to be 18% higher for the graphene-based electrode. The zinc oxide-based platform yielded noise levels consistently higher by 15% than those recorded for the graphene-based formats, with a variability of 2.1-4.8% as compared to 2.5-3.1% for the graphene-based electrodes. Given that the detection limit is dependent on the noise levels of the sensor (estimated at S/N =3), the graphene-based formats are expected to provide lower detectabilities.

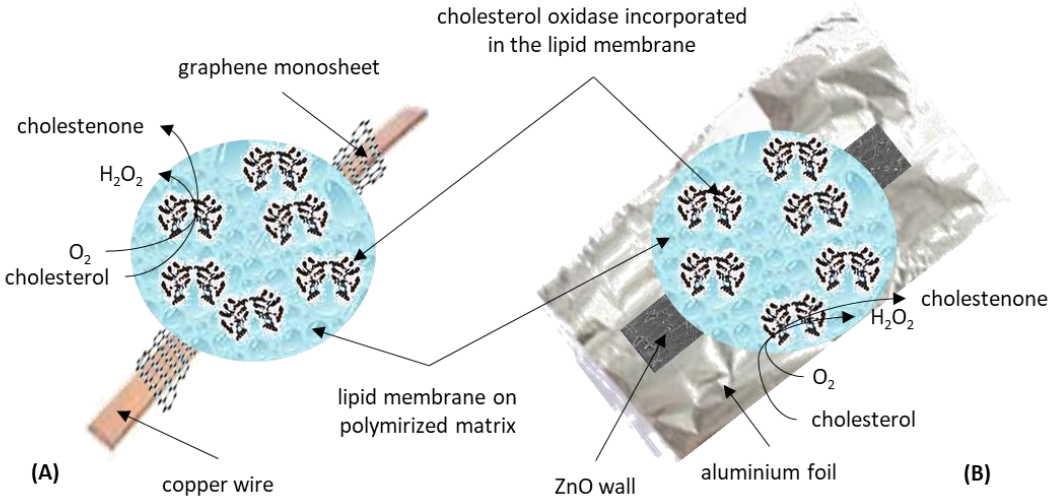

Figure 33. Schematic representation of the polymerized lipid membrane nanosensors that monitor the oxidation of cholesterol. (A) the graphene monosheet is wrapped around a copper wire and mounted on the cholesterol oxidase dopped membrane. (B) the ZnO nanowall is wrapped around aluminium foil and mounted on the cholesterol oxidase dopped membrane. Not drawn in scale.

Both formats proved quite rugged, with breakdown voltage values near 350 mV. The interactions between the two nanomaterials and the membrane or the membrane-bioelement conjugate differ substantially. The reproducibility of the electrochemical response and the low noise levels achieved with the graphene-based platforms could be due to the limited, but significant, anchoring of the lipids to graphene (Du *et al*., 2011); otherwise, graphene does not affect the membrane-bioelement interactions. Conversely, the ZnO nanoconstructs might not enhance membrane stability but they provide for better enzyme accommodation, since their successive positive and negative layering along the ZnO non-polar plane enhances protein adsorption to yield higher sensitivities (Psychoyios *et al*., 2013).

5.4.2 Sensor performance

Preliminary data suggests that the cholesterol oxidase dopped polymerized lipid membrane developed herein yielded comparable results to other biosensor systems for cholesterol detection. The higher surface area of the lipid bilayer network that forms in the polymer pores increases the number of analyte molecules available in the membrane electrolyte interface, thus improving sensitivity of response. Further, the biochemical interaction is known to force the membrane to shift phases to more packed forms that increase transmembrane ion flux (Levitan *et al*., 2010); the effect is amplified herein by the large number of bilayers in the membrane network. In total, the biochemical interaction and the transduction of the response are satisfactory, irrespective of the nanotransduction system used.

The addition of cholesterol yielded a potentiometric response within 5 s in both systems. All measurements involved the relative potential difference between the sensing and the reference electrode (Subchapter 4.2). Satisfactory linearity and acceptable stability have been achieved at pH 7.4 for both formats. The calibration graphs obtained for the two systems are presented in Fig. 34. The sensitivity of the graphene-based format was 64 mV per decade of cholesterol concentration, as compared to 57 mV per decade of cholesterol concentration achieved with the ZnO-based formats; the detection limit for the graphene-based format was 0.52 ng/ml, five times lower than that obtained with the ZnO-based system. The results suggest that graphene-based nanotransducers might be more advantageous to lipid membrane biosensors, the response of which critically depends on membrane-derived signal amplification. In platforms, however, critically dependent on protein activity, such as in immunoassays, the ZnO nanowalls might prove to be more appropriate.

Increasing the enzyme concentration to lower detectability did not produce remarkable results to either system. The response of graphene-based sensor was not altered significantly when the enzyme loading was doubled; the zinc oxide-based sensor demonstrated a slight increase in detectability but the noise level increased by 17%. Possibly, the immobilization of the enzyme occurring during membrane formation during the course of polymerization sets some thresholds on enzyme-lipids ratios.

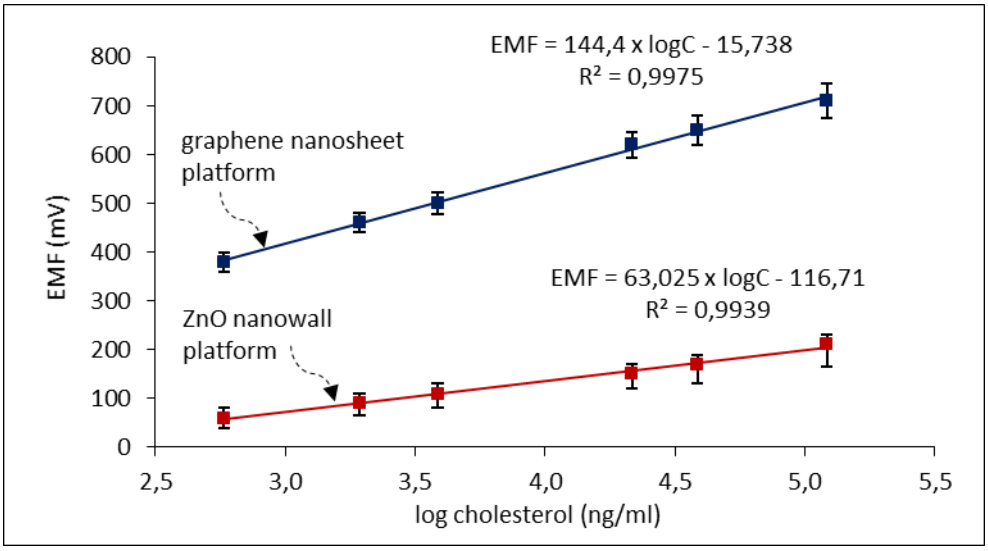

Figure 34. Calibration graphs for the potentiometric response of graphene nanosheets-based and ZnO nanowalls-based cholesterol oxidase lipid membrane biosensors towards cholesterol (pH 7.4 buffered with PBS, 7.5 U of enzyme, 25 °C).

In order to evaluate the reproducibility and the stability of the two formats, five sensors per format have been tested within the same day and one sensor per format has been tested for 4 weeks (kept refrigerated when not in use). The within day reproducibility was similar for both formats; the maximum variability recorded was 3.3% and 5.8% for the graphene-based and the ZnO nanowalls-based formats, respectively. The electrochemical activity of both formats after 4 weeks was satisfactory, indicating a 7.6% drift in the graphene-based sensor and a 11.2% drift in the zinc oxide nanowalls-based sensor.

Sensor reversibility has been investigated herein using washing at high flow rates. At low flow rates, the time required to regenerate the sensor was ca. 15 min for both sensors. At high flow rates, the regeneration time dropped to 1 min, but at the expense of enzyme leaching; further, substantial increase in noise levels has been recorded with the ZnO nanowalls-based sensor for flow rates >2. The best results have been obtained with flow rates 2.5 ml/min for the graphene-based system (2 min) and 1.7 ml/min for the zinc oxide nanowalls-sensor (3 min). The maximum number of assays that could be performed, at an acceptable level of accuracy, was 10 for the graphene-based sensor, irrespective of the cholesterol level, whereas the ZnO nanowalls-based sensor could be used for 6 assays at the low-to-medium cholesterol levels and 4 assays at the high concentration levels.

5.5 Technology evaluation

5.5.1 Metal-supported platforms

The methodological framework proposed herein for biosensor development supported by aquatic modelling and built on an engineering process basis has been proven suitable to guide the construction of detectors for applicability. One generic lipid membrane platform has been dopped with different bioelements and adjusted to the needs of target-analytes of environmental concern to yield different sensors. The design criteria for environmental-relevant and site-specific biosensors for monitoring aquatic ecosystems (Fig. 15) are sufficient for a thorough evaluation of the systems produced, as well as for the identification of the parameters that need improvement or modification.

The manufacturability criteria have been met for the three sensors developed herein. The generic metal-supported lipid membrane platform is easily and reproducibly constructed by minimally trained personnel, whereas the physical chemistry of the membrane offers a bioelement-compatible environment and a built-in signal amplification tool. Bioelement incorporation through physisorption might not be material-effective but it is definitely easy, reproducible over a large number of sensors and reliable over long period of time; the validation studies described herein have not used sensor re-calibration for a large number of operating sensors. The best results have been obtained with the 0.5 mm sensing wire, although the results from the 0.1 mm sensing wire were quite acceptable for sensing but made experimentation difficult; quite possibly circuitry modifications might solve noise problems at smaller diameters.

The analytical performance criteria have been met for phenols and nitrites but not for peroxides, since the detection limit achieved for the latter was not suitable for environmental needs. Notwithstanding, the bioelement-transducer system in the three sensors could be easily controlled with macro-parameter adjustments, namely pH, to tune selectivity (e.g., nitrites over cyanides) and sensor regeneration for multiple analyses. All systems developed exhibited a high tolerance to interference without the need for sample pretreatment or other laborious strategies.

The fitness-for-purpose criteria have been met only for nitrites, since suitability for PAHs and phenolics has not been investigated herein; however, the easy and quick regulation of chemistry and biochemistry has been demonstrated for all systems developed. Assay times (ca. 5 min for water samples) and sample volumes (5-10 μl)

for both, phenols and nitrites, are suitable for routine analysis with the inclusion of electrode washing into the assay protocol. If needed, sensor re-construction is easy, it can be performed in advance and the membrane platform can be stored for > 30h without the bioelement. In any case, the operational lifetime for the sensor is limited to one working day and the storage stability, dependent on the bioelement, to a few hours. The analytical range achieved is quite suitable to serve the environmental norms; higher sample concentrations can be assayed with further sample dilution.

Cost issues for mass production have been considered for the bench-scale set-up used herein. Metal-supported platforms are reproducible, with simple instrumentation at an affordable cost and easily-acquired expertise. Extremely accurate laboratory set-ups can be built at 6,500-8,000 €. Further, the time required to complete analytical investigations may be considered short to medium, as compared to other analytical techniques, such as spectroscopy or chromatography, where the preparation of the system requires longer times.

Marketability criteria have not been considered herein. A competitive advantage for niche applicability has been demonstrated for the bench-scale set-up, but miniaturization and design for mass production have not been investigated in depth. Preliminary results suggest that the electrochemical cell can be downsized to 10 ml or 5 ml and 1 μl sample injectors can be used. Further reduction requires thinner sensing wires but noise compensation should be addressed. Chip integration or screen printing might not be feasible given the lipid membrane self-assembly process employed herein; microelectromechanical technology and microfluidics might decrease the sensor to hand-held size, but automation on lipid membrane formation might not be feasible.

Nonetheless, the construction of versatile, adjustable, tunable, and even dual biosensors has been demonstrated on the same platform; although much work is still required to convert the sensors developed into field detectors, on-the-go multi-analyte monitoring might be feasible within reach.

5.5.2 Nanosensor platforms

The study presented herein, although limited and preliminary, indicated the feasibility of sensor miniaturization on nanotrasduction systems using polymerized lipid membrane platforms. The stability at storage of these membranes (i.e., one month) is

quite satisfactory for applicability, especially because the results refer to the entire biosensor (bioelement included) and not just the membrane platform.

The performance of the nanosensor is comparable to the metal-supported sensor, although the regulation of sensitivity and selectivity is not as simple. The method for membrane formation and for bioelement immobilization is not similar, requiring some expertise, longer times, and more elaborate and careful lipid-bioelement ratio estimations. The metal-supported platforms are amenable to modifications at any time and even during operation, whereas the nanosensors are not. Further, the cost of nanomaterials is a point to consider, although their cost is expected to decrease in the near future (Singh *et al.*, 2017).

Sample throughput has not been increased, despite expectations. Still, a single sensor is a limited-shot device, even if regenerated. In addition, the detection limit has not reached pico-levels. Apparently, the lipid membrane platform has no margin for far-reaching improvements.

Notwithstanding, the nanosensors can be readily integrated into a chip without the need for complicated microfluidics. It seems that the graphene nanosheets are more compatible with the lipid bilayer and more suitable for monitoring enzyme interactions than zinc oxide nanowalls. Granting a significant potential for lab-on-chip development, both systems require further investigation and optimization.

6. Biosensors technological frame

Biochemical processes have a significant role to play in analysis and diagnosis. The need to qualitate and quantitate natural and chemical mixtures prompted the development of analytical methods and relevant instrumentation. Detection, in a fairly large percentage of cases, necessitates some kind of conversion of biological data into analytical information. The pertinency and the opportunity for biosensing is apparent, although not seized appropriately. Through a time span of 50 years (1970-2020), the number of biosensor papers in the Web of Science database reached 28,812, whereas 254,000 papers are retrieved from the Google Scholar database; the number of patent applications for the same period (Google Patents) is 159,844; the number of commercial biosensors available until 2020 were 178 (Casquillas and Houssin, 2020). As evident, less than 0,1% of biosensor research has reached the market, while, roughly, 12% of chemical sensor, 8.7% of chromatographic, 16.3% of spectroscopic and 17% of analytical biochemistry assays (such as ELISA) research have been translated into products.

The reasons are varied and related more to the scope of research than technology hurdles; after all, the high technology adsorption capability observed in the domain of biosensors shifted research from macro-systems to micro-systems and then to nano-systems within only a decade, i.e., 1990-2000 (Siontorou and Batzias, 2014b). The lack of collaborative frameworks in the domain, limited on the one hand the possibility of problem solving and on the other hand the entry of research into the product realization phase to speed delivery to the marketplace (Siontorou and Batzias, 2014b).

The scientific and technological biosensor frames have been recently reviewed for cell-based biosensors (Siontorou, 2020); using the data search strategy described therein (i.e., multiple queries to handle multiple terminologies, data taxonomy and categories grouping), the work has been extended herein to profiling the university biosensor clusters, intra- and multi-disciplinary included, using a representative sample of 1680 papers (confidence level 95%, confidence interval 2.32) from the Web of Science Core Collection data to search the term: affiliation. The results are shown in Table 8, as the percentage of biosensor papers affiliated with a given infrastructure and co-affiliated within the same (intra-disciplinary) or a disparate (multi-disciplinary) infrastructure.

Table 8. The intra- and multi-disciplinarity index of biosensor research within the period 1970-2020

	analytical chemistry, general	analytical chemistry, sensors	biochemistry, cell biology	biochemistry, clinical chemistry	biochemistry, general	chemical engineering, biochemical mechanics	chemical engineering, environmental engineering	chemical engineering, general	chemical engineering, polymer science	electrical engineering, general	electrical engineering, microelectronics &nanoelectronics	electrical engineering, signal processing	mechanical engineering, biosystems	mechanical engineering, general	mechanical engineering, materials	microbiology, bioinformatics	microbiology, computational	microbiology, general	physical chemistry, general	physical chemistry, molecular and supramolecular	physical chemistry, nanostructures	physical chemistry, thermodynamics	Total
analytical chemistry, general	1.87%	2.29%					0.64%	0.17%			1.38%	0.44%	0.17%		0.22%				0.16%		0.16%	0.3%	7.94%
analytical chemistry, sensors	2.29%	1.87%				0.37%	0.76%		0.12%		1.03%	0.64%	0.44%		0.33%	0.12%	0.12%		0.14%	0.51%	0.51%	0.44%	9.76%
biochemistry, cell biology			0.93%	0.61%	0.32%		0.37%					0.37%	0.15%			0.27%	0.08%	0.09%			0.01%		3.24%
biochemistry, clinical chemistry			0.93%	1.15%	0.46%	0.25%		0.03%			0.40%	0.15%	0.23%		0.33%	0.13%	0.03%	0.09%		0.56%	0.71%	0.40%	5.91%
biochemistry, general			0.59%	0.56%	2.55%	0.57%	0.79%					0.19%						0.29%		0.29%			5.86%
chemical engineering, biochemical mechanics		0.16%		0.12%	0.22%	0.57%	0.41%	0.22%	0.05%	0.08%	0.14%	<0.01	0.09%	0.07%	0.07%		0.07%					0.20%	2.55%
chemical engineering, environmental engineering	0.53%	0.63%	0.51%			0.78%	1.08%	0.42%	0.03%				0.39%	0.05%	0.27%	0.20%	0.20%	0.12%				0.03%	5.29%

	analytical chemistry, general	analytical chemistry, sensors	biochemistry, cell biology	biochemistry, clinical chemistry	biochemistry, general	chemical engineering, biochemical mechanics	chemical engineering, environmental engineering	chemical engineering, general	chemical engineering, polymer science	electrical engineering, general	electrical engineering, microelectronics &nanoelectronics	electrical engineering, signal processing	mechanical engineering, biosystems	mechanical engineering, general	mechanical engineering, materials	microbiology, bioinformatics	microbiology, computational	microbiology, general	physical chemistry, general	physical chemistry, molecular and supramolecular	physical chemistry, nanostructures	physical chemistry, thermodynamics	Total
chemical engineering, general	0.09%			0.02%		0.27%	0.27%	0.95%	0.14%		0.07%	<0.01	0.07%			0.06%					0.04%	0.04%	2.08%
chemical engineering, polymer science		0.09%				0.08%	0.03%	0.21%	1.16%						0.48%								2.08%
electrical engineering, general						0.03%				0.24%	0.20%	0.20%	0.04%	0.03%	0.04%								0.81%
electrical engineering, microelectronics & nanoelectronics	0.57%	0.43%		0.18%		0.14%		0.05%		0.53%	0.84%	0.84%	0.74%	0.26%	0.42%					0.26%	0.26%	0.07%	5.68%
electrical engineering, signal processing	0.28%	0.4%	0.39%	0.11%	0.11%	<0.01		<0.01		0.82%	1.30%	1.62%	0.57%	0.41%		0.65%	0.65%			0.41%	0.17%	0.02%	7.99%
mechanical engineering, biosystems	0.06%	0.17%	0.09%	0.09%		0.08%	0.18%	0.05%		0.11%	0.70%	0.34%	0.73%	0.25%	0.25%	0.20%	0.09%	0.09%		0.13%	0.10%	0.01%	3.82%
mechanical engineering, general						0.01%	<0.01			0.02%	0.07%	0.07%	0.07%	0.19%	0.19%	<0.01					0.03%	<0.01	0.69%
mechanical engineering, materials	0.09%	0.14%		0.15%		0.06%	0.13%		0.27%	0.12%	0.43%		0.22%	0.75%	0.85%			0.09%		0.16%	0.16%	0.01%	3.7%

	analytical chemistry, general	analytical chemistry, sensors	biochemistry, cell biology	biochemistry, clinical chemistry	biochemistry, general	chemical engineering, biochemical mechanics	chemical engineering, environmental engineering	chemical engineering, general	chemical engineering, polymer science	electrical engineering, general	electrical engineering, microelectronics &nanoelectronics	electrical engineering, signal processing	mechanical engineering, biosystems	mechanical engineering, general	mechanical engineering, materials	microbiology, bioinformatics	microbiology, computational	microbiology, general	physical chemistry, general	physical chemistry, molecular and supramolecular	physical chemistry, nanostructures	physical chemistry, thermodynamics	Total
microbiology. bioinformatics		0.05%	0.21%	0.07%			0.12%	0.05%				0.49%	0.12%	0.01%		1.39%	1.11%	0.29%		0.38%			4.36%
microbiology. computational		0.02%	0.02%	<0.01		0.02%	0.04%					0.17%	0.04%			0.38%	0.42%	0.38%		0.10%	0.10%		1.74%
microbiology. general			0.04%	0.03%	0.07%		0.04%								0.06%	0.18%	0.68%	0.75%					1.89%
physical chemistry. general	0.25%	0.21%																	0.99%	1.50%	1.46%	1.80%	6.25%
physical chemistry. molecular and supramolecular		0.25%		0.30%	0.12%						0.31%	0.31%	0.16%		0.19%	0.38%	0.30%		0.47%	1.13%	0.99%	0.57%	5.55%
physical chemistry. nanostructures	0.15%	0.42%	0.02%	0.64%				0.06%			0.53%	0.22%	0.22%	0.24%	0.32%		0.51%		0.78%	1.67%	2.08%	0.77%	8.68%
physical chemistry. thermodynamics	0.21%	0.25%		0.25%		0.26%	0.02%	0.04%			0.09%	0.02%	0.02%	0.01%	0.01%				0.66%	0.66%	0.53%	1.04%	4.13%

The findings of this work, differ significantly from previous studies on the biosensor domain that utilized data until 2013 (Siontorou and Batzias, 2014b). As evident, the availability of the nanotools and 3D printing thereafter attracted the attention of more researchers and prompted collaborations within and between different disciplines.

The academic departments that host biosensor research are shown in Fig. 35. Analytical chemistry, general and sensors, accounts for 17.7% of the papers published. Until 2014, this sector was responsible for >46% of the research, owing to the well-established infrastructure inherited by chemical sensors (Siontorou and Batzias, 2014b). In fact, biosensors have been limited to the scopes of chemical sensing for more than 30 years, prohibiting transdisciplinarity, i.e., the creation of a new intellectual framework beyond the disciplinary perspectives. The intra-disciplinarity of the sector remains high, accounting for 23.56% of research (Table 8), as well as its link to physical chemistry for determining the underlying thermodynamics of biochemical reactions. A multi-disciplinary trend started to emerge after 2015, necessitated from both, sensor architecture and problem solving; collaborations occurred with chemical engineering (11.8%), mostly on environmental engineering, electrical engineering (19.8%), mostly on micro- and nano-electronics, and mechanical engineering (7.28%), mostly on biosystems. Microfabrication and nanotechnology have definitely shifted the analytical chemistry scope towards innovations in fabrication.

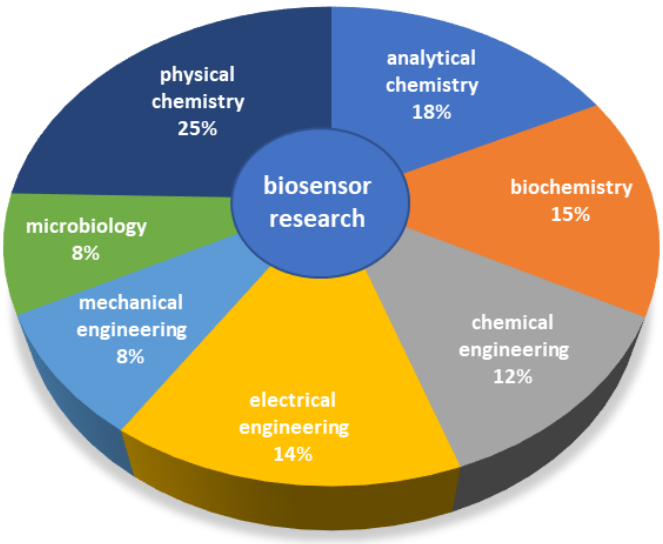

Figure 35. The academic departments that support biosensor research. Data from the Web of Science Core Collection for the period 1970-2020.

The biochemistry sector, including mainly general, cell biology and clinical chemistry, produced 15.01% of research (Table 8), retaining its strong multi-disciplinary profile and the focus in modeling of natural systems; the percentage of monitoring applications that come from this sector is comparable-to-lower than that observed in the earlier study (Siontorou and Batzias, 2014b).

The biosensor systems that have been proposed from the chemical engineering sector have reached 12% of publications (Table 8) and refer mostly to environmental and industrial applications; a sharp 6.5% increase has been noted after 2016. Collaborations with mechanical engineering, materials and biosystems, enhanced by 36.6% since 2013 (Siontorou and Batzias, 2014b), to get hold of modelling design information, packaging and rapid manufacturing. Electrical engineering, on the other hand, retains its high share in microelectronics and nanoelectronics, accounting for 14.48% of biosensor papers; after 2015, 63.12% of publications refer to nanonesing formats.

Mechanical engineering, involving mainly biosystems and materials, demonstrated a remarkable biosensor research share as self-publications, reaching 43% of the sector's papers (Table 8). The interest of the sector to biosensor development becomes significant after 2010, indicating a shifting of the biosensors' domain focus towards process engineering and prototyping; this involvement might foretell the emergence of biosensor systems in the market.

Microbiology, general, bioinformatics and computational, turned into self-publishing after 2013. The sector accounts for 7.99% of total biosensor publications, 70% of which refer to intra-disciplinary teams (Table 8). Still, the sector focuses mostly on cellular and sub-cellular modelling than detection; a similar profile has been observed in the earlier study (Siontorou and Batzias, 2014b).

Physical chemistry, mainly molecular and supramolecular, nanostructures and thermodynamics, has demonstrated a significant participation in biosensor research, reaching 24.61% (Table 8). It is worthwhile noticing that, such an active involvement of physical chemistry has not been seen in the biosensor domain since the late 1960s to mid-1970s (Siontorou and Batzias, 2014b). Strongly multi-disciplinary, the self-publication percentage of 46.32% of the sector's total share, indicates a pressing need to study the entropy of the nanoscale.

In effect, this study identified the progress made in extending the biosensor hub, attracting new players, and slightly shifting towards ready-to-market designing; the technology base has evolved significantly, but the renewed interest of the physical chemistry sector definitely indicates necessary revisions of the science-base. In view of the above, the predicted rate of biosensors reaching the market (Manjrekar and Sumant, 2018) may not be verified.

6.1 The transition from research to market

Besides glucose sensor, a number of biosensor analyzers and probes have reached the market. The main goal of industry is the development of low-cost and multiple-analytes devices for on-site diagnosis. Today North America holds the largest production units for biosensor analyzers while Europe comes first for lab-on-a-chip production (MarketsandMarkets Press, 2019). The industrial development of biosensors requires intensive R&D and large investments; it has been estimated that biosensors for clinical diagnostics require 10 years of R&D and 35-40 million USD to launching (Smit, 2006). There is a quite long and difficult course from the lab to industrial production, involving significant modifications to the systems proposed by the academia in order for biosensors to meet the needs of the market.

In general, R&D may deal with the development of a new product to fulfill the expectations of the end-users or the re-design of a product to optimize capabilities and cost (Casquillas and Houssin, 2020) (Fig. 36). The value cycle becomes critical to development, referring to the engineering value, i.e., whether and how the product can serve its intended purpose, and the analytical value that evaluates the relationship between the functions of the system and the cost required to build these functions during the production process (Temiz *et al*., 2015). Some trade-offs are eminent at this stage, mainly between system operation and value to the end-user; for example, the cost of supreme analytical advantages may not always correspond to user needs, especially when lower-cost alternatives are available.

Biosensor assembly and chip integration at large scales are usually multi-step and care-intensive processes (Fig. 36). 3D printing technology is used nowadays in integration, miniaturization and production, coupled with femtosecond laser-assisted etching to assure the required precision manufacturing (Tsao, 2016). A major complication in chip fabrication comes for the biochemical system; a new and emerging trend in

industry is the development of *in situ* polymerization of biological moieties for enhancing the compatibility between the inorganic parts assembly and the vulnerability of the organic components (Tsao, 2016).

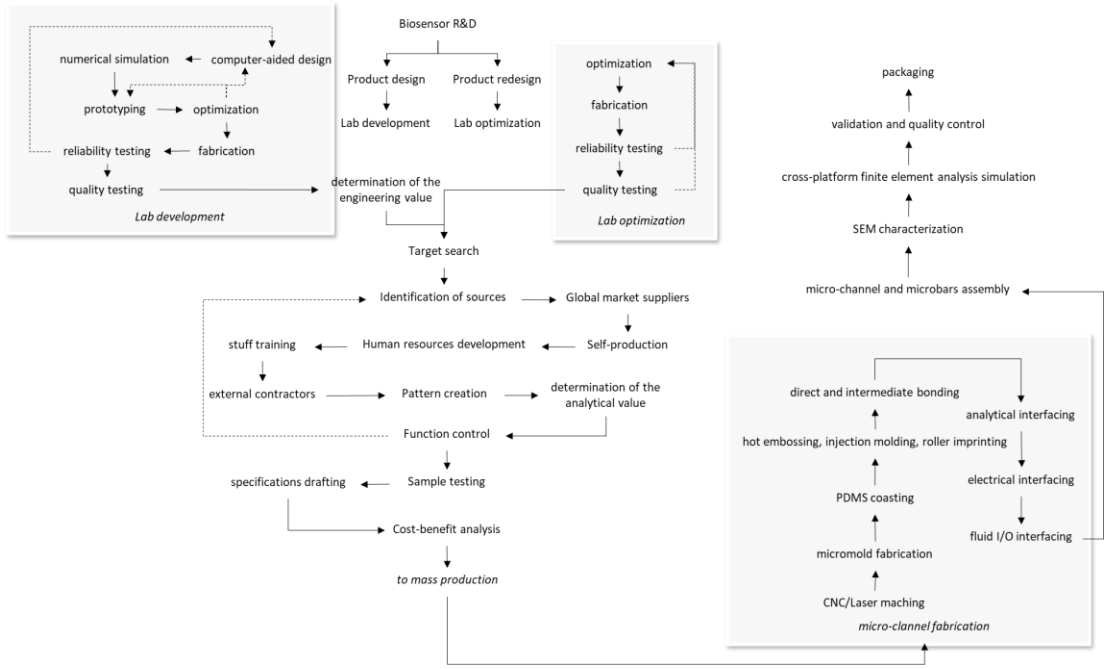

Figure 36. An overview of the R&D and mass production of lab-on-a-chip biosensors. The flow chart was created with data collected from Casquillas and Houssin, 2020, Temiz et al., 2015, and Tsao, 2016.

6.2 Worldwide market

The market for biosensors is growing, but it is still narrow despite the innovations produced; market penetration is slow, mainly due to limited patenting by the academia (Manjrekar and Sumant, 2018). Nonetheless, a biosensor may need ca. 10 years to launching (Smit, 2006) and probably 8-10 more years before any reasonable profit is seen (Manjrekar and Sumant, 2018). It is therefore not surprising that high-profile corporations dominate the biosensor market. The acquisition of Biacore, the first company to manufacture and market surface plasmon resonance biosensors, by General Electric in 2006, is a pertinent example.

Presently, biosensors have reported most revenues from electrochemical and optical systems. Market shares have grown within 2003 to 2018 (MarketsandMarkets, 2019) but not considerably, whereas a turn-down appeared in annual growth rate from 2009 to 2012 (Fig. 37). The clinical diagnostics market represents almost 48% of the total biosensor market (MarketsandMarkets, 2019). Roadmaps generally predict that the medical market will continue to increase, while security and biodefense may become

important sources of revenue for the industry in the near future (Manjrekar and Sumant, 2018).

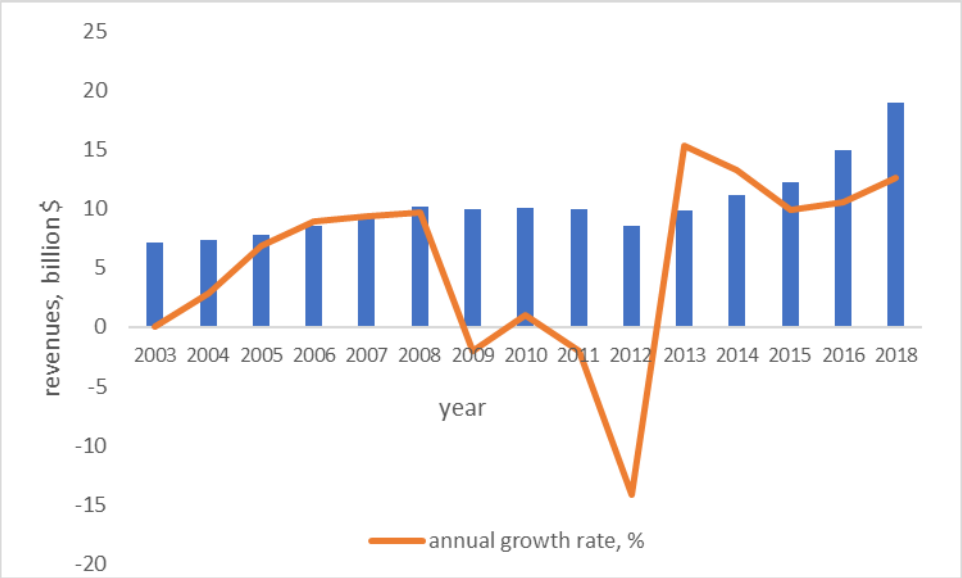

Figure 37. Revenues and annual growth rate (AGR) of biosensors market 2003–2018

The biosensor market is currently part of the sensors market, with chemical sensors being direct competitors. The global market for sensors reached 138.9 billion $ in 2018 at an annual growth rate of 9.5% (Patil, 2018). Biosensor revenues represent an average of 15.74% of the total sensors market (Fig. 38). Compared to sensors, the low marketability has been attributed to high production costs, availability of comparable alternative technologies, stability issues and quality assurance issues.

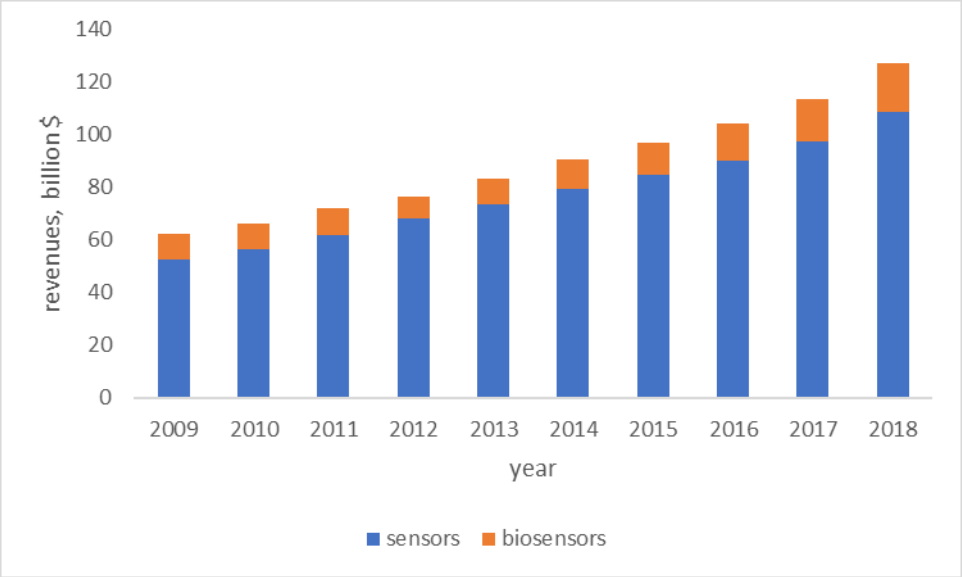

Figure 38. Sensors and biosensors global market revenues for the period 2009-2018.

Opportunities for biosensors rise from the point-of-care and point-of-testing demands using portable and integrated devices (Manjrekar and Sumant, 2018); pollution increase worldwide may also boost environmental markets. Electrochemical biosensors are expected to grow at faster rates until 2026, while China might take the lead in biosensor production over North America (MarketsandMarkets, 2019).

In view of the above, the strategy deployed herein for biosensor development utilizing fit-for-purpose criteria to yield target- and environment-specific electrochemical biosensors for niche applicability might prove beneficial to accelerate and improve biosensor penetration into the market.

7. Conclusions

The work presented herein implemented a novel strategy for the design and development of biosensors for monitoring aquatic ecosystems based on built-in environmental constrains and techno-economic criteria.

Modelling of aquatic systems utilized an ontological platform to define and project critical interactions at different scales, like mass and energy exchanges, within a given ecosystem. Starting with the description of the system, considered as a natural and economic environment with many stakeholders, and moving to functional and systemic analysis, the governing interfaces are revealed, the monitoring of which could provide a reliable assessment for the fate of pollutants and stressors, occurring or transpiring, in the ecosystem. This modelling process has been proven successful in identifying the critical stressors of the southwest shorelines of Attiki, as well as in predicting the course of events for the oil spill from the tanker Agia Zoni in the Saronic Gulf.

Further, the local stress- or anti-stress response mechanisms of the ecosystem have been used as molecular tools for developing tailored-to-the-environment biosensor systems. The development of such systems on the basis of their intended use and their evaluation under real environmental conditions and samples has not been reported before in literature.

Three novel biosensors have been constructed herein on peroxidase-peroxide interactions, as a proof-of-principle model for the detection of polycyclic aromatic hydrocarbons, priority pollutants for waters and sediments, tyrosinase-phenol interactions, as a proof-of-concept sensor for the detection of the widely distributed and highly toxic phenolic and polyphenolic compounds, and methemoglobin-nitrite interactions for the detection of nitrites in water and sediments; the latter is, in fact, a dual sensor, since methemoglobin can be also used for the detection of cyanides. The analytical performance of the tyrosinase-phenol and the methemoglobin-nitrite sensors was very satisfactory as per selectivity, sensitivity, detection limit, and analytical range. The peroxidase-peroxide sensor yielded detection limits higher than those reported for similar technology systems; further, the limited, but significant, interactions observed between the lipid bilayer and peroxide might complicate the upgrade of the system for polycyclic aromatic hydrocarbons. Nonetheless, the bioelement-membrane-transducer system in all biosensors developed herein could be easily controlled with macro-

parameter adjustments, namely pH, to tune selectivity (e.g., nitrites over cyanides) and sensor regeneration for multiple analyses. All devices produced exhibited a high tolerance to interference and matrix effects without the need for sample pretreatment or other laborious strategies.

The replacement of the metal-supported lipid platform with polymerized membranes and the conversion of the transducer to zink oxide nanowalls or graphene nanosheet electrodes yielded nanoplatforms readily amenable to downsizing. Although limited and preliminary, this study indicated a substantial improvement in sensor stability at storage; the entire biosensor (bioelement included) could be stored for one month at 0-4 ^{o}C without reducing functionality or affecting operability. The performance of the nanoplatforms was comparable to the metal-supported sensors, although the regulation of sensitivity and selectivity was not as simple. Due to the nanosensor architecture, the protocols for membrane formation and bioelement immobilization differ significantly than those applied to the metal-supported platform, requiring more expertise, longer times, and more elaborate and careful lipid-bioelement ratio estimations. The metal-supported platforms were amenable to modifications at any time and even during operation, whereas the nanoplatforms were not. Further, the cost of nanomaterials is a point to consider, although their cost is expected to decrease in the near future.

In conclusion, the strategy deployed in this work for biosensor development utilizing fit-for-purpose criteria to yield target- and environment-specific electrochemical biosensors for niche applicability might prove beneficial to accelerate and improve biosensor penetration into the market as the biosensor opportunities highlighted in recent market reports, i.e., point-of-testing, portable and integrated devices, environmental applicability and electrochemical platforms, can be seized with the technology produced herein.

References

Adamski, J., Nowak, P., and Kochana, J., 2010. Simple sensor for the determination of phenol and its derivatives in water based on enzyme tyrosinase. *Electrochim. Acta*, 55, pp. 2363–2367.

Aloraefy, M., Pfefer, T.J., Ramella-Roman, J.C., and Sapsford, K.E., 2014. In vitro evaluation of fluorescence glucose biosensor response. *Sensors*, 14, pp. 12127-12148.

Álvarez, R., Ordóñez, A., Loredo, J., and Younger, P.L., 2013. Wetland-based passive treatment systems for gold ore processing effluents containing residual cyanide, metals and nitrogen species. *Environ. Sci. Proc. Imp.*, 15, pp. 2115-2124.

Anku, W.W., Mamo, M.A., and Govender, P.P., 2017. Phenolic compounds in water: sources, reactivity, toxicity and treatment methods. In Soto-Hernandez, M., Palma-Tenango, M., and del Rosario Garcia-Mateos, M. (Eds), *Phenolic Compounds - Natural Sources. Importance and Applications*, IntechOpen.

Arhonditsis, G.B., and Brett, M.T., 2004. Evaluation of the current state of mechanistic aquatic biogeochemical modelling. *Mar. Ecol.-Progr. Ser.*, 271, pp. 13-26.

Aziz, A., Asif. M.. Ashraf. G., Farooq, U., Yang. Q., and Wang, S., 2021. Trends in biosensing platforms for SARS-CoV-2 detection: A critical appraisal against standard detection tools. *Curr. Opin. Colloid In.*, 101418.

Bahadir, E.B., and Sezgintürk, M.K., 2015. Applications of commercial biosensors in clinical, food, environmental, and biothreat/biowarfare analyses. *Anal. Biochem.*, 478, pp. 107-120.

Balogun, A.-L., Yekeen, S.T., Pradhan. B., and Wan Yusof, K.B., 2021. Oil spill trajectory modelling and environmental vulnerability mapping using GNOME model and GIS. *Environ. Pollut.*, 268, 115812.

Barry, S., and O' Riordan, A., 2015. Electrochemical nanosensors: advances and applications. *Rep. Electrochem.*, 6, pp. 1-14.

Bashir, I., Lone, F.A., Bhat, R.A., Mir, S.A., Dar, Z.A., and Dar, S.A., 2020. Concerns and threats of contamination on aquatic ecosystems. *Bioremed. Biotechnol*., 27, pp. 1–26.

Batzias, F.A., and Siontorou, C.G., 2012. Creating a specific domain ontology for supporting R&D in science-based disciplines – The case of biosensors. *Expert Syst. Appl.*, 39, pp. 9994-10015.

Batzias, F.A., Siontorou, C.G., and Spanidis, P.M.-P., 2011. Designing a reliable leak bio-detection system for natural gas pipelines. *J. Hazard. Mater*., 186, pp. 35-58.

Benkovitz, A., Matthews, A., Teutsch, N., Poulton, S.W., Bar-Matthews, M., and Almogi-Labin, A., 2020. Tracing water column *Euxinia* in Eastern Mediterranean Sapropels S5 and S7. *Chem. Geol.*, 545, 119627.

Bennett, N.D., Croke, B.F.W., Guariso, G., Guillaume, J.H.A., Hamilton, S.H., Jakeman, A.J., Marsili-Libelli, S., Newham, L.T.H., Norton, J.P., Perrin, C., Pierce, S.A., Robson, B., Seppelt, R., Voinov, A.A., Fath, B.D., and Andreassian, V., 2013. Characterising performance of environmental models. *Environ. Model. Softw.*, 40, pp. 1-20.

Beutel, M.W., Horne, A.J., Taylor, W.D., Losee, R.F., and Whitney, R.D., 2008. Effects of oxygen and nitrate on nutrient release from profundal sediments of a large. oligo-mesotrophic reservoir, Lake Mathews, California. *Lake Reserv. Manag*., 24, pp. 18-29.

Bhalla, N., Jolly, P., Formisano, N., and Estrela, P., 2016. Introduction to biosensors. *Essays Biochem.*, 60, pp. 1-8.

Budi, S., Susanto, F., de Souza, P., Timms, G., Malhotra, V., and Turner, P., 2018. In search for a robust design of environmental sensor networks. *Environ. Technol.*, 39, pp. 683-693.

Burger, J., 2008. Environmental management: Integrating ecological evaluation, remediation, restoration, natural resource damage assessment and long-term stewardship on contaminated lands. *Sci. Total Environ.*, 400, pp. 6-19.

Casquillas, G.V., and Houssin, T., 2020. Introduction to lab-on-a-chip 2020: review, history and future. Microfluidic Reviews, ELVE Flow Microfluidics Innovation Centre.

Chen, H.-C., Wu, P.-C., Huang, J.-Y., and Chen, L.-A., 2010. Uncertainty analysis for measurement of measurand. *Measurement*, 43, pp. 1250–1254.

Chen, L.-C., Wang, E., Tai, C.-S., Chiu, Y.-C., Li, C.-W., Lin, Y.-R., Lee, T.-H., Huang, C.-W., Chen, J.-C., and Chen, W.L., 2020. Improving the reproducibility,

accuracy, and stability of an electrochemical biosensor platform for point-of-care use. *Biosens. Bioelectr.*, 155, 112111.

Chen, Q., Ai, S., Zhu, X., Yin, H., Ma, Q., and Qiu, Y., 2009. A nitrite biosensor based on the immobilization of cytochrome c on multi-walled carbon nanotubes-PAMAM-chitosan nanocomposite modified glass carbon electrode. *Biosens. Bioelectr.*, 24, pp. 2991-2996.

Clegg, J.R., Wagner, A.M., Shin, S.R., Hassan, S., Khademhosseini. A., and Peppas, N.A., 2019. Modular fabrication of intelligent material-tissue interfaces for bioinspired and biomimetic devices. *Progr. Mater. Sci.*, 106, 100589.

Cushing, D.H., 1983. The decline of the herring stocks and the gadoid outburst. *J. Cons. Int. Explor. Mer.*, 39, pp. 70-81.

Dai, Z., Bai, H., Hong, M., Zhu, Y., Bao, J., and Shen, J., 2008. A novel nitrite biosensor based on the direct electron transfer of hemoglobin immobilized on CdS hollow nanospheres. *Biosens. Bioelectr.*, 23, pp. 1869-1873.

Ding, Y., Wang, Y., Li, B., and Lei, Y., 2010. Electrospun hemoglobin microbelts based biosensor for sensitive detection of hydrogen peroxide and nitrite. *Biosens. Bioelectr.*, 25, pp. 2009-2015.

Du, D., Wang, L., Shao, Y., Wang, J., Engelhard, M.H., and Lin, Y., 2011. Functionalized graphene oxide as a nanocarrier in a multienzyme labeling amplification strategy for ultrasensitive electrochemical immunoassay of phosphorylated p53 (s392). *Anal. Chem.*, 83, pp. 746–752.

Duan, G., Zhang, Y., Luan, B., Weber, J.K., Zhou, R.W., Yang, Z., Zhao, L., Xu, J., Luo, J., and Zhou, R., 2017. Graphene-induced pore formation on cell membranes. *Sci. Rep.*, 7, 42767.

Duran, R., and Cravo-Laureau, C., 2016. Role of environmental factors and microorganisms in determining the fate of polycyclic aromatic hydrocarbons in the marine environment. *FEMS Microbiol. Rev.*, 40, pp. 814–830.

Dutt, J., and Davis, J., 2002. Current strategies in nitrite detection and their application to field analysis. *J. Environ. Monit.*, 4, pp. 465-471.

EC, 2007. European Communities (Drinking Water) (No. 2) Regulations. S.I. No. 278 of 2007, The Stationary Office, Dublin.

Ensafi, A.A., Rezaei, B., and Nouroozi, S., 2004. Simultaneous spectrophotometric determination of nitrite and nitrate by flow injection analysis. *Anal. Sci*., 20, pp. 1749-1753.

Evangeliou, N.H., Florou, H.M., and Scoullos, M., 2011. POC and particulate 234th export fluxes estimated using 234Th/238U disequilibrium in an enclosed Eastern Mediterranean region Saronikos Gulf and Elefsis Bay. Greece in seasonal scale. *Geochim. Cosmochim. Acta*., 75, pp. 5367-5388.

Fartas, F.M., Abdullah, J., Yusof, N.A., Sulaiman, Y., and Saiman, M.I., 2017. Biosensor based on tyrosinase immobilized on graphene-decorated gold nanoparticle/chitosan for phenolic detection in aqueous. *Sensors (Basel)*, 17, 1132.

Fiamegos, Y.C., Nanos, C.G., Pilidis, G.A., and Stalikas, C.D., 2003. Phase-transfer catalytic determination of phenols as methylated derivatives by gas chromatography with flame ionization and mass-selective detection. *J. Chromatogr. A*., 983, pp. 215-223.

Forsberg, M.M., Huotari, M., Savolainen, J., and Männistö, P.T., 2005. The role of physicochemical properties of entacapone and tolcapone on their efficacy during local intrastriatal administration. *Eur. J. Pharm. Sci*., 24, pp. 503–511.

Frihy, O.E., 2001. The necessity of environmental impact assessment (EIA) in implementing coastal projects: Lessons learned from the Egyptian Mediterranean coast. *Ocean Coast Manage.*, 44. pp. 489-516.

Galanopoulou, S., Vgenopoulos, A., and Conispoliatis, N., 2005. DDTs and other chlorinated organic pesticides and polychlorinated biphenyls pollution in the surface sediments of Saronikos Gulf. Greece. *Mar. Pollut. Bull.*, 50, pp. 520-525.

Gao, H., Scherson, Y.D., and Wells, G.F., 2014. Towards energy neutral wastewater treatment: methodology and state of the art. *Environ. Sci. Proc. Imp*., 16, pp. 1223-1246.

Gelfand, I., and Yakir, D., 2008. Influence of nitrite accumulation in association with seasonal patterns and mineralization of soil nitrogen in a semi-arid pine forest. *Soil Biol. Biochem.*, 40, pp. 415-424.

Georgopoulos, K.N., and Siontorou, C.G., 2016. A planar bilayer lipid membrane biosensor based on enzymes in the service of environmental monitoring. *Water Pollution XIII*.. 209. WIT PRESS.

Goetz, B.I., Shields, H.W., Basu, S., Wang, P., King, S.B., Hogg, N., Gladwin, M.T., and Kim-Shapiro, D.B., 2010. An electron paramegnetic resonance study of the affinity of nitrite for methemoglobin. *Nitric Oxide*, 22, pp. 149-154.

Gould, S.B., 2018. Membranes and evolution. *Curr. Biol*., 28, pp. 381–385.

Grieshaber, D., MacKenzie, R., Vörös, J., and Reimhult, E., 2008. Electrochemical biosensors - Sensor principles and architectures. *Sensors (Basel)*, 8, pp. 1400–1458.

Guan, H., Liu, X., and Wang, W., 2013. Encapsulation of tyrosinase within liposome bioreactors for developing an amperometric phenolic compounds biosensor. *J. Solid State Electrochem.*, 17, pp. 2887–2893.

Hanrahan, G., Patila, D.G., and Wang, J., 2004. Electrochemical sensors for environmental monitoring: design, development and applications. *J. Environ. Monit.*, 6, pp. 657-664.

Hesse, C., Krysanova, V., Päzolt, J., and Hattermann, F.F., 2008. Ecohydrological modeling in a highly regulated lowland catchment to find measures for improving water quality. *Ecol. Model.*, 218, pp. 135-148.

Hianik, T., 2011. Mechanical properties of bilayer lipid membranes and protein–lipid interactions. In Iglič, A. (Ed.), *Advances in Planar Lipid Bilayers and Liposomes*, Vol. 13, Academic Press, pp. 33-72.

ICH, 2005. *Validation of Analytical Procedures: Text and Methodology Q2(R1)*.

Ji, R., and Brune, A., 2006. Nitrogen mineralization, ammonia accumulation, and emission of gaseous NH_3 by soil-feeding termites. *Biogeochemistry*, 78, pp. 267–283.

Justino, C., Gomes, A.R., Freitas, A.C., Duarte, A.C., and Rocha-Santos, T., 2017. Graphene-based sensors and biosensors. *Trends Anal. Chem.*, 91, pp.53-61.

Kavita, V., 2017. DNA biosensors – A review. *J. Bioeng. Biomed. Sci.*, 7, 222.

Kiani, M.R., and Rahimpour, M.R., 2020. Aquatic/water environment contamination, treatment, and use. In Figoli, A., Li, Y., and Basile, A. (Eds), *Current Trends and Future Developments on (Bio-) Membranes*, Elsevier, pp. 213-238.

Knoke, T., and Seifert, T., 2008. Integrating selected ecological effects of mixed European beech–Norway spruce stands in bioeconomic modelling. *Ecol. Model.*, 210, pp. 487-498.

Kotis, K., Vouros, G. A., and Stergiou, S., 2006. Towards automatic merging of domain ontologies: the HCONE-MERGE approach. *Web Sem.*, 4, pp. 60-79.

La Rota Hernandez, C.E., Werberich, D.S., and D'Elia, E., 2008. Electroenzymatic oxidation of polyaromatic hydrocarbons using chemical redox mediators in organic media. *Electrochem. Commun*., 10, pp. 108-112.

Laanbroek, H.J., Bar-Gilissen, M.-J., and Hoogveld, H.L., 2002. Nitrite as a stimulus for ammonia-starved *Nitrosomonas europaea*. *Appl. Environ. Microbiol*., 68, pp. 1454–1457.

Lang, C., Mission, E.G., Fuaad, A.A.-H.A., and Shaalan, M., 2021. Nanoparticle tools to improve and advance precision practices in the Agrifoods Sector towards sustainability - A review. *J. Clean. Prod.*, 126063.

Larsen, L.H., Damgaard, L.R., Kjaer, T., Stenstrom, T., Lynggaard-Jensen, A., and Revsbech, N.P., 2000. Fast responding biosensor for on-line determination of nitrate/nitrite in activated sludge. *Water Res*., 34, pp. 2463–2468.

Laterreur, J., and English, A.M., 2007. Hemoglobin S-nitrosation on oxygenation of nitrite/deoxyhemoglobin incubations is attenuated by methemoglobin. *J. Inorg. Biochem.*, 101, pp. 1827-1835.

Lawal, A.T., 2018. Progress in utilisation of graphene for electrochemical biosensors. *Biosens. Bioelectr.*, 106, pp. 149-178.

Levitan, I., Fang, Y., Rosenhouse-Dantsker, A., and Romanenko, V., 2010. Cholesterol and ion channels. In: Harris, J. (eds), *Cholesterol Binding and Cholesterol Transport Proteins: Subcellular Biochemistry*, vol 51, Springer.

Liu, L., Jin, X., Yang, S., Chen, Z., and Lin, X., 2007. A highly sensitive biosensor with (Con A/HRP)n multilayer films based on layer-by-layer technique for the detection of reduced thiols. *Biosens. Bioelectr*., 22, pp. 3210-3216.

Liu, L., Xi, F., Zhang, Y., Chen, Z., and Lin, X., 2009. Selective analysis of reduced thiols with a novel bionanomultilayer biosensor based on the inhibition principle. *Sens. Actuators B Chem*., 135, pp. 642-649.

Liu, S., and Ju, H., 2003. Nitrite reduction and detection at a carbon paste electrode containing hemoglobin and colloidal gold. *Analyst*, 128, pp. 1420-1424.

Liu, Y., Gupta, H., Springer, E., and Wagener, T., 2008. Supporting sustainable water management: making environmental decisions for an integrated modeling approach. *Environ. Model. Softw.*, 23, pp. 846-858.

López Pasquali, C.E., Gallego-Picó, A., Fernández Hernando, P., Velasco, M., and Durand Alegría, J.S., 2010. Two rapid and sensitive automated methods for the determination of nitrite and nitrate in soil samples. *Microchem. J.*, 94, pp. 79–82.

Luka, G., Ahmadi, A., Najjaran, H., Alocilja, E., DeRosa, M., Wolthers, K., and Hoorfar, M., 2015. Microfluidics integrated biosensors: A leading technology towards lab-on-a-chip and sensing applications. *Sensors (Basel)*, 1512, pp.30011–30031.

Manjrekar, S., and Sumant, O., 2018. Biosensors market by product (wearable biosensors and non- wearable biosensors), technology (electrochemical biosensors, optical biosensors, piezoelectric biosensors, thermal biosensors, and nanomechanical biosensors): global opportunity analysis and industry forecast, 2019–2026. Allied Market Research Institute, Canada.

Marbà, N., Duarte, C.M., Holmer, M., Calleja, M., Álvarez, E., Díaz-Almela, E., and Garcias-Bonet, N., 2008. Sedimentary iron inputs stimulate seagrass (*Posidonia oceanica*) population growth in carbonate sediments. *Estuar. Coast. Shelf Sci.*, 76, pp. 710-713.

MarketsandMarkets, 2019. Biosensors market worth $31.5 billion by 2024. Press Releases, https://www.marketsandmarkets.com/ PressReleases/ biosensors.asp.

Martins, M.A.F., Requião, R., and Kalid, R.A., 2011. Generalized expressions of second and third order for the evaluation of standard measurement uncertainty. *Measurement*., 44, pp. 1526–1530.

Matthews, C.J., Andrews, E.S.V., and Patrick, W.M., 2021. Enzyme-based amperometric biosensors for malic acid – a review. *Anal. Chim. Acta*., 338218.

Mendes, P.M., 2008. Stimuli-responsive surfaces for bio-applications. *Chem. Soc. Rev.*, 37, pp. 2512-2529.

Michalski, R., and Kurzyca, I., 2006. Determination of nitrogen species (nitrate, nitrite and ammonia ions) in environmental samples by ion chromatography. *Pol. J. Environ. Stud.*, 15, pp. 5-18.

Mohanty, S.P., and Kougianos, E., 2006. Biosensors: a tutorial review. *IEEE Potentials*, 252, pp.35-40.

Morales, M.A., and Halpern, J M., 2018. Guide to selecting a biorecognition element for biosensors. *Bioconj. Chem.*, 29, pp. 3231–3239.

Motornov, M., Roiter, Y., Tokarev, I., and Minko, S., 2010. Stimuli-responsive nanoparticles, nanogels and capsules for integrated multifunctional intelligent systems. *Prog. Polym. Sci*., 35, pp. 174-211.

Narwal, V., Deswal, R., Batra, B., Kalra, V., Hooda, R., Sharma, M., and Rana, J.S., 2019. Cholesterol biosensors: A review. *Steroids*, 143, pp. 6-17.

Naveh, Z., Allen, E., Laszlo, E., and Antrop, M., 2007. *Transdisciplinary Challenges in Landscape Ecology and Restoration Ecology – An Anthology*, Springer, pp. 353-402.

Nayak, A.P., Katzenmeyer, A.M., Gosho, Y., Tekin, B., and Islam, M.S., 2012. Sonochemical approach for rapid growth of zinc oxide nanowalls. *Appl. Phys. A*., 107, pp. 661–667.

Nikoleli, G.-P., Israr, M.Q., Tzamtzis, N., Nikolelis, D.P., Willander, M., and Psaroudakis, N., 2012. Structural characterization of graphene nanosheets for miniaturization of potentiometric urea lipid film-based biosensors. *Electroanal*., 24, pp. 1285–1295.

Nikoleli, G.-P., Siontorou, C.G., Nikolelis, M.-T., Bratakou, S., and Bendos, D.K., 2019. Recent lipid membrane-based biosensing platforms. *Appl. Sci.*, 9, 1745.

Nikolelis, D., Ntanos, N., Nikoleli, G.-P., and Tampouris, K., 2008. Development of an electrochemical biosensor for the rapid detection of naphthalene acetic acid in fruits by using air stable lipid films with incorporated auxin-binding protein 1 receptor. *Protein Pept. Lett*., 15, pp. 789–794.

Nikolelis, D.P., and Siontorou, C.G., 1995. Bilayer-lipid membranes for flow-injection monitoring of acetylcholine. urea. and penicillin. *Anal. Chem*., 67, pp. 936-944.

Nikolelis, D.P., and Siontorou, C.G., 1996. Flow injection monitoring and analysis of mixtures of simazine, atrazine and propazine using filter-supported bilayer lipid membranes (BLMs). *Electroanal.*, 8, pp. 907-912.

Nikolelis, D.P., Raftopoulou, G., Nikoleli, G.-P., and Simantiraki, M., 2006. Stabilized lipid membrane based biosensors with incorporated enzyme for repetitive uses. *Electroanal*., 18, pp. 2467–2474.

Nishio, M., Teranishi, Y., Morioka, K., Yanagida, A., and Shoji, A., 2020. Real-time assay for exosome membrane fusion with an artificial lipid membrane based on enhancement of gramicidin A channel conductance. *Biosens. Bioelectr*., 150, 111918.

Olson, N., and Bae, J., 2019. Biosensors - Publication trends and knowledge domain visualization. *Sensors*, 19, 2615.

Oshima, A., and Sumitomo, K., 2017. Vesicle fusion with bilayer lipid membrane controlled by electrostatic interaction. *Biochem. Biophys. Rep*., 11, pp. 58–63.

Panjan, P., Ohtonen, E., Tervo, P., Virtanen, V., and Sesay, A.M., 2017. Shelf life of enzymatic electrochemical sensors. *Proc. Technol.*, 27, pp. 306-308.

Papageorgiou, N., Kalantzi, I., and Karakassis, I., 2010. Effects of fish farming on the biological and geochemical properties of muddy and sandy sediments in the Mediterranean Sea. *Mar. Environ. Res.*, 69, pp. 326-336.

Parinos, C., Hatzianestis, I., Chourdaki, S., Plakidi, E., and Gogou, A., 2019. Imprint and short-term fate of the Agia Zoni II tanker oil spill on the marine ecosystem of Saronikos Gulf. *Sci. Total Environ*., 693, 133568.

Patil., A., 2018. Sensor market by type (radar sensor, optical sensor, biosensor, touch sensor, image sensor, pressure sensor, temperature sensor, proximity & displacement sensor, level sensor, motion & position sensor, humidity sensor, accelerometer & speed sensor, and others), technology (CMOS, MEMS, NEMS, and others), and end user (electronics, IT & telecom, industrial, automotive, aerospace & defense, healthcare, and others): global opportunity analysis and industry forecast, 2012–2025. Allied Market Research Institute, Canada.

Paton, G.I., Reid, B.J., and Semple, K.T., 2009. Application of a luminescence-based biosensor for assessing naphthalene biodegradation in soils from a manufactured gas plant. *Environ. Pollut.*, 157, pp. 1643-1648.

Pawełczyk, A., 2012. Assessment of health hazard associated with nitrogen compounds in water. *Water Sci. Technol*., 66, pp. 666-672.

Peng, X., Wang, Z., Yang, C., Chen, F., and Mai, B., 2006. Simultaneous determination of endocrine-disrupting phenols and steroid estrogens in sediment by gas chromatography–mass spectrometry. *J. Chromatogr. A*., 1116, pp. 51-56.

Pham, X.-H., Li, C.A., Han, K.N., Huynh-Nguyen, B.-C., Le, T.-H., Ko, E., Kim, H.H., and Seong, G.H., 2011. Electrochemical detection of nitrite using urchin-like palladium nanostructures on carbon nanotube thin film electrodes. *Sens. Actuat. B,* 193, pp. 815–822.

Pietrzak, M., and Meyerhoff, M.E., 2009. Polymeric membrane electrodes with high nitriteselectivity based on rhodium(III) porphyrins and salophens as ionophores. *Anal.Chem*., 81, pp. 3637–3644.

Ponzoni, A., Zappa, D., Comini, E., Sberveglieri, V., Faglia, G., and Sberveglieri, G., 2012. Metal oxide nanowire gas sensors: application of conductometric and surface ionization architectures. *Chem. Eng. Trans.*, 30, pp. 31-36.

Psychoyios, V.N., Nikoleli, G.-P., Tzamtzis, N., Nikolelis, D.P., Psaroudakis, N., Danielsson, B., Israr, M.Q., and Willander, M., 2013. Potentiometric cholesterol biosensor based on ZnO nanowalls and stabilized polymerized lipid film. *Electroanal.*, 25, pp. 367–372.

Ramsden, C.A., and Riley, P.A., 2014. Tyrosinase: The four oxidation states of the active site and their relevance to enzymatic activation, oxidation and inactivation. *Bioorg. Med. Chem.*, 22, pp. 2388-2395.

Rebaud, S., Maniti, O., and Girard-Egrot, A.P., 2014. Tethered bilayer lipid membranes (tBLMs): Interest and applications for biological membrane investigations. *Biochimie*., 107, pp. 135–142.

Rems, L., Kasimova, M.A., Testa, I., and Delemotte, L., 2020. Pulsed electric fields can create pores in the voltage sensors of voltage-gated ion channels. *Bioph.J.*, 119, pp. 190–205.

Sabirovas, T., Valiūnienė, A., Gabriunaite, I., and Valincius, G., 2020. Mixed hybrid bilayer lipid membranes on mechanically polished titanium surface. *Biochim. Biophys. Acta – Biomembranes*, 1862, 183232.

Saem, S., Shahid, O., Khondker, A., Moran-Hidalgo, K., Rheinstädter, M.C., and Moran-Mirabal, J., 2020. Benchtop-fabricated lipid-based electrochemical sensing platform for the detection of membrane disrupting agents. *Sci. Rep.*, 10, 4595.

Salimi, A., Hallaj, R., Mamkhezri, H., and Hosaini, S.M.T., 2008. Electrochemical properties and electrocatalytic activity of FAD immobilized onto cobalt oxide nanoparticles: application to nitrite detection. *J. Electroanal. Chem*., 31, pp. 619–620.

Samouilov, A., Woldman, Y.Y., Zweier, J.L., and Khramtsov, V.V., 2007. Magnetic resonance study of the transmembrane nitrite diffusion. *Nitric Oxide*, 16, pp. 362–370.

Schwab, D.E., Stamler, J.S., and Singel, D.J., 2009. Nitrite-methemoglobin inadequate for hypoxic vasodilation. *Nat. Chem. Biol*., 5, pp. 366–366.

Shukla, S., Jin, R., Robustelli, J., Zimmerman, Z.E., and Baumgart, T., 2019. PIP2 reshapes membranes through asymmetric desorption. *Biophys. J.*, 117, pp. 962-974.

Sillero, N., 2011. What does ecological modelling model? A proposed classification of ecological niche models based on their underlying methods. *Ecol. Model.*, 222, pp. 1343-1346.

Silveira, C.M., Gomes, S.P., Araujo, A.N., Montenegro, M.C., Todorovic. S., Viana, A.S., Silva, R.J., Moura, J.J., and Almeida, M.G., 2010. An efficient non-mediated amperometric biosensor for nitrite determination. *Biosens. Bioelectr*., 25, pp. 2026-2032.

Simon, D., Marzocchi, A., Flecker, R., Lunt, D.J., Hilgen, F.J., and Meijer, P.Th., 2017. Quantifying the Mediterranean freshwater budget throughout the late Miocene: New implications for sapropel formation and the Messinian Salinity Crisis. *Earth Planet. Sci. Lett.*, 472, pp. 25-37.

Singh, T., Shukla, S., Kumar, P., Wahla, V., and Bajpai, V.K., 2017. Application of nanotechnology in food science: perception and overview. *Front. Microbiol.*, 8, 1501.

Siontorou, C.G., 2014. Aquatic modelling: An interplay between scales. *Int. J. Environ. Ecol. Geol. Mining Eng*., 8, pp. 555-561.

Siontorou, C.G., 2015. Bilayer lipid membrane constructs: A strategic technology evaluation approach. In: Tiwari. A., Patra, H.K., and Turner, A.P. (eds), *Advanced Bioelectronic Materials*, Wiley.

Siontorou, C.G., 2020. University-industry relationships for the development and commercialization of biosensors. In: Thouand, G. (ed), *Handbook of Cell Biosensors*, Springer Cham.

Siontorou, C.G., and Batzias, F.A., 2014a. Determining the sources of measurement uncertainty in environmental cell-based biosensing. *IEEE Trans. Instrum. Meas*.. 63, pp.794–804.

Siontorou, C.G., and Batzias, F.A., 2014b. A methodological combined framework for roadmapping biosensor research: a fault tree analysis approach within a strategic technology evaluation frame. *Crit. Rev. Biotechnol*., 34, pp. 31-55.

Siontorou, C.G., Batzias, F.A., and Tsakiri, V., 2010. A knowledge-based approach to online fault diagnosis of FET biosensors. *IEEE Trans. Instrum. Meas*., 59, pp. 2345-2364.

Siontorou, C.G., and Georgopoulos, K.N., 2014. Stimuli-responsive platforms for integrated multifunctional intelligent systems. *Chem. Eng. Trans.*, 39, pp. 811-816.

Siontorou, C.G., and Georgopoulos, K.N., 2015. Tyrosinase biosensor for phenol monitoring in water. *Proceedings of the International Conference on Chemical. Agricultural and Biological Sciences 2015 (CABS 2015)*, 10.17758/ERPUB.ER915036.

Siontorou, C.G., and Georgopoulos, K.N., 2016. A biosensor platform for soil management: the case of nitrites. *J. Clean. Prod.*, 111, pp. 133-142.

Siontorou, C.G., Georgopoulos, K.N., and Nalantzi, M.-M., 2017. Designing biosensor networks for environmental risk assessment of aquatic systems. *Crit. Rev. Environ. Sci. Technol.*, 47, pp. 40-63.

Siontorou, C.G., Georgopoulos, K.N., Nikoleli, G.-P., Nikolelis, D.P., Karapetis, S.K., and Bratakou, S., 2016. Protein-based graphene biosensors: optimizing artificial chemoreception in bilayer lipid membranes. *Membranes (Basel)*, 6, 43.

Siontorou, C.G., and Nikolelis, D.P., 1997. Cyanide ion minisensor based on methemoglobin incorporated in metal supported self-assembled bilayer lipid membranes and modified with platelet-activating factor. *Anal. Chim. Acta*, 355, pp. 227-234.

Siontorou, C.G., Nikolelis, D.P., and Krull, U.J., 1997. A carbon dioxide biosensor based on hemoglobin incorporated in metal supported bilayer lipid membranes (BLMs): Investigations for enhancement of response characteristics by using platelet-activating factor. *Electroanal.*, 9, pp. 1043-1048.

Siontorou, C.G., Nikolelis, D.P., Tarus, B., Dumbrava, J., and Krull, U.J., 1998. DNA biosensor based on self-assembled bilayer lipid membranes for the detection of hydrazines. *Electroanal.*, 10, pp.691-694.

Smit, P.J., 2006. *Medical and Biological Sensors and Sensor Systems*. Kalorama Information, 2nd ed., N.Y. USA.

Sreekumar, N.V., Narayana, B., Hegde, P., Manjunatha, B.R., and Sarojini, B.K., 2003. Determination of nitrite by simple diazotization method. *Microchem. J*., 74, pp. 27-32.

Stoytcheva, M., Zlatev, R., Velkova, Z., Valdez, B., and Ovalle, M., 2009. Analytical characteristics of electrochemical biosensors. *Portugaliae Electrochim. Acta*., 27, pp. 353-362.

Temiz, Y., Lovchik, R.D., Kaigala, G.V., Delamarche, E., 2015. Lab-on-a-chip devices: How to close and plug the lab? *Microelectron. Eng.*, 132, pp. 156-175.

Tepper, A.W., 2010. Electrical contacting of an assembly of pseudoazurin and nitrite reductase using DNA-directed immobilization. *J. Am. Chem. Soc*., 132, pp. 6550-6557.

Thévenot, D.R., Toth, K., Durst, R.A., Wilson, G.S., 1999. Electrochemical biosensors: Recommended definitions and classification. *Pure Appl. Chem.*, 71, pp. 2333-2348.

Thomas, G.E., Cameron, T.C., Campo, P., Clark, D.R., Coulon, F., Gregson, B.H., Hepburn, L.J., McGenity, T.J., Miliou, A., Whitby, C., and McKew, B.A., 2020. Bacterial community legacy effects following the Agia Zoni II oil-spill. Greece. *Front. Microbiol*., 11, 1706.

Tsao, C.-W., 2016. Polymer microfluidics: simple, low-cost fabrication process bridging academic lab research to commercialized production. *Micromachines*, 7, 225.

Van Dael, H., and Ceuterickx, P., 1984. The interaction of phenol with lipid bilayers. *Chem. Phys. Lipids*, 35, pp. 171-181.

Vanbeneden, N., Delvaux, F., and Delvaux, F.R., 2006. Determination of hydroxycinnamic acids and volatile phenols in wort and beer by isocratic high-

performance liquid chromatography using electrochemical detection. *J. Chromatogr. A*, 1136, pp. 237-242.

Vashchenko, O.V., Sadchenko, A.O., Budianska, L.V., and Lisetski, L.N., 2017. The combined effects of nitrates on multibilayer lipid membranes: Thermodynamic effects. *Biophys*., 62, pp. 227–232.

Walcarius, A., Shelley, D., Minteer, J.W., Yuehe, L., and Arben, M., 2013. Nanomaterials for bio-functionalized electrodes: recent trends. *J. Mater. Chem. B*, 1, pp. 4878-4908.

Wang, Y., Wang, J., Zhao, X., Song, X., and Gong, J., 2016. The inhibition and adaptability of four wetland plant species to high concentration of ammonia wastewater and nitrogen removal efficiency in constructed wetlands. *Biores. Technol*., 202, pp. 198-205.

Weiss, P.S., 2008. Functional molecules and assemblies in controlled environments: formation and measurements. *Acc. Chem. Res.*, 41, pp. 1772-1781.

Werlen, C., Jaspers, M.C.M., and van der Meer, J.R., 2004. Measurement of biologically available naphthalene in gas and aqueous phases by use of a *Pseudomonas putida* biosensor. *Appl. Environ. Microbiol.*, 70, pp. 43-51.

WHO, 2008. *Guidelines for Drinking Water Quality*, 3rd edition, vol. 1, Geneva.

WHO, 2018. A global overview of national regulations and standards for drinking-water quality, CCBY-NC-SA3.0IGO.

Wu, Y., and Lin, J.M., 2006. Determination of phenol in landfill leachate by using microchip capillary electrophoresis with end-channel amperometric detection. *J. Sep Sci*., 29, pp. 137-143.

Yang, L., Wang, Z., and Xu, L., 2006. Simultaneous determination of phenols (bibenzyl, phenanthrene, and fluorenone) in dendrobium species by high-performance liquid chromatography with diode array detection. *J. Chromatogr. A*, 1104, pp. 230-237.

Yildiz, H.B., Castillo, J., Guschin, D.A., Toppare, L., and Schuhmann, W., 2007. Phenol biosensor based on electrochemically controlled integration of tyrosinase in a redox polymer. *Microchim. Acta*, 159, pp. 27-34.

Zacharias, I., and Fakiris, E., 2005. Application of Landsat imagery, to verify nearshore water circulation of Saronikos Gulf. as resulted from numerical modelling. *Appl. Num. Anal. Comput. Math.*, 2, pp.281-290.

Zakharian, E., 2013. Recording of ion channel activity in planar lipid bilayer experiments. *Methods Mol. Biol*., 998, pp. 109–118.

Zhai, Q., and Cheng, W., 2019. Soft and stretchable electrochemical biosensors. *Mater. Today Nano*, 7, 100041.

Zhang, J., Zhao, S.Q., Zhang, K., and Zhou, J.Q., 2014. Cd-doped ZnO quantum dots-based immunoassay for the quantitative determination of bisphenol A. *Chemosphere*, 95, pp. 105-110.

Zhu, C., Yang, G., Li, H., Du, D., and Lin, Y., 2015. Electrochemical sensors and biosensors based on nanomaterials and nanostructures. *Anal. Chem.*, 871, pp. 230-249.